PERIODICAL Kobe Marine Observ. Memoirs
V. 14
LIBRARY
AUG 15 1960
FISH & WILDLIFE SERVICE
V. 1

神戸海洋気象台

欧文報告

第14巻

（堀口由己先生記念論文集）

THE MEMOIRS of the KOBE MARINE OBSERVATORY KOBE, JAPAN

Vol. XIV

Dr. Y. Horiguti's Anniversary Volume

KOBE

March 1960

This is the last issue of our MEMOIRS. We are also discontinuing THE JOURNAL OF OCEANOGRAPHY OF K.M.O.

We are planning to continue to publish BULLETIN OF THE KOBE MARINE OBSERVATORY once or twice a year in the form of collected papers.

Journal of Oceanography	Vol. 8,1-6	(completed)
	Vol. 9,1-2	(")
	Vol.10,1	(discontinued)

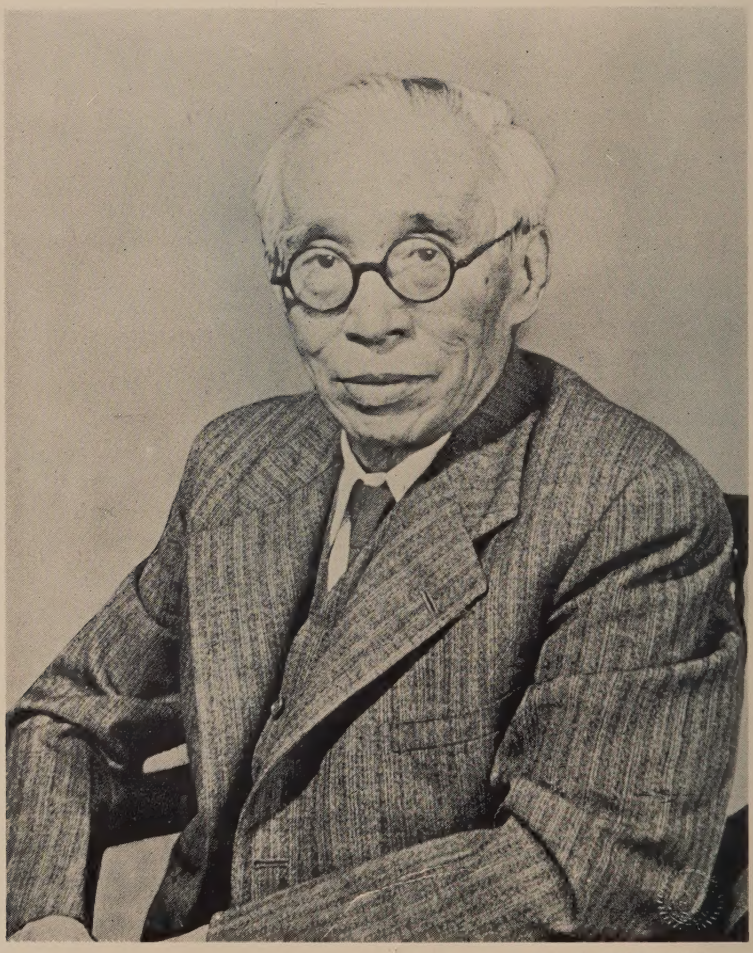

Dr. Y. HORIGUTI

The Memoirs of the Kobe Marine Observatory Vol. XIV

Dr. Y. Horiguti's Anniversary Volume

Contents

In Memory of Dr. Y. Horiguti. (Y. Shibata) 1

Oceanography

Z. Yasui and **K. Hata**: On the Seasonal Variations of the Sea Conditions in the Tsugaru Warm Current Region 3

H. Iida: On the Dynamical Structure of the Tsugaru Warm Current 13

S. Moriyasu: On the Monthly Sea Level on the South Coast of Japan 19

K. Hidaka: On the Equatorial Upwelling 32

Y. Saito: The Cold Water-Mass off the South Coast of Central Japan (I) 35

K. Hishida: On the Subsidence of Ground Level at Amagasaki Region, especially with the Relation to the Tidal Level 44

M. Uda: On the Fluctuation and Prediction of Ocean Temperature in the North Pacific 53

M. Ohwada: Vertical Distribution of Living and Dead Diatoms down to One Thousand Meters off Sanriku, Northern Japan 69

Y. Kawarada: A Contribution of Microplankton Observations to the Hydrography of the Northern North Pacific and Adjacent Seas (III) 74

K. Furuhashi and **Y. Matsudaira**: On the Vertical Distribution of Pelagic Copepoda Collected from the Kuroshio Region South of Honshū 81

Meteorology

K. Suda: Summer Temperature in North Japan Related to the Tropospheric Zonal Wind Profile 89

H. Matano: On the Evolution of a Tropical Cyclone in Relation to Its Life Cycle 96

K. Kanaya: On an Example of Cyclone Development 101

I. Sano, Y. Fujitani and **Y. Maena**: The Ice-Nucleating Property of Some Substances and its Dependence on Particle Size 107

T. Ogata: On the Relation of the Generation and Passage of a Typhoon to Sea Surface Conditions 119

S. Akai: On the Wind Velocity Profile near the Surface and Accumulation of Sand Grains at a Coastal Sand Dune 129

K. Akedo: On the Northwesterly Monsoon around Japan in Winter Season 134

M. Ōta: The Role of Vertical Structure of Atmospheric Circular Vortex in the Movement of its Center 145

K. Koenuma: Some Statistical Studies on Typhoons attacking Japan Islands 156

In Memory of Dr. Yosiki Horiguti

By

Yoshiji Shibata

Director of the Kobe Marine Observatory

The disastrous War of the Pacific ended at last and in the following year, 1946, a repatriator arrived home in Gifu Prefecture. Ill of polyartiritis rheumatica, he spent 10 odd years since, fighting for his health at home until he passed away on January 17, 1959, age 74. The man was the second Director of the Kobe Marine Observatory of Japan — Dr. Yosiki Horiguti himself.

In the heart of the rural Gifu Prefecture — Kamino-ho, Itonuki-mura, Motosu-gun, Gifu Prefecture — he was born on September 15, 1885. After graduated in June 1911 from the Physics Course, College of Science, Tokyo Imperial University, he started working at the Tsu Weather Station, then moved to Kobe the next year as the Chief of the Kobe Weather Station. Thus began the career of Dr. Horiguti in Kobe.

It was in 1920 that the Imperial Marine Observatory was established in Kobe. In cooperation with Dr. Takematsu Okada, the former director of the Central Meteorological Observatory, he made incredibly great efforts to set up the very Observatory of Kobe. For 19 long years since then until 1939, he contributed very much to the weather analysis of the North Pacific Ocean, working in that Observatory as the Chief of the Weather Chart Section of North Pacific Ocean.

Weather Stations in Japan had been under the command of the local prefectural governments until October 1939, when all such Stations came under the control of the State. It was then that our Dr. Yosiki Horiguti was appointed the second Director of the Imperial Marine Observarory of Kobe, as the successor to Dr. Takematsu Okada. The following year, he was also given the additional post of the Director of the Osaka District Meteorological Observatory. So to say, he was now the top director of all the official meteorological works of air, land and sea in Western Japan.

In 1942, following the outbreak of the Pacific War in December 1941, he went to Singapore to be the Chief of the Meteorological Department, General Headquarters of Military Administration of Japan at Singapore. There he was taken ill and, as we already know, he came home to Japan soon after the War to spend the rest of his life for the recovery of his health.

But for the War, this excellent scientist — truly one of the best meteorologists in Japan — could have lived many long years thereafter. For this never can we regret too much.

He left behind him many excellent achievements in the research of such meteor-

ological phenomena as typhoon, the heavy rain, etc. Among them most notable are his studies of typhoon.

In 1929, he was awarded the Prize of the Imperial Academy for his work "On the Typhoon of the Far East." When the notorious Typhoon Muroto came to hit Japan in 1934, he collected all obtainable data of observations from many places and made evident its structure as well as the origin of its energy. It was a great step forward along the way of researches about typhoon.

In his last years from 1957 to 1959, he was the President of the Marine Meteorological Society.

He had little of eloquency. Never in his life did he allow himself to resort to flattery or the like, nor did he forget to do anybody rights. Many people who once worked with him say that their first impression of him was that of a very difficult man; but having made his acquaintance, they soon found in him a warm humane heart.

Among the leading officials of the Japan Meteorological Agency today, there are many meteorologists who have once worked under Dr. Horiguti. In their view and way of thinking as well as in their memory, still live Dr. Horiguti and his influences so clearly that we can see.

On the Seasonal Variations of the Sea Conditions in the Tsugaru Warm Current Region

By

Zen'ichi Yasui and Katsumi Hata

Hakodate Marine Observatory

ABSTCRACT

(1) The northward transport of the Tsushima Warm Current is $3\sim6\times10^6$ m^3 /sec and corresponds to the 50 to 70% of the northward transport of the current off Yakushima, Kyūshū District.

(2) The seasonal variations of the heat transported by the Tsushima Warm Current which is computed from the temperature distributions in the vertical section off Henashizaki, have maxima in April and October, and minima in July and November. From this fact we can deduce that the rapid supplies of warm water from south occur in June and October. These supplies of warm water are different year by year and this gives important effects on the catches of sagittated calamary in the south of Hokkaidō District.

(3) The variations of the northward transport off Yakushima give some effects to the variations of the Tsugaru Warm Current several months later. And this gives some great influence to the catches of sagittated calamary.

(4) About 70% of the water of the Tsushima Warm Current enters into the Tsugaru Straits, but the current patterns of the Tsushima Warm Current make the transports into the straits change from 50% to 100%.

(5) The heat content in the Tsugaru Warm Current Region varies g-cal and corresponds to the heat transported during 15 to 60 days by the Tsushima Warm Current.

1. Introduction

It is said that the most significant period of the variations of the Tsushima Warm Current is 7 years (Hidaka, 1950). Generally speaking, a branch of the Kuroshio enters into the Japan Sea through the Tsushima Straits. It, meandering, flows northwards along the island of Japan proper and then the 70% of its water flows into the Tsugaru Straits and the rest continues to flow northwards along the west coast of Hokkaidō District and enters into the Okhotsk Sea.

The flow of the warm water which flows into the Tsugaru Straits is called the Tsugaru Warm Current and it makes a tongue-like warm region in the sea east of Tōhoku District—an eastward extension of the Tsugaru Warm Current—after passing the straits. One part of the warm water flows into the Bay of Uchiura and the most parts of the rest go down southwards along the east coast of Tōhoku District. Uda (1934, 1936, 1950 and 1958) investigated the physical structure of the

Tsugaru Warm Current, Miyazaki (1952) the heat budget of the Japan Sea, Kimura (1956) the catches of mackerel in the Tsugaru Straits and the sea regions adjacent to them, Sugiura (1952, 1957 and 1958) the sea conditions of the Tsugaru Warm Current, Hata (1951, 1957, 1958) the sea conditions of the Tsugaru Warm Current, and many other authors many other valuable facts.

In the straits and the sea adjacent to them, the catches of fish are very important to the local economy. The catches of sagittated calamary which have decreased since 1956 are specially important to Hokkaidō District.

Stuff of the Hakodate Marine Observatory have forecasted the sea condition of the summer in the sea east of Tōhoku District. If we can forecast those of the four seasons, that will be sure to give many profits to the people. So we devote our efforts to developing the method of forecasting the sea conditions. As the first step, the variations of the sea conditions in the sea regions or the sea conditions in the Tsushima Warm Current Region in the sea west of the Tsugaru Straits where there is the water mass before entering into the straits, and those in the northern part of the sea east of Tōhoku District where there is the water mass after flowing out the straits, will be investigated and next to these the connection between these sea conditions will be studied.

2. Sea conditions in the sea west of the Tsugaru Straits

(1) Mass transports

Papers which treated the mass transports in the sea region are very scarce. But according to the investigations on the Tsushima Warm Current by the Nagasaki Marine Observatory (1958), the mass transports had been $4\sim13\times10^6$ m^3/sec and had shown the tendency of decrease during the years 1955 to 1957, where they thought that the mass transports were able to be computed only by the northward components of the velocities in the vertical section west of Yakushima. And Miyazaki (1952) also computed the transports and got the values of $0.8\sim2.8\times10^6$ m^3/sec which were a little smaller than the former. Fig. 1 shows that the breadths of the Tsushima Warm Current west of Aomori prefecture are 30~80 sea miles, where the breadth of the current are smallest and those of the higher temperature belt are smaller than 50 sea miles. (Report of the synthetic investigations of the Tsushima Warm Current, vol. 1).

Using the hydrographic data observed in the sea west of Henashizaki and Gongenzaki in March, May, August and November every year since May, 1957, by the 1st Regional Maritime Safety Headquarter, we computed the mass transports through two pairs of observation points on the two lines west of Henashizaki and Gongenzaki, where the observations were held to the deeper layers than 400m. (In Fig. 1 the two pairs of observation points are shown St. 1 and St. 2 off Gongenzaki, and St. 3 and St. 4

off Henashizaki, respectively). The distances from the coast to St. 1 and St. 2 are 30 and 100 sea miles, respectively and to St. 3 and St. 4 are 10 and 80 sea miles, respectively. We computed the following values Q at the two pairs of points.

$$Q = \int_0^{400} \Delta D(Z)dz,$$ where Z is the depth and $\Delta D(Z)$ the value of dynamic anomaly at the depth Z.

The differences of Q's at the two points on the same lines which are the transports between the two points from surface to the 400m layer, are shown in

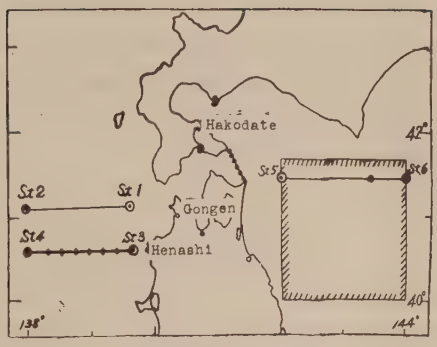

Fig. 1. Obsevation stations used in our computatinns and the sea region in which the Area of the Tsugaru Warm Current is computed.

Table 1. Transports in $10^6 m^3$/sec of the Tsushima Warm Current off Henashizaki and off Gongenzaki.

Season / Sea Region / Year	March		May		August		November	
	off Henashi	off Gongen	off Henashi	off Gongen	off Henashi	off Gongen	off Henashi	off Gongen
1957			3.5	0.9	3.3	3.3	6.6	1.3
1958	3.7	0.5	3.2	1.0	3.2	1.4	2.9	0.4

Table 1. The transports through the two lines contain the transports of the proper cold water of the Japan Sea but these are negligiblly small, so we may think the whole transports as the northward transports of the Tsushima Warm Current. The transports of the Tsushima Warm Current passing these lines are about 50~70% of those near Yakushima.

The transports passing between St. 1 and St. 2 are $0.4 \sim 3 \times 10^6$ m^3/sec, and have the maximum value in summer and the minimum in winter. Those between St. 3 and 4 are 15~45% of the former. The differences of the transports passing the two lines which have larger values than the transports passing between St. 3 and 4 almost all the years except in August, 1957, may be regarded as the transports between Gongenzaki and St. 1. The transports between St. 1 and 2, and those between St. 1 and Gongenzaki correlate in the reverse sign in winter.

(2) Sea conditions off Henashizaki

The variations of the heat transported by the Tsushima Warm Current through the vertical section off Henashizaki and the area of the Tsushima Warm Current in the vertical section were investigated, by using the data observed from 1950 to 1958 except 1951 and 1952 by the Aomori Fisheries Research Institute. Generally,

in summer the discontinuous layer which is significant in the Japan Sea developes at 30m and the axis of the Tsushima Warm Current are in 40 sea miles from the coast and the horizontal temperature gradients are larger there. In the deeper layers than 100 or 200m is there the proper cold water of the Japan Sea, whose temperatures are lower than 2°C.

Using the data observed in the sea from the coast to 50 sea miles where more observations were held, we computed the area A_1 with higher temperatures than 6°C in a vertical section, where the layers from surface to 50m which effected very much by the climate were excepted and the layers from 50 to 300m were considered, and then the heat C_1 contained in the area A_1. These are shown in Fig. 2. We use these values as the characteristics of the variations of the northward

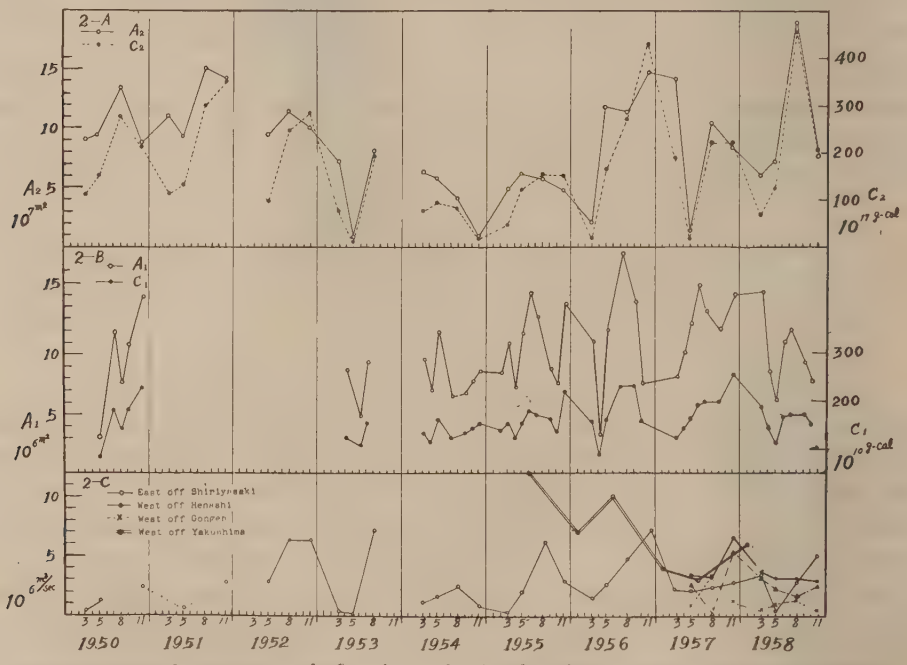

Fig. 2a. Seasonal variations of the Area A_2 in the above mentioned area occupied by the Tsugaru Warm Current Water, and those of the heat C_2 contained in the water mass.

2b. Seasonal variations of the Area A_1 occupied by the water mass warmer than 6°C in the layers from 50 to 300m in the vertical section west of Henashizaki, and those of the heat C_1 passing through the area in the section.

2c. Seasonal variations of the transports in the sections shown in Fig. 1.

flow of the Tsushima Warm Current. The minima of A_1 and C_1 in the mean values over 6 years appear two times a year, in April and October and the maxima also appear two times in July and November. These are seemed to have occurred by the cause of the rapid supplies of warm waters in June and October.

The variations of A_1 are much larger than those of C_1, do not show any outstanding persistency, and C_1 relates better to the transports through this area A_1 than to A_1. In November, 1957, in our results C_1 reaches its maximum value and at the same time the transport was a larger value, 6×10^6 m^3/sec, but it is wonderful that inspite of such a condition the transports of the water flowing into the Tsugaru Straits was very small.

3. Sea conditions off the east mouth of the Tsugaru Straits

(1) Mass transports

According to Hata (1959), the transport of the Tsugaru Warm Current in the northern parts of the sea east of Tōhoku District is minimum ($0.2\sim3.6\times10^6$ m^3/sec) in March to May and maximum ($1.0\sim7.7\times10^6$ m^3/sec) in August to November and its variations are due to the variations of the sea conditions off the west mouth of the straits.

Table 2. Transports in 10^6m^3/sec in the sea east of Shiriyazaki.

Year \ Season	Feb.-Mar.	May	Aug.	Nov.
1950	0.3	1.3	—	2.3
51	—	0.6	—	2.8
52	—	2.8	6.3	6.3
53	0.3	0.2	7.7	—
54	1.1	1.8	2.6	1.0
55	0.2	2.0	6.2	2.8
56	1.5	2.6	4.7	7.4
57	2.2	2.0	2.4	2.8
58	3.6	0.4	2.9	5.0

(2) Temperature distributions in the northern part of the sea east of Tōhoku District

Seasonal and yearly variations of the eastward extension of the Tsugaru Warm Current in the northern part of the sea east of Tōhoku District are very large and these variations have great effects on the sea conditions of the region.

The extension of the warm current is greatly changed by the variations of the current axis and the northward transports of the Tsushima Warm Current off the west mouth of the straits. It is also effected by the other elements in the sea east of Tōhoku District, that is, the variations of the Oyashio front or the relation between the water from Kuroshio and the coastal branch of the Oyashio Currents.

As a characteristic quantity of the eastward extension, we choose in the sea region (40°00′N to 41°40′N and 142°E to 144°E) the area in which the mean water temperatures of the upper 200m layer are higher than a certain definite temperature in each season; 4°C in March, 6°C in May, 8°C in August and 10°C

in November.

The equi-thermal contour of the definite temperature is considered as a representation of the boundary of the warm current in the season, because the temperature gradient near this contour is largest.

We computed A_2 and C_2 heat contained in the water column 0 to 200m occupying the area A_2 by the use of the data observed on board of the R. M. S. Yūshio Maru and Ryōfū Maru during the year 1950 to 1958.

A_2 and C_2 are shown in Fig. 2.

A_2 is $1 \sim 20 \times 10^7$ m^2 and ten times larger than A_1 off Henashizaki, and the minimum of A_2 appears in March and the maximum appears in August or sometimes in November.

C_2 is $10 \sim 450 \times 10^{17}$ g-cal and shows the same tendency of variations as A_2, but its maximum appears mainly in November. This fact is due to the increase of the depth of the warm water or the developement of the anticyclonic current system in autumn.

According to Miyazaki (1952), the heat given by the Tsushima Warm Current to the Tsugaru Current is about 5×10^{17}g-cal/day. Using this value, the heat content in the Tsugaru Warm Current Region in the sea east of Tōhoku District is equivalent to the heat transported through the Tsugaru Straits during 15 days in March, 20 days in May, 50 days in August and 60 days in November. This fact is very important to study the persistency of the eastward extension.

If the southward flow of the Tsugaru Warm Current is checked by any cause, it is natural that an extraordinary sea condition appears in the sea region.

Next to this, the relation of A_2 to the transports mentioned in (1) of § 3 shows that in May and November the two quantities correlate well with each other, but in March and August they do not correlate to some extent. The cause of this is that there are many examples of the extraordinary sea condition in summer. As shown in Fig. 3, in spite of the fact that in November, 1951 and August, 1958, the transports of the Tsugaru Warm Current are small, the eastward extensions of the Tsugaru Warm Current are large. This fact is, of course, due to the checking effect of the water from the Kuroshio. And contrary cases occured in August, 1953 and 1958. This is due to the fact that the southward flow of the warm current was extraordinarily large along the east coast of Tōhoku District.

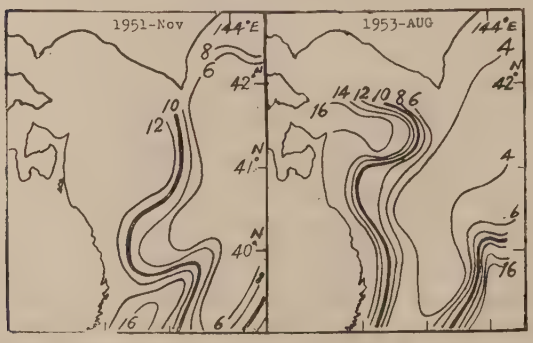

Fig. 3. Mean temperature distribution in the layers from 0 to 200m in the sea region east of the Tsugaru Straits.

4. Relations between the sea conditions off the east mouth and the west mouth of the straits

(1) It can be thought that the variations of the Tsugaru Warm Current in the sea east of Tōhoku District will occur 5 or 6 months after the variations of the Tsushima Warm Current off Yakushima.

In Fig. 3 the relation between the northward transports off Yakushima in January and June and the transport of the Tsugaru Warm Current since 1955 is shown. The variations of the two quantities coincide well in the difference of several months inspite of the defect of data.

(2) The transport of the water into the Tsugaru Straits from the Tsushima Warm Current is about $0.4 \sim 1.3 \times 10^6$ m³/sec according to Miyazaki (1952). Other investigations on the transport can not be found, but it is said that the 70% of the transport of the Tsushima Warm Current flows into the Straits. The southward transport of the Tsugaru Warm Current in the sea east of Tōhoku District is $3 \sim 5 \times 10^6$ m³/sec in spring and summer according to Sugiura (1957), and $0.2 \sim 8 \times 10^6$ according to Hata (1958).

From these values we can understand that the 50~100% of the water flowing west of Henashizaki enters into the straits. A few extreme cases are shown in Table 3, and if we call as A-type the temperature distribution of the case where the 50% of water flows into the straits and as B-type temperature distribution of the case where the 100% flows into the straits, then the B-type can occur in any season.

Table 3. Transports in 10^6 m³/sec off Henashizaki and Shiriyazaki and ratios of the transports off Shiriyazaki and those off Henashizaki.

Year	A Type 1957 Nov.	B Type 1958 Mar.	B Type 1958 Aug.
off Henashi	66	37	31
off Shiriya	28	36	29
	42%	98%	94%

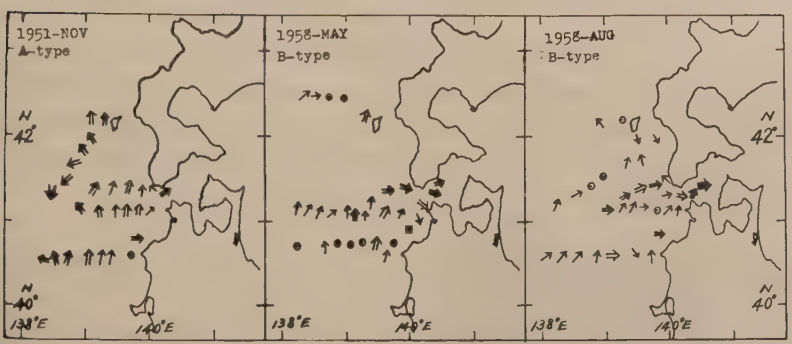

Fig. 4. Surface Currents by G. E. K. measurements in the sea region west of the Tsugaru Straits.

Examples of the A and B-type are shown in Fig. 4. In B-type (March and August, 1958), the whole northward flow off Henashizaki goes on flowing between St. 1 and St. 2, turns to the right off Shirakami-misaki and flows back into the straits.

In A-type (November, 1957), the axis of the Tsushima Warm Current is in 40～70 sea miles from Henashizaki and in 30～60 sea miles from Gongenzaki; so we can not see any inflows to the straits. From this fact we can understand the reason why the extreme cases of the transport occur. At the same time it can be said that the transport into the straits depends on the position of the axis of the Tsugaru Warm Current.

(3) If we investigate the relation between the transports between St. 1 and St. 2, and the areas of the eastward extension in Fig. 5, we can find the correlation between the two except in the extraordinary season, August, 1958, of which we mentioned in (2) of § 3. That is, when the transport is larger, the extension is larger, too.

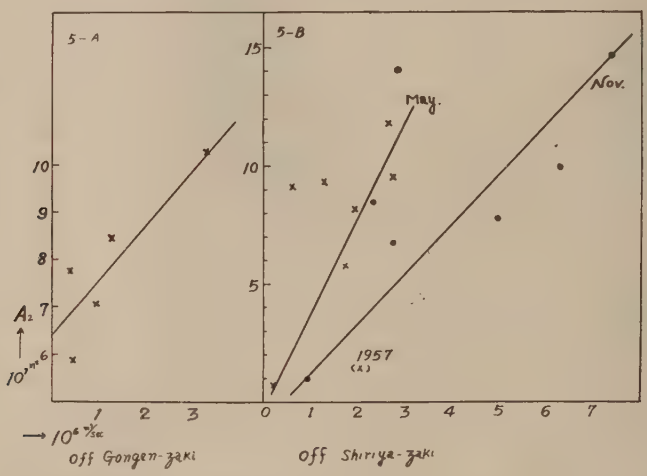

Fig. 5. Relations between the areas occupied by the water mass of the Tsugaru Warm Current and the transports off Shiriyazaki and Gongenzaki.

(4) If we compare A_2 and C_2 in the sea east of Tōhoku District with A_1 and C_1 in the sea west of Henashizaki, it can be found that their variations coincide nearly, that is they have minima in 1954 and 1955 and maxima in 1956 and 1957.

To variations of more short periods we can not give any conclusion for the shortness of data. This point will be investigated some day.

5. Influences of the variations of the sea conditions and the catches of sagittated calamary

The catches of sagittated calamary in the sea south of Hokkidō District are

influenced by the sources of it in the sea region and the sources are influenced by the variations of sea conditions, so we investigated the relation between the two facts.

In recent years the catches of it have decreased rapidly and those in 1958 reached the one-fourth in 1958. See Fig. 6.

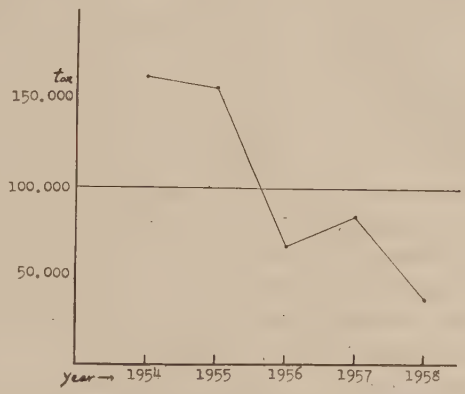

Fig. 6. Catches of sagittated calamary in these five years in the sea south of Hokkaido.

As already mentioned in § 3, the northward transports of the warm water mass off Henashizaki occur in June and October, but they vary year by year in the points of time and strength. See Fig. 2b.

When the seasons of the northward transports of the warm water mass are agree with the seasons of the tour of schools of sagittated calamary, larger sources of it are thought to be found in the sea south of Hokkaidō District. So we investigated the seasons of the warm northward transport from year to year. The result is that in 1954, 1955 and 1957 the seasons were in May to June and in 1956 and 1958, in July. In the former cases the catches of sagittated calamary were larger and in the later they were smaller.

The relation of the catches to the transports into the Tsugaru Straits is considered to be significant, that is, the tendency of decrease of the transports to the same tendency of the catches. And in the years, 1956 and 1958, when the southward transports off Hidaka made a sudden increase in summer to autumn, we had smaller catches and on the contrary, we had larger catches in the years, 1954 and 1955, when the transports made a decrease.

There were the year (1954) when the extent of the water mass of the Tsugaru Warm Current off Hidaka was stable in all seasons, and the years (1956, 1957, and 1958) when the extent was unstable season by season. We may suppose that this fact also gives a great effect on the catches of fish and the seasonal variations of it. Specially, the sea condition in the Tsugaru Warm Current Region in 1958 was the most extreme case in these ten years. In that year the transports out of the Tsugaru Straits increased in summer to autumn, but the area of the Tsugaru Current Region decreased. This shows that the warm water flowed down southwards along the east coast of Tōhoku Disrtict more rapidly.

As mentioned above the transports, the extensions and their seasonal variations of the Tsugaru Warm Current have connection with the catches of the sagittated calamary in the sea south of Hokkaidō District.

We convince that by means of the sea conditions, we shall be able to forecast

the fishery conditions in the sea south of Hokkaidō.

References

(1) Miyazaki, M. (1952): Heat budget in the Japan Sea, *Reports of the Hokkaidō Fishery Research Institute*, Vol. 4.

(2) Japan Meteorological Agency (1952): *Reports of the Marine Meteorological and Oceanographical Observations*, Vol. 6, No. 2, pp. 17-21.

(3) Japan Meteorological Agency (1958): *Reports of the Marine Meteorological and Oceanographical Observations*, Vol. 7, No. 1, pp. 49-52.

(4) Hata, K. (1953): Influences of the Tsugaru Warm Current on the sea conditions in the sea east of Tōhoku District. *Reported in the 3rd Conference on the Observation Technique in the Sea east of Tōhoku District.*

(5) Hata, K. (1959): Connection of the sea conditions on the passage of ferry-boats in the Tsugaru Straits, in printing.

(6) Sugiura, J. (1954): Sea conditions of spring and summer in the sea east of Tōhoku District in the point of view of the transports of current. *Reports of the Marine Meteorological and Oceanographical Observations*, Vol. 3, No. 3.

(7) Sugiura, J. (1957): Seasonal variations of the transports of currents in the sea east of Tōhoku District. *Journal of Meteorological Research*, Vol. 9, No. 2.

(8) Sugiura, J. (1958): On the Tsugaru Warm Current. *Geophysical Magazine*, Vol. 28, No. 3.

(9) Kimura, K. (1956): Mackerels in the Tsugaru Straits and in the sea adjacent to the straits. *Reports of the Tōhoku Fishery Research Institute*, Vol. 7.

On the Dynamical Structure of the Tsugaru Warm Current

By

H. Iida

Hakodate Marine Observatory

ABSTCRACT

The relations between the temperatures in the 200m and the dynamic depth anomalies at *P*-db. have seasonal variations.

The $\Delta D(P)$ values in February and May are smaller than those in August and November.

From these relations the author could compute the upwelling and sinking in the Tsugaru Warm Current Region.

1. Introduction

The density structure of the Tsugaru Warm Current Region has not been studied so well. But the sea conditions in the region have been studied by many authors. Among their works the author found some interesting and important facts on the density structure.

J. Sugiura (1958) thought that the structure of the current in the region is very much like that of the Kuroshio Current.

Mi. Miyazaki (1952) computed the volume transport of the Tsugaru Warm Current and found it varies between the minimum value, about 3.8×10^{16} cm^3/day, in February and the maximum, about 11×10^{16} cm^3/day, in September to October. And Mi. Miyazaki (1953) and M. Akagawa (1954) said there are the coastal water and the intermediate waters of the Tsushima Warm Current near the western mouth of the Tsugaru Straits in the layers shallower than 200m, and the waters of temperature warmer than 6°C flow into the straits.

Since 1949, the observations in the Tsugaru Warm Current Region have been held in February, May, August and November on board R. M. S. Yūshio Maru. On the basis of these data and by refering the above mentioned works, the author tries to get some fact on the density structure of the region.

2. T-Cl relations

In Fig. 1a, 1b, Fig. 2a and 2b the T-σ_t relations and the T-Cl relations in the four seasons are shown. It is shown that the patterns of the T-Cl relations in February and May are different from those in August and November only in the parts of temperature lower than 7°C and that the patterns in the higher temperature parts are different very much season by season and the patterns in August and November are very near but the pattern in May is much isolated from the former.

The same relations are seen from the T-σt relations in Figs. 1a and 2a.

In short, the T-Cl structure in May is similar to that in February and that in November is similar to that in August, and the water in the Tsugaru Warm Current Region consists of two layers, one in which the T-Cl relation can vary season by season and the other in which the relation can not vary.

Thus, it is found that the density structure is comparatively simple and has a simple seasonal variation. From these facts the author thinks the dynamic anomaly is presumed to be obtained by some comparatively few observational data which can be got by the easier observation than the serial hydrographical observation to the depth of no current.

3. $T_{200}\sim D(P)$ relations

Using the data north of 40°00′N and west of 143°30′E, the author obtained the relations between the temperatures in the 200m layer and $\Delta D(P)$, dynamic depth anomaly at the P deci-bar layer, which are shown in Tables I and II or Fig. 3a and 3b. In Tables I and II, $F(P)$ and $G(P)$ are the coefficients of the $T_{200}\sim D(P)$ relations which are assumed to be linear as follows

$$\Delta D(P)=F(P)T_{200}-G(P) \qquad (1)$$

These tables show that $\Delta D(P)\sim T_{200}$ relations in February and May are lower than those in August and November, have greater seasonal variations in shallower layers and no seasonal variation at the depth of about 1000-db.

Table I. Coefficients of linear relations between T_{200} and $\Delta D(P)$ in February and May.

	$T<4$°C		$T>4$°C	
P(d.b.)	F	G	F	G
400	0.0273	0.467	0.0193	0.499
600	0.0365	0.641	0.0243	0.690
800	0.0393	0.819	0.0278	0.865
1000	0.0403	1.007	0.0298	1.085

Table II. Coefficients in August and November.

	$T<4$°C		$T>4$°C	
P(d.b.)	F	G	F	G
400	0.0325	0.548	0.0246	0.580
600	0.0353	0.743	0.0267	0.777
800	0.0380	0.916	0.0284	0.954
1000	0.0403	1.007	0.0298	1.085

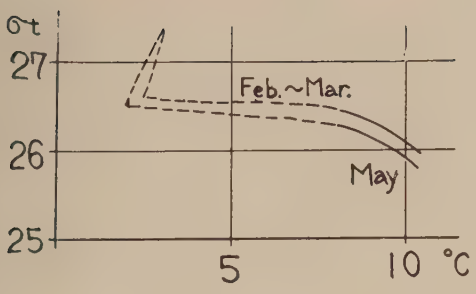

(1a)

Fig. 1a. T-σt relations in February and May.

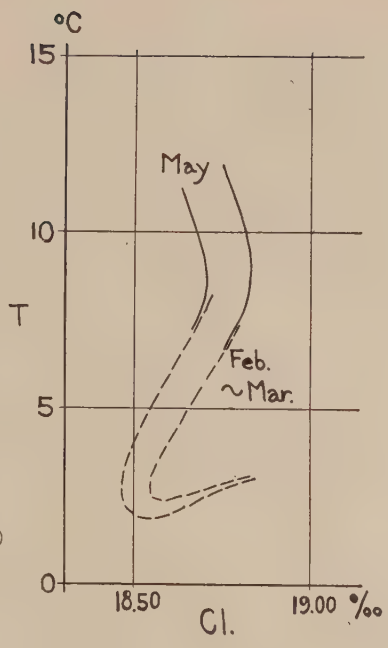

Fig. 1b. T-Cl relations in February and May.

(1b)

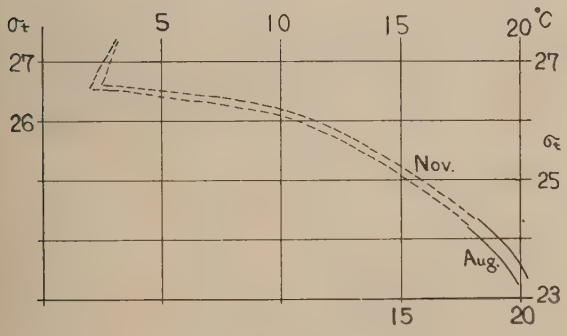

(2a)

Fig. 2a. T-σt relations in August and November.

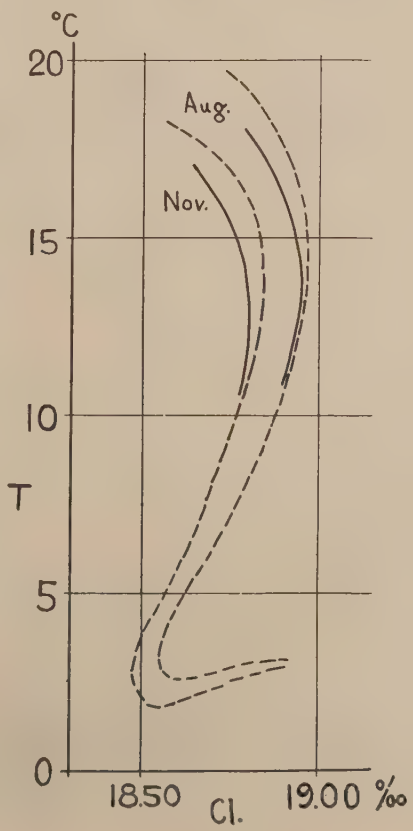

Fig. 2b. T-Cl relations in August and November.

(2b)

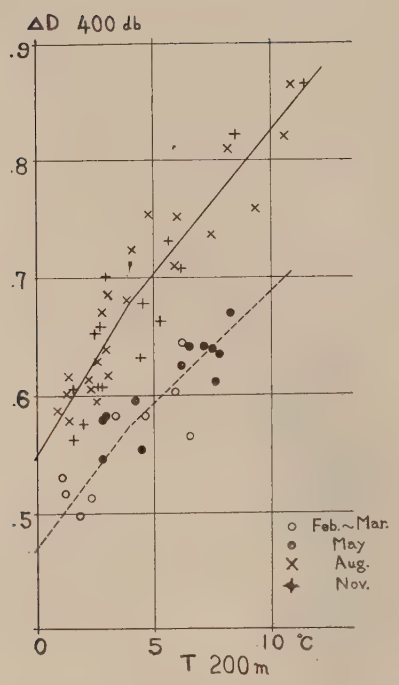

Fig. 3a. Relations between the temperatures in the 200m layer and the dynamic depth anomalies at the 400 db. layer.

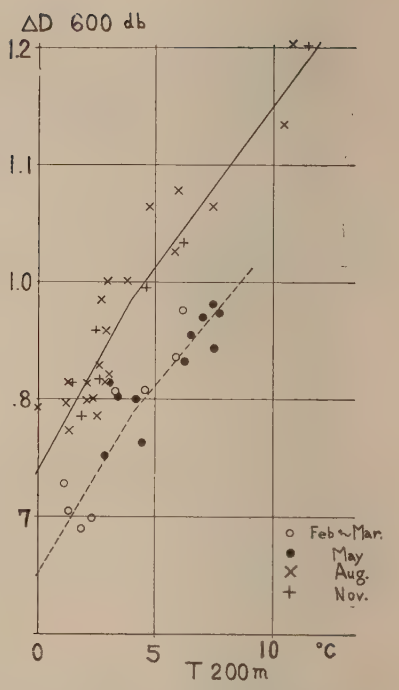

Fig. 3b. Relations between the temperatures in the 200m layer and the dynamic depth anomalies at the 600 db. layer.

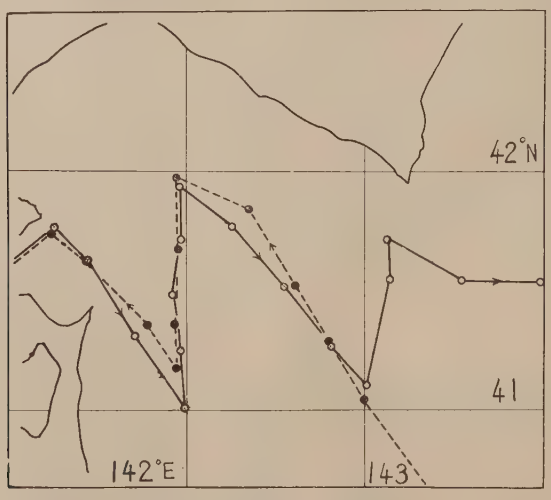

Fig. 4a. Observation stations on May 19, —○—, and on May 30, 1958. ···●···

4. Applications

The author assumes the depth of no currents about 1000 db. surface.

Then $$\frac{\partial P}{\partial x}=\rho\frac{\partial\{D(1000)-D(P)\}}{\partial x}=\rho\frac{\partial\{\Delta D(1000)-\Delta D(P)\}}{\partial x}=\rho\{F(1000)-F(P)\}\frac{\partial T_{200}}{\partial x} \quad (2)$$

where x-axis points eastwards, ρ is density at P-db. and $D(P)$ is dynamic depth at P-decibar. From (2), assuming geostrophic balance, we can compute the vertical velocity at P-db. as follows

$$\rho w\Big|_P=-\frac{\beta}{f^2}\int_P^{1000}\frac{\partial P}{\partial x}dP=-\frac{\beta}{f^2}\left[\int_P^{1000}\rho\{F(1000)-F(P)\}dP\right]\frac{\Delta T_{200}}{\Delta x} \quad (3)$$

So the vertical velocity is in February and May

$$w_{200}=-\begin{cases}1.8\times10^{-3}\,\Delta T_{200}\ m/sec, & T>4^\circ C\\ 1.5\times10^{-3}\,\Delta T_{200}\ m/sec, & T<4^\circ C\end{cases} \quad (4)$$

and in August and November

$$w_{200}=-\begin{cases}1.4\times10^{-3}\,\Delta T_{200}\ m/sec, & T>4^\circ C\\ 1.0\times10^{-3}\,\Delta T_{200}\ m/sec, & T<4^\circ C\end{cases} \quad (5)$$

where ΔT_{200} is east value minus west value of T_{200} and Δx is about 2×10^7 meters and w_{200} is positive in the sinking region.

If this relationship (this corresponds to the assumptions of geostrophic balance and the above mentioned T_{200}-ΔD relations) holds in the region, the author can compute upwelling and sinking. When there are upwellings, the temperatures at 200m will decrease and when there are sinkings, the temperatures will incease. From this fact we can prove the above relation.

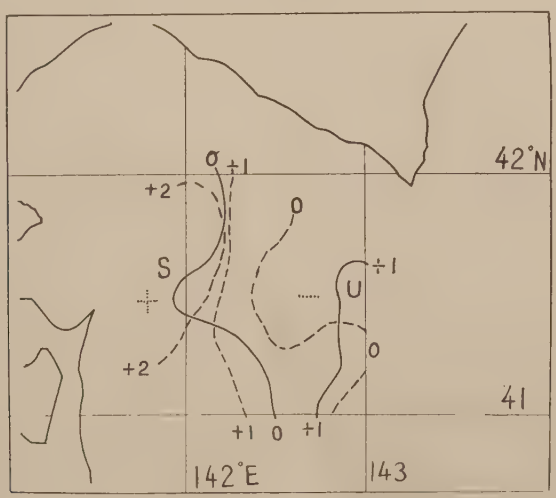

Fig. 4b. Distributions of the ΔT_{200} in solid and the increases of temperature in those ten days in broken lines.

In fact, in Fig. 4b the author shows the good coincidence between ΔT_{200} and the increases of temperature during May 19 to 30, 1958. It can be assumed that during such a short period the transport of the Tsugaru Straits does not change so much and does not give some large effects on the structure of the Tsugaru Warm Current.

5. Conclusions

These show that the relationship of $T_{200} \sim \Delta D$ and the assumption of geostrophic balance hold approximately.

But the reason why the $T_{200} \sim \Delta D$ relations hold and the seasonl variations of them arise, will be investigated in future. The author thanks Mr. Yasui, Mr. Sugiura and Mr. Hata for their kind encouragements and advices.

References

(1) Sugiura, J. (1957): Variations of sea conditions in the sea south of Hokkaidō. *Oceanog. Mag.* Vo. 9, No. 1, 1957.

(2) Miyazaki, Mi. (1952): Heat budget in the Japan Sea, *Reports of the Hokkaidō Fishery Research Institute*, Vol. 4.

(3) Yoshida, K. and Han-Lee Mao (1957): A theory of upwelling of large horizontal extent. *Jour. Mar. Res.*, Vol. 16, No. 1, 1957.

On the Monthly Sea Level on the South Coast of Japan

By

S. Moriyasu

Kobe Marine Observatory

1. Introduction

The monthly sea level around the Kii Peninsula has been studied and its close relation with the fluctuation in the oceanographic conditions has been made clear (Moriyasu, 1958 b). In this paper, we make the monthly sea level at Aburatsu (Miyazaki Prefecture), Shimizu (Kochi Prefecture), Uwajima (Ehime Prefecture), Toba (Mie Prefecture) and Maisaka (Shizuoka Prefecture) an object of the study in addition to around the Kii Peninsula and discuss its dependence upon the oceanographic conditions. The location of the tidal station is shown in Fig. 1.

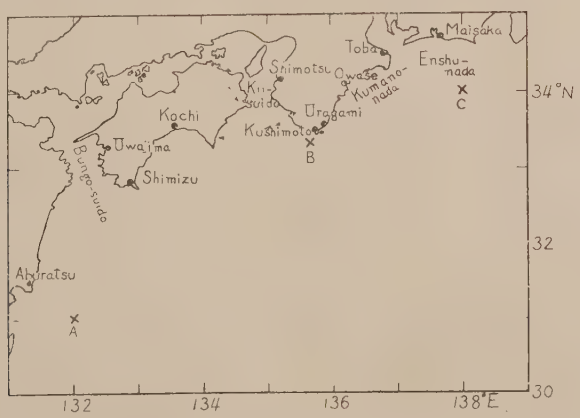

Fig. 1. The position of the tidal station (●) and the oceanographic station (×).

The source of data is Tidal Observations (C. M. O., 1956; J. M. A., 1957, 1958). The barometric effect is statically eliminated as follows. On the assumption that the monthly sea level becomes higher (lower) by 1 cm according to the decrease (increase) of 1 mb in the atmospheric pressure, the monthly sea level is reduced to the standard atmospheric pressure (1013.3 mb) by using the monthly mean pressure at the weather station which is located nearest to the concerned tidal station.

2. The normal monthly value

The mean value of the monthly sea level from 1951 to 1956 is called the normal monthly value in each month in this paper. The variation of the normal monthly

values is common to every tidal station (Fig. 2), that is, the maximum and the minimum occur in September ~ October and in February ~ March, respectively. The results of harmonic analysis show that the amplitude of annual variation is about 10 cm and that the amplitude of semi-annual variation is less as compared with that of annual variation i.e. below one fourth of the latter. By Pattullo et. al. (1955), it was pointed out that the semi-annual variation is slight in the Kuroshio region. Though we use the data in 6 years, the feature shown by them appears distinctly in our results. The amplitude of annual variation is great at Kochi, Uragami, Toba and Maisaka, while it is least at Aburatsu. Furthermore, it is noteworthy that the amplitude is not great in the inland sea.

We have briefly described the mean feature of the annual variation in the monthly sea level so that we may have the preliminary knowledge for the discussions in the following sections.

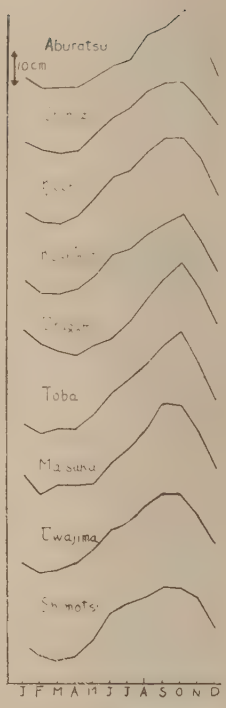

Fig. 2. The normal monthly sea level from 1951 to 1956.

3. The relation between the monthly sea level and the dynamic height

In the previous paper (Moriyasu, 1958 b), we found a close connection between the monthly sea level at Kushimoto and the dynamic height anomaly at 33°20'N, 135°40'E. This implies that the monthly sea level at the tidal station which faces the open-sea fluctuates according to the oceanographic conditions in the neighbourhood. Therefore, we try to find the relation at Aburatsu and Maisaka in the same manner. In Fig. 3, we show the scatter diagram between the monthly sea level at Aburatsu and Maisaka and the dynamic height anomaly above the 800 db surface at 31°N, 132°E and 34°N, 138°E, respectively. The position of the hydrographic station is not necessarily suitable for the purpose and the dynamic height anomaly is extrapolated in some cases. Though the treatment is not sufficient in such a manner, the correlation can be found at the significance level of 2%. The

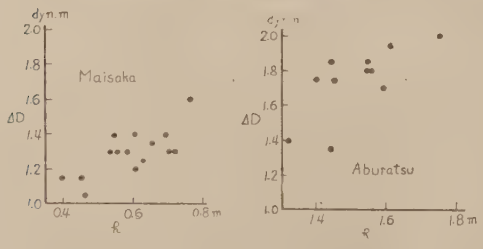

Fig. 3. The relation between the monthly sea level (h) and the dynamic height anomaly (ΔD) near the tidal station.

correlation coefficient is shown in Table 1.

Table 1. The correlation coefficient between the monthly sea level and the dynamic height anomaly near the tidal station.

tidal station	oceanographic station	r	N	2% point
Aburatsu	A (31°N, 132°E)	0.697	11	0.6851
Maisaka	C (34°N, 138°E)	0.863	15	0.5923
Kushimoto	B (33°20′N, 135°40′E)	0.830	16	0.5742

r: correlation coefficient; N: number of samples.

The result makes us conclude that the monthly sea level is regarded as the steric surface and is related with the fluctuation of the oceanographic conditions. At Aburatsu, the monthly sea level becomes higher when the current axis of the Kuroshio approaches to the coast in general. At Maisaka, the monthly sea level becomes higher when the counter-clockwise eddy in the cold water region develops and *vice versa*. Hence, we can deduce the oceanographic conditions in the offing from the monthly sea level to some extent.

4. The fluctuation in the annual variation of the monthly sea level

We pointed out that the annual variation of the monthly sea level fluctuated from year to year (Moriyasu, 1958 b). Now, we will again ascertain the fact by

Table 2. The results of analysis of variance of the monthly sea level.

		sum of squares	D	unbiased estimates	F	F_0 (5%)	F_0 (1%)
Aburatsu	months	3081	11	280	7.37	2.01	2.68
	years	532	4	133	3.50	2.58	3.78
	interaction	1680	44	38			
Shimizu	months	3213	11	292	8.34	2.01	2.68
	years	425	4	106	3.03	2.58	3.78
	interaction	1558	44	35			
Kochi	months	5704	11	519	13.66	1.97	2.59
	years	437	5	87	2.29	2.38	3.37
	interaction	2095	55	38			
Kushimoto	months	4265	11	388	11.41	1.97	2.59
	years	526	5	105	3.09	2.38	3.37
	interaction	1891	55	34			
Uragami	months	5083	11	462	11.55	1.97	2.59
	years	853	5	171	4.28	2.38	3.37
	interaction	2184	55	40			
Toba	months	6766	11	615	14.30	1.97	2.59
	years	1305	5	261	6.07	2.38	3.37
	interaction	2380	55	43			
Maisaka	months	3841	11	349	21.81	2.09	2.84
	years	1452	3	484	30.25	2.89	4.44
	interaction	532	33	16			
Uwajima	months	4498	11	409	16.36	1.97	2.59
	years	219	5	44	1.76	2.38	3.37
	interaction	1371	55	25			
Shimotsu	months	2887	11	262	7.49	2.26	2.18
	years	59	2	30	1.17	19.45	99.45
	interaction	780	22	35			

D: degree of freedom; F_0: 5% and 1% point for the distribution of F.

means of the analysis of variance (Kenney, 1939). The result of the analysis of variance is shown in Table 2. At Uragami, Toba and Maisaka, significance differences can be found in the variance of the deviations in each month from the annual mean sea level at the significance level of 1%, while at Aburatsu, Shimizu and Kushimoto, those can be found at the significance level of 5%. Nevertheless, those can not be found even at the significance level of 5% at Kochi, Uwajima and Shimotsu. Thus, we may conclude that the annual variation fluctuates from year to year on the coast of the open-sea, while the significant difference can not be found in the annual variation of the sea level at the stations which are not in good exposure to the open-sea. At the latter stations, the influence of oceanographic conditions in the open-sea is diminished. Therefore, the fluctuation of the oceanographic conditions contributes to the fluctuation in the annual variation of the sea level with year. Here, the annual mean sea level is not treated, but the departure of the monthly sea level from the annual sea level is discussed by means of the analysis of variance.

5. The departure from normal monthly values

The departure is the deviation from the mean values and occurs under the influence of the fluctuation in the oceanographic conditions etc. Since the effect of the atmospheric pressure is eliminated from the monthly sea level, it is not included in the departure. In Fig. 4, we show the departure at every station. The vertical land deformation must be noticed, but the progressive deformation can not be found in the figure.

The standard deviation of the departure makes the degree of the fluctuation in the monthly sea level clear. According to Table 3, the standard deviation is greater on the coast of the Kumano-nada and the Enshu-nada, while it is less on the coast of Kyushu and Shikoku. Hence, the fluctuation of the oceanographic conditions is expected to be remarkable in the Kumano-nada and the Enshu-nada. This expectation has a considerable basis, that is, the cold water region fluctuated strikingly in the concerned period (Moriyasu, 1959). At the station which does not face the open-sea,

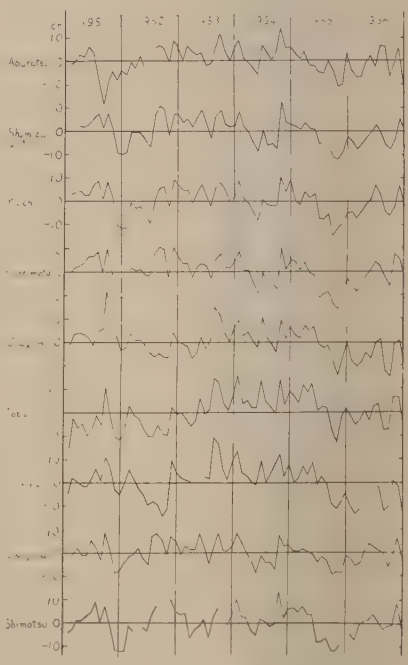

Fig. 4. The departure from the normal monthly sea level.

Table. 3. The standard deviation of the departure from the normal monthly sea level in each year (cm).

	1951	1952	1953	1954	1955	1956	1951~1956
Aburatsu	7.2	5.0	5.0	5.9	5.5	6.5	5.9
Shimizu	6.0	6.5	5.1	6.3	6.2	4.5	5.8
Kochi	6.5	6.4	4.4	5.7	7.3	4.7	5.9
Kushimoto	6.5	6.7	3.8	5.9	8.5	5.0	6.2
Uragami	7.4	4.1	6.4	5.7	6.3	8.1	6.5
Toba	8.7	6.6	6.6	8.1	7.4	5.0	7.2
Maisaka	4.7	8.1	8.7	7.0	6.2	9.3	7.4
Uwajima	4.7	4.9	4.2	5.4	4.8	3.8	4.7
Shimotsu	5.9	6.5	4.0	5.6	7.9	3.8	5.7

the standard deviation is generally less. This is based upon the fact that the fluctuation of the oceanographic conditions in the open-sea does not extend there in the original condition.

The standard deviation in each year fluctuates from year to year as shown in Table 3. Accordingly, though the feature noted above is not always seen, it can be admitted in general. The fluctuation with year is irregular and has no common tendency, and so the fluctuation in the departure is not similar to every station.

Now, we will discuss the fluctuation in the departures with month by using the standard deviation (Table 4). Generally, the standard deviation is maximum in

Table 4. The standard deviation of the departure from the normal monthly sea level in each month (cm).

	Jan.	Feb.	Mar.	Apr.	May	June	July	Aug.	Sept.	Oct.	Nov.	Dec.
Aburatsu	4.7	4.0	4.2	2.4	4.1	4.5	5.0	8.6	7.6	7.6	7.0	7.3
Shimizu	6.0	4.0	2.9	3.3	5.6	4.8	5.4	6.6	8.8	7.3	6.8	5.2
Kochi	6.6	3.8	3.3	3.0	5.2	6.5	5.0	4.3	8.4	6.8	7.7	7.3
Kushimoto	6.3	3.9	3.1	2.8	4.6	5.7	6.8	6.4	9.4	8.9	7.4	6.2
Uragami	5.4	5.1	5.9	3.7	4.2	5.0	3.5	8.6	12.7	8.4	3.4	5.3
Toba	10.0	3.6	6.4	4.3	7.8	7.6	5.0	7.5	8.8	9.3	5.6	7.1
Maisaka	7.4	6.4	5.6	2.1	5.2	5.7	4.5	10.3	12.0	8.9	5.5	7.8
Uwajima	4.1	3.2	2.2	1.9	5.3	3.8	4.1	4.4	7.8	5.0	6.5	4.3
Shimotsu	7.5	4.3	4.2	2.3	3.0	4.6	5.7	4.4	6.1	9.0	8.1	6.7

September and is minimum in April. However, there are following exceptions: at Uragami the minimum occurs in November, and at Toba the maximum and minimum occur in January and February, respectively. Thus, the standard deviation is subject to annual variation whose phase is similar to the phase of the annual variation in the monthly sea level. At Uragami, the standard deviation is above 8 cm from August to October, while it is below 6 cm in other months. At Toba, the standard deviation oscillates conspicuously with short period. In such manner, the deviation from the sine curve is conspicuous at some stations. The general feature is interpreted as the effect of the meteorological conditions. For example, from summer to autumn, the standard deviation is great, because the intensity of the solar radiation and the amount of the precipitation fluctuate strikingly and so the density of the sea water fluctuates strikingly under their influence, too. Besides, the variation of the oceanic current may be a cause, but we can not conclude from the available materials when the variation of the oceanic current is most active. According to the analysis of variance (Table 2), we can find the significant difference among months in the variance of the deviation at the significance level of 1% at all stations.

It is accepted that the sea level is dependent upon the density of sea water. Since the precipitation is a factor which affects the density of sea water, it is expected that there is a close connection between the sea level and the amount of the precipitation. In Fig. 5, we give a relation between the deviation of the

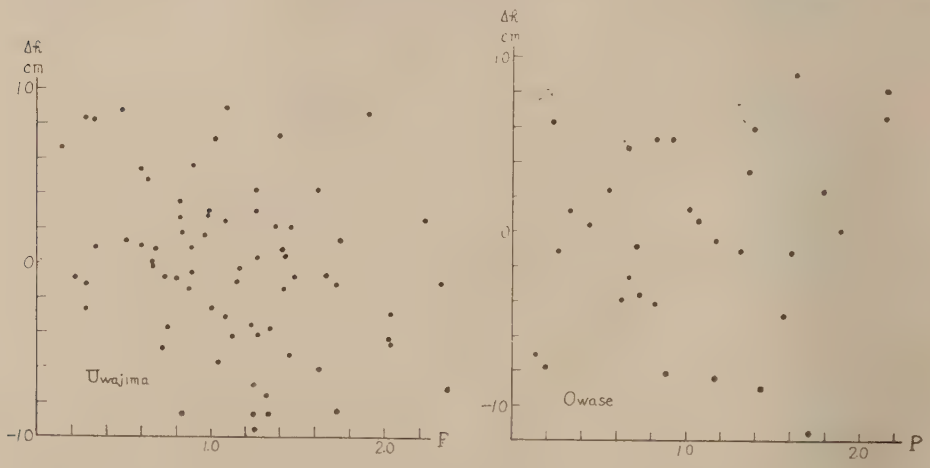

Fig. 5. The relation between the departure from the normal mothly sea level (Δh) and the percentage of the monthly precipitation to the normal (P).

monthly sea level from the normal value and the percentage of monthly precipitation to the normal value at Uwajima and Owase, where the influence of the precipitation upon the density of sea water is considered to predominate (the data are given in Geophysical Review published by J.M.A.). The scattering is striking and the

relation between them seems to be at random. As pointed out by Ichiye (1954), the density of sea water is under the influence of the precipitation in the manner proper to each station, for example, the time lag is not common. Accordingly, the precipitation at the end of the month exerts the sea level in the following month in some cases. The influence of the precipitation is restricted only in the surface layer and does not continue for a long time. By taking these into account, it can be considered to be natural that the monthly precipitation is not closely related with the deviation of the monthly sea level from the normal value. On the other hand, the surface water temperature seems to correlate with the sea level. Fig. 6 shows an example. The correlation coefficient is +0.623 for 36 samples (the significance point of 0.1% is 0.5259). In this case, the increase (decrease) of water temperature causes the decrease (increase) of density and so the rise (fall) of sea level. However, the surface water temperature fluctuates under the influence of many factors, one of which is the precipitation. Accordingly, we may consider that the precipitation influences implicitly the monthly sea level, but the role of the precipitation can not be quantitatively estimated.

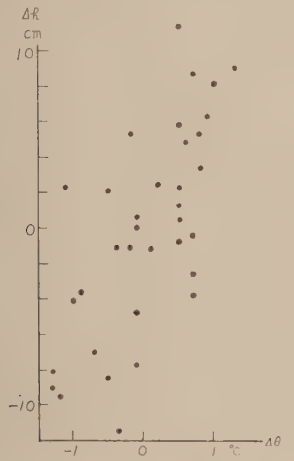

Fig. 6. The relation between the departure from the normal monthly sea level (Δh) and the departure from the normal monthly value of surface water temperature ($\Delta \theta$) at Owase.

The cause of the departure is expected to be common to the stations which are not distant. From this point of view, we calculate the correlation coefficient of the departure among various stations. Since the effect of the Kuroshio appears at Aburatsu and Kushimoto and the effect of the cold water region appears at Maisaka as noted in Section 3, we calculate the correlation coefficient between Shimizu and Kushimoto and between Kushimoto and Maisaka to see the influence of the Kuroshio and the cold water region. As Uwajima and Shimotsu are situated in the Bungo-suido and the Kii-suido, respectively, the influence due to the coastal water is predominant and the effect of the Kuroshio is diminished. Therefore, when we calculate the correlation coefficient between Uwajima and Shimizu and between Shimotsu and Kushimoto, we can see how the effect appears there. The results are shown in Table 5.

The coefficient fluctuates with year even in the same combination and the significance of the coefficient is not always found. On the other hand, the coefficient is significant in some combinations throughout the period and the appearance of the effect is in the common way. Especially, noticeable points are as follows:

Table 5. The correlation coefficient of the departure from the normal monthly sea level between stations.

	1951	1952	1953	1954	1955	1956	1951～1956
Aburatsu — Shimizu	0.023*	0.929	0.794	0.673*	0.843	0.447*	0.586
Shimizu — Kochi	0.981	0.871	0.962	0.859	0.970	0.922	0.934
Shimizu — Kushimoto	0.969	0.943	0.894	0.984	0.977	0.719	0.940
Kochi — Kushimoto	0.953	0.783	0.822	0.887	0.951	0.784	0.888
Kushimoto — Uragami	0.536*	−0.179*	0.671*	0.642*	0.773	0.650*	0.520
Kushimoto — Maisaka	0.638*	−0.177*	0.822	0.442*	0.669*	0.666*	0.443
Uragami — Toba	0.216*	0.918	0.981	0.942	0.856	0.741	0.689
Toba — Maisaka	0.579*	0.895	0.955	0.910	0.817	0.667*	0.781
Uwajima — Shimizu	0.901	0.942	0.895	0.975	0.977	0.838	0.918
Shimotsu — Kushimoto	0.847	0.932	0.769	0.810	0.947	0.767	0.880

The mark * indicates that the correlation coefficient is not significant at the level of 1%.

(1) the coefficient is great between Shimizu and Kochi and between Shimizu and Kushimoto;

(2) the coefficient is not great between Kushimoto and Uragami and between Kushimoto and Maisaka;

(3) the influence of the open-sea is not definitely modified at Uwajima and Shimotsu.

As we are based on the standpoint that the monthly sea level is dependent upon the oceanographic conditions near the station, it is deduced that the oceanographic conditions near the station are commonly influenced if the correlation coefficient in the departure of the monthly sea level is great. At Shimizu and Kushimoto, the departure fluctuates similarly according to the fluctuation of the Kuroshio and at Toba and Maisaka the departure is similarly dependent upon the fluctuation of the cold water region. At Kushimoto and Uragami, the effect of the Kuroshio and of the cold water region appear in the way varying with the oceanographic conditions, and the correlation is significant only when the cold water region develops and its effect influences the monthly sea level at both stations (for example in 1955). In a word, the Kuroshio affects the sea level at Aburatsu, Shimizu, Kochi and Kushimoto, and the effect of the cold water region in the Enshu-nada appears at Uragami, Toba and Maisaka. In the above expression, we consider the fluctuation of the cold water region to be independent of the fluctuation of the Kuroshio. However, it may be deduced that the influence of the Kuroshio appears indirectly where the cold water region affects the monthly sea level, because the fluctuation of the cold water region seems to be connected with the fluctuation of the Kuroshio.

6. The difference in the monthly sea level between the successive months

In this section, we will discuss the difference in the monthly sea level from the previous month. Here, the effect of the atmospheric pressure is eliminated as in other sections.

The frequency distribution of the difference is nearly symmetric as shown in Fig. 7. Therefore, we study the distribution by using the absolute value of the difference. The difference of the absolute value less than 4.9 cm and greater than 10 cm occurs at about 50% and at about 20%, respectively. Furthermore, the variation greater than 15 cm does not frequently occur (Table 6). At Uwajima and Shimotsu, the absolute value of the difference is generally less as compared with that at other stations. Hence, the monthly sea level varies more strikingly on the coast of the open-sea. The variation of the frequency with the season is not taken into account in the expression noted above, but the annual variation of the frequency is clearly found. Namely,

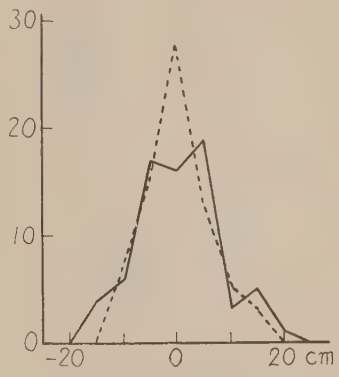

Fig. 7. The frequency distribution of the difference in the monthly sea level between the successive months (full line) and the departure from the normal difference (broken line) at Kushimoto. The frequency for 10 cm is that for the value between 7.5 cm and 12.5 cm, etc.

Table 6. The frequency (%) of the difference in the monthly sea level between the successive months and its departure from the normal difference.

	difference			departure		
	>10cm	<4.9cm	>15cm	>10cm	<4.9cm	>15cm
Aburatsu	21	53	3	7	57	0
Shimizu	12	58	4	6	67	1
Kochi	23	49	4	7	63	0
Kushimoto	17	51	6	10	66	1
Uragami	20	58	10	11	61	1
Toba	21	48	13	20	58	1
Maisaka	23	52	12	12	63	3
Uwajima	18	58	6	6	63	1
Shimotsu	14	52	2	8	65	0

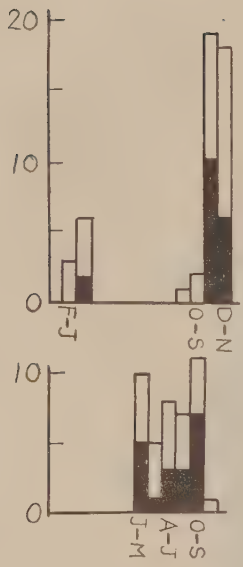

Fig. 8. The histogram of the difference in the monthly sea level between the successive months on the coast of the open-sea. The white bar represents the frequency of the difference above 10 cm, and the black bar represents the frequency of the difference above 15 cm. (upper: negative difference; lower: positive difference)

the difference greater than 10 cm does not occur in the period from February to May, while it occurs frequently from summer to autumn (Fig. 8), and the fall above 10 cm and the rise above 10 cm are most frequent in the period from October to December and from May to October, respectively. The result consists with one which is expected from the annual variation of water temperature and chlorinity and so density, because the variation of density is conspicuous in the period. The variation above 15 cm occurs rarely and the period of the occurrence is similar to that above 10 cm. The frequency is greater at Uragami, Toba and Maisaka. This will imply that the sea level in the Enshu-nada varies strikingly under the influence of the oceanographic conditions. The frequency of the variation above 10 cm and 15 cm are 1.3~2.5 times and 0.3~1.5 times a year on the average, respectively. Therefore, we can deduce that the remarkable difference does not occur in general when we compare the monthly sea level in the successive months.

Next, we will express the departure of the difference from the normal difference, which is the difference in the normal monthly sea level between the successive months. The frequency distribution of the departure is nearly symmetric (Fig. 7). The departure less than 4.9 cm and greater that 10 cm occur at the percentage greater than 50% and about 10%, respectively (Table 6). The frequency of the great departure is great east of Kushimoto in general, for example, the departure greater than 10 cm occurs at 20% at Toba and the departure greater than 15 cm occurs at 3% at Maisaka. Accordingly, the great departure tends to occur where the difference in the monthly sea level between successive months is great. As the departure is dependent upon the departure in the oceanographic conditions from their normal annual variation, the conspicuous departure in the oceanographic conditions does not occur in general. We illustrate the frequency of the departure greater than 10 cm in each month on the coast of the open-sea in Fig. 9. The great departure occurs in the period from September to October. Summarizing the results, we deduce that the departure does not frequently exceed 10 cm and that the departure in the oceanographic conditions from the normal annual variation is not conspicuous, that is, the departure in the oceanographic conditions from the normal conditions tends to

be conserved. At Uwajima and Shimotsu, the great departure is rarely found and the conspicuous departure in the oceanographic conditions does not frequently occur in the inland sea.

Pattullo et al. (1955) discussed the steric sea level. We will discuss the relation between the difference in the monthly sea level and the variation of specific volume after them. The variation of the sea level is written as follows:

$$\Delta z = 10 g^{-1} \int_{p_a}^{p_0} \Delta\alpha \, dp = 10 g^{-1} \int_{p_a}^{p_0} \Delta\delta \, dp,$$

where $\Delta\alpha$ and $\Delta\delta$ are the amount of the fluctuation in specific volume and specific volume anomaly, respectively, and p_a and p_0 are the atmospheric pressure and the pressure to which the integration has been carried. As pointed out in the previous paper (Moriyasu, 1958 a), the annual variation of water temperature and of chlorinity and so of density are restricted in the upper 100 m layer near the coast when the variation of the dynamic conditions (the movement of the current axis etc.) does not appear. Therefore, it is expected in this case that the annual variation of the normal monthly value is due to the variation of the specific volume in the upper 100 m layer. If we assume that the monthly sea level varies during a month by 10 cm and that $\Delta\alpha$ is independent of the depth, we have

$$\Delta\delta = 10^{-3},$$

which is equivalent to the variation of 1.00 in σ_t. The variation of 1.00 in σ_t is due to the variation of 3.5°C in water temperature (θ) for $Cl = 19‰$ or to the variation of 0.7‰ in chlorinity (Cl) for $\theta = 22.8$°C. Therefore, the variation of this magnitude in water temperature or chlorinity can cause the variation of the sea level. When the water temperature and the chlorinity fluctuates with the period of one year from 16.0°C to 28.0°C and from 19.2‰ to 18.8‰, respectively, σ_t and δ fluctuates from 25.53 to 21.64 and from 247×10^{-5} to 618×10^{-5}, respectively. If it is assumed that σ_t and δ fluctuate according to the sine curve with the period of one year, the sea level is given by

$$z = \int_{p_a}^{p_0} \alpha \, dp = \int_{p_a}^{p_0} (\alpha_{35,0,p} + \delta) \, dp = \int_{p_a}^{p_0} \alpha_{35,0,p} dp + [432.5 + 185.5 \cos(30° \times t - 60°)] \times 10^{-3},$$

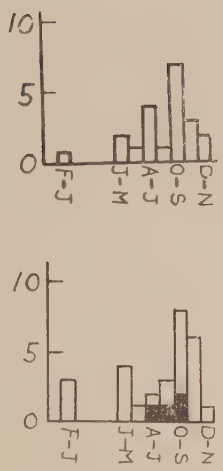

Fig. 9. The histogram of the departure of the difference in the monthly sea level from the normal difference on the coast of the open-sea. The white bar represents the frequency of the departure above 10 cm and the black bar represents the frequency of the departure above 15 cm. (upper: negative departure; lower: positive departure)

where the maximum of δ is assumed to appear in August and t is the month. The maximum amount of the variation in the sea level during a month is about 10 cm on the basis of the formula. Since this consideration is made on the assumption that the variation of δ is homogeneous in the layer, the variation is considerably overestimated in the lower part of the layer. However, it is natural that we find the amount of this magnitude in the variation of the monthly sea level as the normal variation. Accordingly, the variation above 10 cm during a month is scarcely expected if the dynamic conditions are nearly constant throughout the year. When the dynamic conditions vary or the abnormal variation of water temperature and of chlorinity appear under the influence of the meteorological conditions, the departure from the difference in the sea level between successive normal months occurs. This is usually below 10 cm as stated above and their effect does not make so great variation in the monthly sea level. Though the variation of short period is found in the oceanographic conditions, the influence is not conspicuous on the average when the variation of the scale of a month is the subject for discussion.

7. Summary

The results mentioned above are summarized as follows. Here, the effect of the atmospheric pressure is statically eliminated.

The monthly sea level at Aburatsu and Maisaka are closely connected with the dynamic height near the station and so with the oceanographic conditions. According to the results of the analysis of variance, the annual variation of the monthly sea level fluctuates from year to year on the coast of the open-sea and does not in the inland sea. The departure of the monthly sea level from the normal value is great on the coast of the Kumano-nada and the Enshu-nada where the oceanographic conditions fluctuate noticeably. The departure fluctuates according to the year and the month. The monthly sea level is not directly connected with the monthly amount of the preciptiation, but it is connected with the surface water temperature. The correlation of the departure implies that the monthly sea level west of Kushimoto depends upon the fluctuation of the Kuroshio and that the monthly sea level east of Kushimoto depends upon the oceanographic conditions in the Enshu-nada, that is, the fluctuation of the cold water region. The difference in the monthly sea level between the successive months is less than 10 cm in general and the remarkable variation in the monthly sea level does not occur during a month. And the departure from the normal difference is also less than 10 cm and the abnormal variation in the oceanographic conditions occurs rarely. The seasonal variation in the difference and in its departure are clear and can be considered to be connected with the oceanographic conditions. The difference between the successive normal monthly values is expected to be 10 cm at most. Taking account of these, we can conclude that the monthly sea level can be an indicator of the

fluctuation in the oceanographic conditions.

The author wishes to express his gratitude to Dr. K. Hishida for his revision.

References

(1) Ichiye, T. (1954): On the change of density of the coastal water due to the precipitation. *Oceanogr. Rep. C.M.O.*, Vol. 3, No. 3 (in Japanese).

(2) Kenney, J. F. (1939): *Mathematics of statistics.* D. Van Nostrand Company, New York.

(3) Moriysau, S. (1958 a): On the fluctuation of the Kuroshio south of Honshū (2). *Mem. Kobe Mar. Obs.*, Vol. 12, No. 2.

(4) Moriyasu, S. (1958 b): On the fluctuation of the Kuroshio south of Honshū (4). *Journ. Oceanogr. Soc. Japan*, Vol. 14, No. 4.

(5) Moriyasu, S. (1959): Supplementary note on the dynamical property of the cold water region. *Oceanogr. Mag.*, Vol. 11, No. 1.

(6) Pattullo, J., W. Munk, R. Revelle and E. Strong (1955): The seasonal oscillation in sea level. *Journ. Mar. Res.*, Vol. 14, No. 1.

On the Equatorial Upwelling

By

Koji Hidaka

Geophysical Institute, Faculty of Science, Tokyo University.

ABSTRACT

A finite expression for upwelling valid at and only at the equator is worked out, assuming a balance between pressure gradients, Coriolis forces and vertical mixing. It enables us to estimate the amount of equatorial upwelling in terms of density distribution and the wind stresses both computed from observations.

1. In recent years, a number of theories has been published on the upwelling, or the steady vertical motion of sea water. (Hidaka 1955, Stommel 1956). However, most of the expressions for computing the upwelling given by these theories are not valid at the equator, because they have the sines of latitude in the denominators. In the present paper, the author is going to give an expression for computing the upwelling at the equator from distribution of density and wind stress, both obtainable from observations. In establishing the theory, only a balance between pressure gradients, Coriolis forces and vertical mixing was assumed. Effects of field accelerations and horizontal mixing will be neglected.

2. We start with the hydrodynamical equations:

$$\left.\begin{aligned} \mu\frac{\partial^2 u}{\partial z^2}+2\omega\rho\sin\phi v&=-\frac{\partial p}{\partial x}\,;\\ \mu\frac{\partial^2 v}{\partial z^2}-2\omega\rho\sin\phi u&=\frac{\partial p}{\partial y}\,. \end{aligned}\right\} \tag{1}$$

In these expressions, we take x-, y- and z- axis positive eastwards, northwards and downwards respectively; u and v are the components of current velocity parallel to x- and y- axis, μ the coefficient of vertical mixing supposed constant, p the pressure, ρ the density of sea water, both function of x, y and z, ω the angular velocity of the earth and ϕ the geographical latitude.

In addition to (1) we need the surface condition:

$$z=0\ :\ -\mu\frac{\partial u}{\partial z}=\tau_x\ ;\ -\mu\frac{\partial v}{\partial z}=\tau_y \tag{2}$$

where τ_x and τ_y are the components of wind stress, being generally functions of x and y, and the bottom conditions:

$$z=h\ :\ \frac{\partial u}{\partial z}=\frac{\partial v}{\partial z}=0 \tag{3}$$

where $z=h$ represents the sea bottom, supposed horizontal.

Two equations in (1) lead to

$$\mu\frac{\partial^2}{\partial z^2}\left\{\frac{\partial}{\partial z}(u+iv)\right\}-i\cdot 2\omega\rho\sin\phi\left\{\frac{\partial}{\partial z}(u+iv)\right\}=g\left(\frac{\partial\rho}{\partial x}+i\frac{\partial\rho}{\partial y}\right), \tag{4}$$

where the space variation of ρ is neglected against those of u and v.

Further, by an operation $\frac{\partial}{\partial x}-i\frac{\partial}{\partial y}$, and taking into account that $\frac{\partial}{\partial y}=\frac{1}{R}\frac{\partial}{\partial\phi}$ where R is the radius of the earth, we have from (4)

$$\left(\mu\frac{\partial^2}{\partial z^2}-i\cdot 2\omega\rho\sin\phi\right)\cdot\left\{\frac{\partial}{\partial z}\left(\frac{\partial u}{\partial x}+\frac{\partial v}{\partial y}\right)+i\frac{\partial}{\partial z}\left(\frac{\partial v}{\partial x}-\frac{\partial u}{\partial y}\right)\right\}$$
$$-\frac{2\omega\rho}{R}\cos\phi\cdot\frac{\partial}{\partial z}(u+iv)=g\left(\frac{\partial^2\rho}{\partial x^2}+\frac{\partial^2\rho}{\partial y^2}\right). \tag{5}$$

3. Putting $\phi=0$ or $\sin\phi=0$, $\cos\phi=1$ in (4) and (5), and taking real parts only, we have at the equator

$$\frac{\partial^2}{\partial z^2}\left(\mu\frac{\partial u}{\partial z}\right)=g\frac{\partial\rho}{\partial x} \tag{6}$$

and

$$\frac{\partial^2}{\partial z^2}\left\{\mu\frac{\partial}{\partial z}\left(\frac{\partial u}{\partial x}+\frac{\partial v}{\partial y}\right)\right\}=\frac{2\omega\rho}{R}\cdot\frac{\partial u}{\partial z}+g\left(\frac{\partial^2\rho}{\partial x^2}+\frac{\partial^2\rho}{\partial y^2}\right) \tag{7}$$

respectively.

Integrating (6) subject to the conditions (2) and (3), we have

$$\frac{\partial u}{\partial z}=-\frac{\tau_x}{\mu}\cdot\frac{h-z}{h}-\frac{g}{\mu}\int_0^h\frac{\partial\rho}{\partial x}K(z,s)ds \tag{8}$$

where z in ρ is replaced by s, and $K(z,s)$ is a symmetric kernel of the type:

$$\left.\begin{aligned}K(z,s)&=\frac{(h-z)s}{h}\qquad(s<z)\\&=\frac{z(h-s)}{h}\qquad(s>z)\end{aligned}\right\} \tag{9}$$

Substitution of (8) in (7) gives

$$\frac{\partial^2}{\partial z^2}\left\{\mu\frac{\partial}{\partial z}\left(\frac{\partial u}{\partial x}+\frac{\partial v}{\partial y}\right)\right\}$$
$$=-\frac{2\omega\rho}{\mu Rh}\cdot\tau_x\cdot(h-z)-\frac{g}{\mu}\int_0^h\frac{\partial\rho}{\partial x}K(z,s)ds+g\left(\frac{\partial^2\rho}{\partial x^2}+\frac{\partial^2\rho}{\partial y^2}\right). \tag{10}$$

Since

$$\mu\frac{\partial}{\partial z}\left(\frac{\partial u}{\partial x}+\frac{\partial v}{\partial y}\right)=\frac{\partial}{\partial x}\left(\mu\frac{\partial u}{\partial z}\right)+\frac{\partial}{\partial y}\left(\mu\frac{\partial v}{\partial y}\right)$$

we have, after substitution from (2), two following boundary conditions:

$$z=0:\ \mu\frac{\partial}{\partial z}\left(\frac{\partial u}{\partial x}+\frac{\partial v}{\partial y}\right)=-\left(\frac{\partial\tau_x}{\partial x}+\frac{\partial\tau_y}{\partial y}\right) \tag{11}$$

$$z=h:\ \mu\frac{\partial}{\partial z}\left(\frac{\partial u}{\partial x}+\frac{\partial v}{\partial y}\right)=0 \tag{12}$$

then the solution of (10) becomes

$$\mu\frac{\partial}{\partial z}\left(\frac{\partial u}{\partial x}+\frac{\partial v}{\partial y}\right)=-\left(\frac{\partial\tau_x}{\partial x}+\frac{\partial\tau_y}{\partial y}\right)\cdot\frac{h-z}{h}+\frac{2\omega\rho}{\mu R}\cdot\tau_x\int_0^h\frac{(h-s)}{h}K(z,s)ds$$
$$+g\int_0^h\left(\frac{\partial^2\rho}{\partial x^2}+\frac{\partial^2\rho}{\partial y^2}\right)K(z,s)ds-\frac{2\omega\rho g}{\mu R}\int_0^h\frac{\partial\rho}{\partial x}K^{(2)}(z,s)ds \tag{13}$$

where $K(z,s)$ is the same as that given by (9) and

$$K^{(2)}(z,s)=\int_0^h K(z,\sigma)\ K(\sigma,s)d\sigma \tag{14}$$

4. If we neglect the space variation of density compared with those of velocity components, we have from the equation of continuity

$$\frac{\partial u}{\partial x}+\frac{\partial v}{\partial y}=-\frac{\partial w}{\partial z} \tag{15}$$

where w is the vertical velocity components counted downwards positive. Substituting (15) in (13), we have

$$\mu\frac{\partial^2 w}{\partial z^2}=\left(\frac{\partial \tau_x}{\partial x}+\frac{\partial \tau_y}{\partial y}\right)\frac{h-z}{h}-\frac{2\omega\rho}{\mu R}\tau_x\cdot\frac{z(h-z)(2h-z)}{6}$$
$$+g\int_0^h\left(\frac{\partial^2\rho}{\partial x^2}+\frac{\partial^2\rho}{\partial y^2}\right)_s K(z,s)ds-\frac{2\omega\rho g}{\mu R}\int_0^h\frac{\partial\rho}{\partial x}K^{(2)}(z,s)ds \tag{16}$$

Integrating this equation subject to the conditions:

$$w=0 \quad \text{for} \quad z=0 \quad \text{and} \quad z=h, \tag{17}$$

and again disregarding the space variation of ρ, we have

$$w=-\frac{1}{\mu}\left(\frac{\partial\tau_x}{\partial x}+\frac{\partial\tau_y}{\partial y}\right)\cdot\frac{z(h-z)\ (2h-z)}{6h}$$
$$+\frac{2\omega\rho}{6\mu^2Rh}\cdot\tau_x\cdot\left(\frac{2}{15}h^3+\frac{2}{15}h^2z-\frac{1}{5}hz^2+\frac{1}{20}z^3\right)\cdot z(h-z)$$
$$-\frac{g}{\mu}\int_0^h\left(\frac{\partial^2\rho}{\partial x^2}+\frac{\partial^2\rho}{\partial y^2}\right)_s K^{(2)}(z,s)ds+\frac{2\omega\rho g}{\mu^2R}\int_0^h\frac{\partial\rho}{\partial x}K^{(3)}(z,s)ds \tag{18}$$

where

$$K^{(3)}(z,s)=\int_0^h K^{(2)}(z,\sigma)K(\sigma,s)d\sigma \tag{19}$$

5. The equation (18) is the expression for computing the equatorial upwelling. Of course, it is valid at the equator only. The vertical velocity w is counted positive downwards. Two last terms on the left-hand member represent the contribution correlated with density distribution, while the two first ones give the upwelling produced by the stress of winds sweeping the sea surface.

We see that convergence of wind stresses and westward wind are correlated with upwelling or negative value of w. Although both of the functions $(2h-z)\,z\,(h-z)$ and $\left(\frac{2}{15}h^3+\frac{2}{15}h^2z-\frac{1}{5}hz^2+\frac{1}{20}z^3\right)\cdot z(h-z)$ vanish at $z=0$ and $z=h$ only and nowhere in between, the joint effect of the two wind terms working together may be able to result in some depth or depths where there is no vertical motion. Further discussion and explanation of this expression will be left for later study.

References

(1) Hidaka, Koji (1954): A contribution to the theory of upwelling and coastal currents. *Amer. Geophys. Union Trans.*, Vol. 35, 431-444.

(2) Stommel, Henry (1956): On the determination of the depth of no meridional motion. *Deep-Sea Res.*, Vol. 3, 273-278.

The Cold Water-Mass off the South Coast of Central Japan (Part I)

(On a Phenomenological Research on the Oceanographical States)

By

Yukimasa Saito

Osaka City University

1. Introduction

It has long been known that off the south coast of central Japan, a large cold water-mass sometimes appears and causes a large deformation in the course of the Kuroshio. The oceanographical studies on this phenomena have already been made by many authors and it is understood that this cold water-mass is formed by a large-scale upwelling of the subpolar intermediate water.

In the region bounded by latitude 29°N, longitude 140°E and the Japanese Islands, seasonal observations have been carried on since April 1956 on the surveying ship "Shumpu-Maru" of Kobe Marine Observatory and much data have been obtained.

In this paper, making use of these data, the water masses in this region were re-examined with the aid of T-S diagrams; and then their distribution and the ocean structure were determined. The movements of the water were also inferred from the relation between each water-mass and the distribution of densities.

Lastly, it was also attempted to explain the mechanism of the upwelling on the basis of the obtained results.

2. The structure of the upper layer

In the previous paper[1] it has already been shown that the mixing state of water-masses in most parts of the ocean, excepting the region adjacent to the Polar front, is usually determined by transversal mixing alone; and the mixing going on stationary between two different water-masses in layer or in juxtaposition moving parallel to each other with different velocities can be shown on the T-S diagrams by a straight line that connects two points corresponding to the temperatures and the salinities of both water-masses. The straight line is called the "Mixing line" for convenience's sake. We have also known that, according to a similar consideration, the mixing state of three or more water-masses flowing parallel to each other is represented by a curve which is in contact with two or more mixing lines forming a zigzag shape. These are the fundamental concepts of the water mass analysis.

As ocean waters flow mainly along the nearly horizontal isentropic surfaces, to distinguish between the different waters, it is convenient to use two kinds of T-S diagram; that is, one derived from the vertical distribution of temperatures and salinities at any station and representing the mixing state of several strata, and another obtained from their horizontal distribution in a plane of any depth and showing the mixing state of water-masses in juxtaposition. To simplify we shall call them the T-S diagram of the lst type and that of the 2nd type.

In a region far from the Polar front where the water flows mainly along the isentropic surfaces, the T-S diagrams of the 2nd type always coincide with any part of the synthesized T-S diagram of the lst type; this fact is particularly true in the intermediate water. In the subtropical region of the Pacific the T-S diagrams of both types are usually shaped like an inverted S, and broken or zigzag parts can hardly be seen on the T-S curves. This is seen in Figs. 1 (a) and (b)

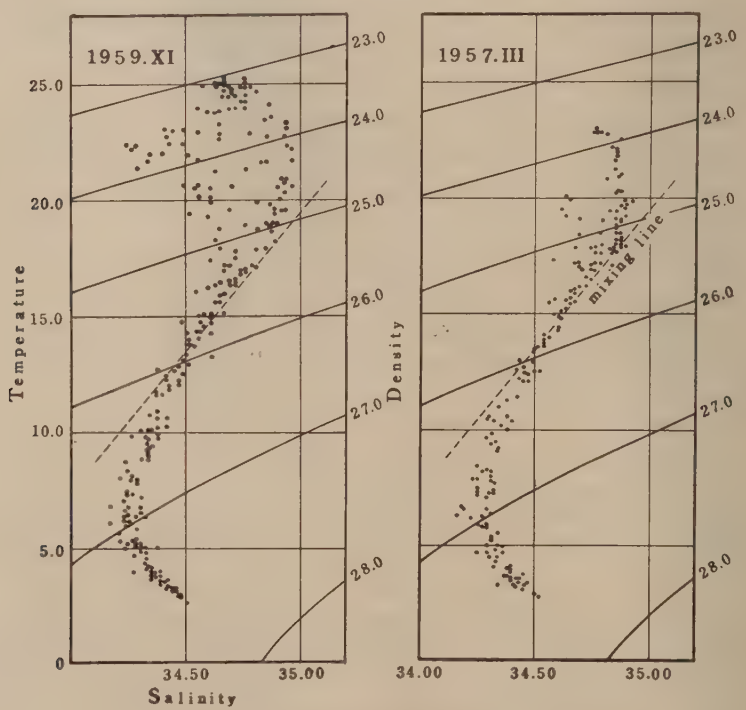

Fig. 1. The Synthesized T-S relation of the lst type.

which are respectively the synthesized T-S diagrams of the lst type of the region under consideration in early spring and autumn. Fig. 2 shows the T-S diagram of the 2nd type upon the surface of the 50m depth in this region, and it has been found to have a strong resemblance to the patterns shown in Fig. 1. But in such

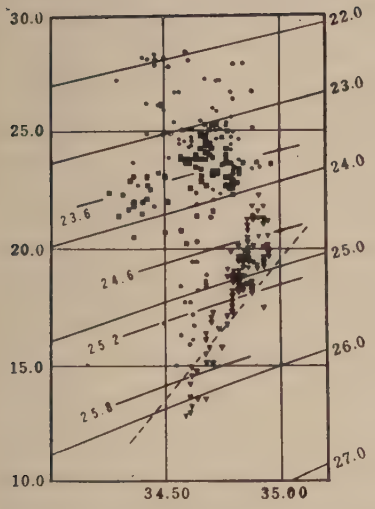

Fig. 2. The Synthesized T-S relation of the 2nd type obtained at the surface of 50m depth.
▼ March. ● August. ■ November.

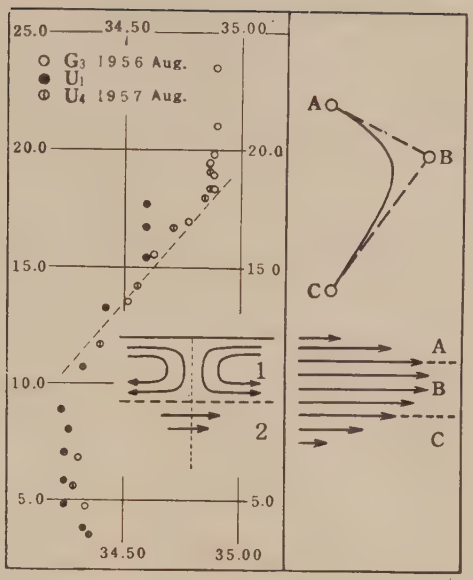

Fig. 3. T-S diagrams (lst type) at the selected stations showing the breaking point (left) and the usual T-S diagram (right), and the mechanisms of mixing. (Stations are shown in Fig. 5)

a case when, by a vertical flow like a convection, the water of the top-most layer invades the lower waters while mixing with the surrounding waters, there may occur a breaking point on the T-S curves as shown schematically in Fig. 3. The breaking point in the lst type should correspond to the lower limit of the layer where the vertical flow occurs, and that which is in the 2nd type should correspond to the boundary of the vertical flow region. Several T-S diagrams of the 2nd type obtained in the region under consideration are shown in Fig. 4. In this case we excluded the data from the top-most layer of 50m thickness which is greatly influenced by the atmosphere. It will be found that the T-S diagrams of the 2nd type in the upper layer are triangles. This is particularly true in the cold season when the layer of the upper water becomes thinnest. The temperatures and salinities of the vertexes of the triangles in early spring and autumn are as follows,

A(T=18.3°C, S=34.70‰) B(T=14.6°C, S=34.38‰) C(T=18.3°C, S=34.70‰)
in early spring
A(T=25.0°C, S=34.50‰) B(T=14.6°C, S=34.38‰) C(T=18.3°C, S=34.70‰)
in autumn

where A represents a vertex and BC the base; BC is on the mixing line between the subpolar intermediate water and the southern upper water.

For trial, if the water belonging to these two sides AB and AC is divided by the median through A, and the water lighter than the density σ_t =23.6 is defined

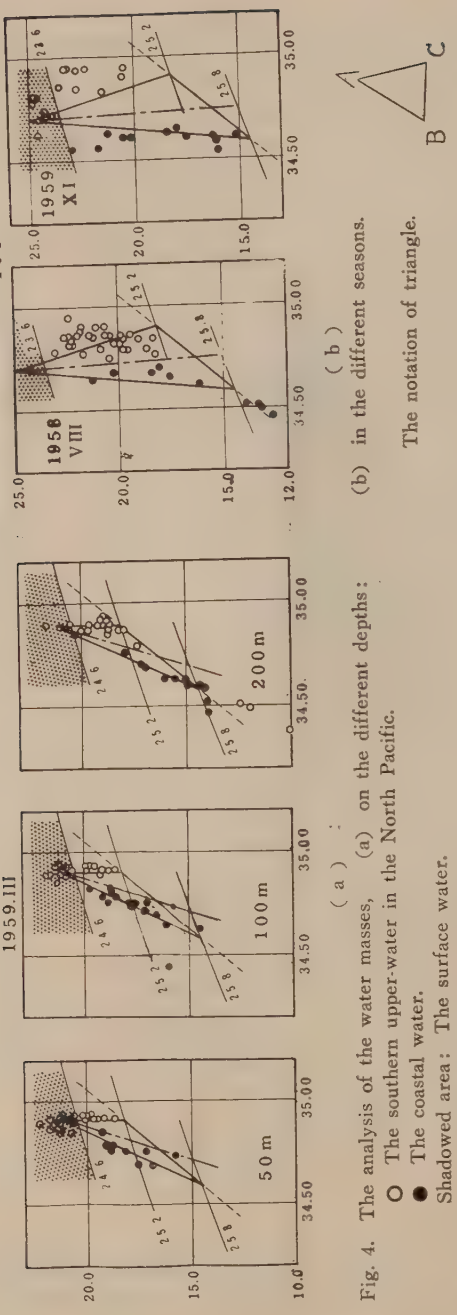

Fig. 4. The analysis of the water masses, (a) on the different depths; (b) in the different seasons.
○ The southern upper-water in the North Pacific.
● The coastal water.
Shadowed area: The surface water.
The notation of triangle.

as "surface water" we can divide the water into different kinds of water-masses within horizontal planes and vertical cross-sections. Two of the figures obtained by these procedures are shown in Fig. 5. Both of them have been obtained at the surface of the 100m depth. Since it is found from these figures that the stations which belong to the two sides AB and AC of the triangles are separated completely by the surface water, AB and AC should be considered as the mixing lines between the less dense surface water A and the denser B and C which represent the waters corresponding to the different stages of mixing in the subpolar intermediate water respectively. From Figs. 4 (a), we may understand that the vertical flow is the descending current, and that the lowest limit where the surface water can reach is around 200m in depth. This is also ensured by the distribution of densities in a vertical section taken across the descending current region or convergence shown in Fig. 8; that is, the marked depression of isopycnal $\sigma_t = 25.00$ which should have been brought about by the decending of the less dense water occurs at the boundary between the two masses AB and AC. The half of the belt of the converged surface water at the side of the coastal water (AB mass) is found to be the Kuroshio and that its maximum velocity appears along its edge.

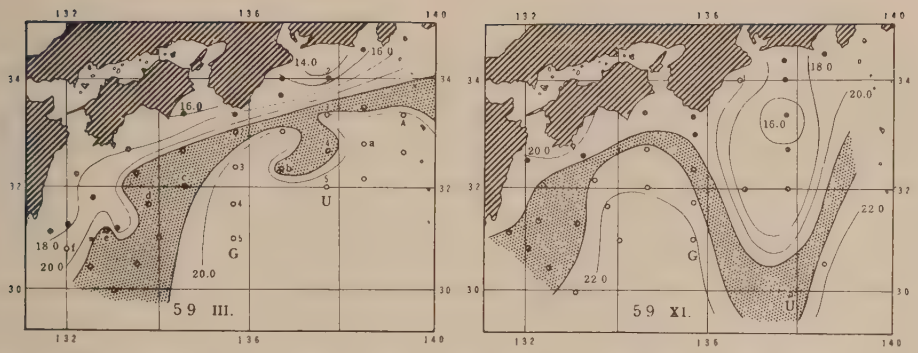

Fig. 5. The distributions of water-masses on the surface of 100m depth by the use of Fig. 4.
○ The southern upper-water in the North Pacific.
● The coastal water.
Shadowed area: The surface water.

3. The state of the deeper part of the ocean and the interpretation of the upwelling of a cold water mass.

Up to now our consideration has been limited mainly to the upper part of the ocean. Next we shall study the state of the deeper part of the ocean. The depth of the core of the subpolar intermediate water which corresponds to the layer of the lowest salinity and the isopycnal of 27.00 may be a good clue for this purpose. The figure showing the depth of the core in this region is Fig. 6. It will be seen from this figure that the depth of the core is shallowest along the land and rapidly becomes deeper on the outside. This narrow shallowest zone may correspond to that of the coastal water. The subpolar intermediate water which goes down under the southern upper water from the Polar front mainly at the west end where it protrudes in the shape of a tongue flows with a considerable velocity through a narrow zone along the Japanese coast which may correspond to the shallowest zone of the core shown in Fig. 6.

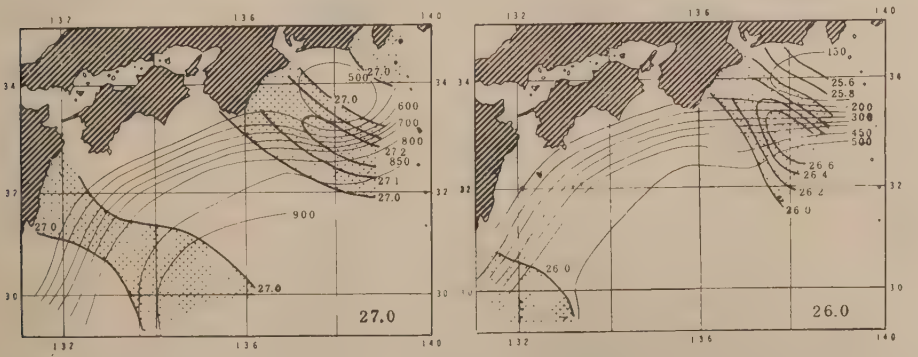

Fig. 6. The distributions of densities in Nov. 1957 on each of the topographic surfaces corresponding to the isopycnic surfaces $\sigma_t = 27.00$ and $\sigma_t = 26.00$ in Aug. 1957.
Thin lines: Topographies of each of the isopycnic surfaces (unit: meter).
Shadowed zone: Upwelling regions.

Selecting any two successive seasons and studying the distribution of densities in the latter season on the surface corresponding to any specified isopycnic surface of the former season, we can determine the regions where the water had upwelled during the two seasons; because in such regions the densities should become larger than the index value of the specified isopycnic surface. The two examples are shown in Fig. 6 where the selected two successive seasons are the summer and autumn of 1957, and the index value of the specified isopycnic surfaces of the former season are 27.00 and 26.00 respectively. A marked upwelling area appears in the north-eastern part of this region and the other parts of this region correspond to a weak descending area. There seems also to be a weak upwelling area in the south-western part.

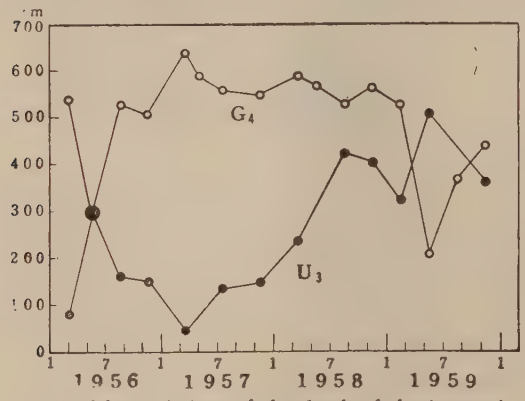

Fig. 7. The variations of the depth of the isopycnic surface $\sigma t = 26.00$ at two stations G and U (cf. Fig. 5).

The variations of the depth of the isopycnal of 26.00 from April 1956 to November 1959 at stations G_4, and U_3 which may be considered to be in the main upwelling and the descending area respectively, are shown in Fig. 7. From this it will be seen that these variations show a negative correlation.

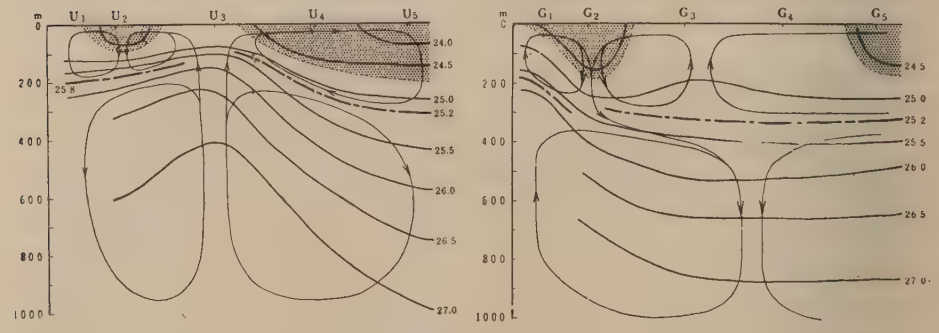

Fig. 8. The distributions of densities in the two cross-sections along the lines G and U (cf. Fig. 5). (March. 1959.)
Shadowed areas: Surface water.
—— - —— - : Boundaries between the intermediate waters and the upper waters which correspond to $\sigma t = 25.2$ and $\sigma t = 25.80$ in the water masses AC and AB respectively.

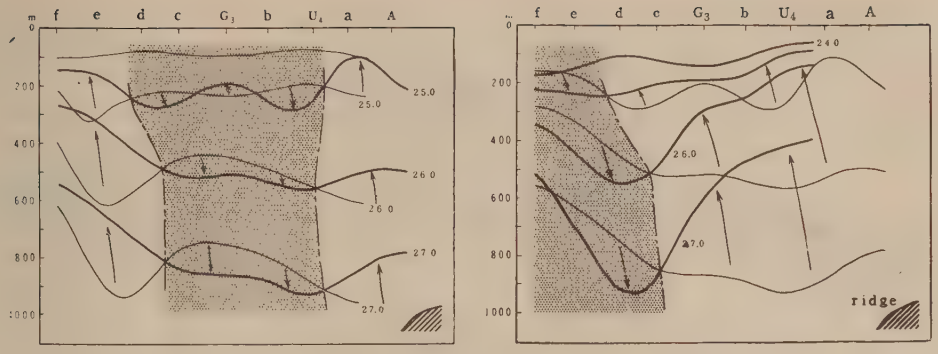

Fig. 9. The changes of the distributions of densities in the cross-section through Sts. A~f (cf. Fig. 5).
(a) Thin lines: Aug. 1958.
Thick lines: Feb. 1959.
(b) Thin lines: Feb. 1959.
Thick lines: Nov. 1959.
Shadowed zones: The descending current regions during the successive seasons.

The distributions of densities in the two cross-sections along the lines G and U (cf. Fig. 5) shown in Fig. 8, and Fig. 9 shows, in a cross-section parallel to the land, the changes of the distribution of densities during each of the three successive seasons. According to Figs. 7 and 9 the upwelling and descending regions seem to turn their position by the season. It will be seen clearly from Fig. 9 that the axes of upwelling is tilting upwards to the west from the plateau of the Zunan ridge shown in Fig. 10.

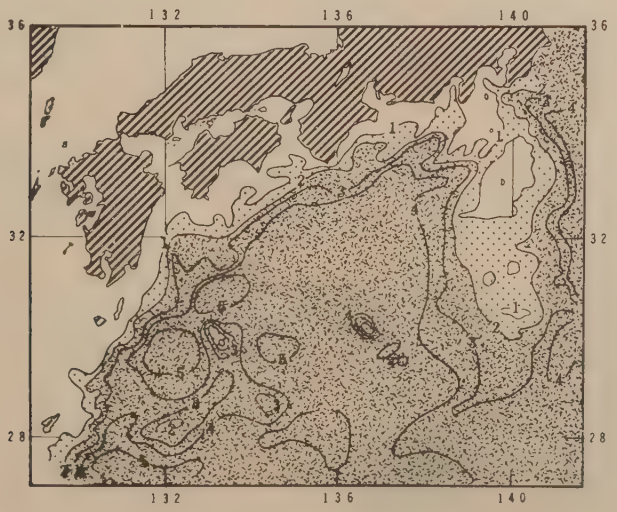

Fig. 10. The topographic map.

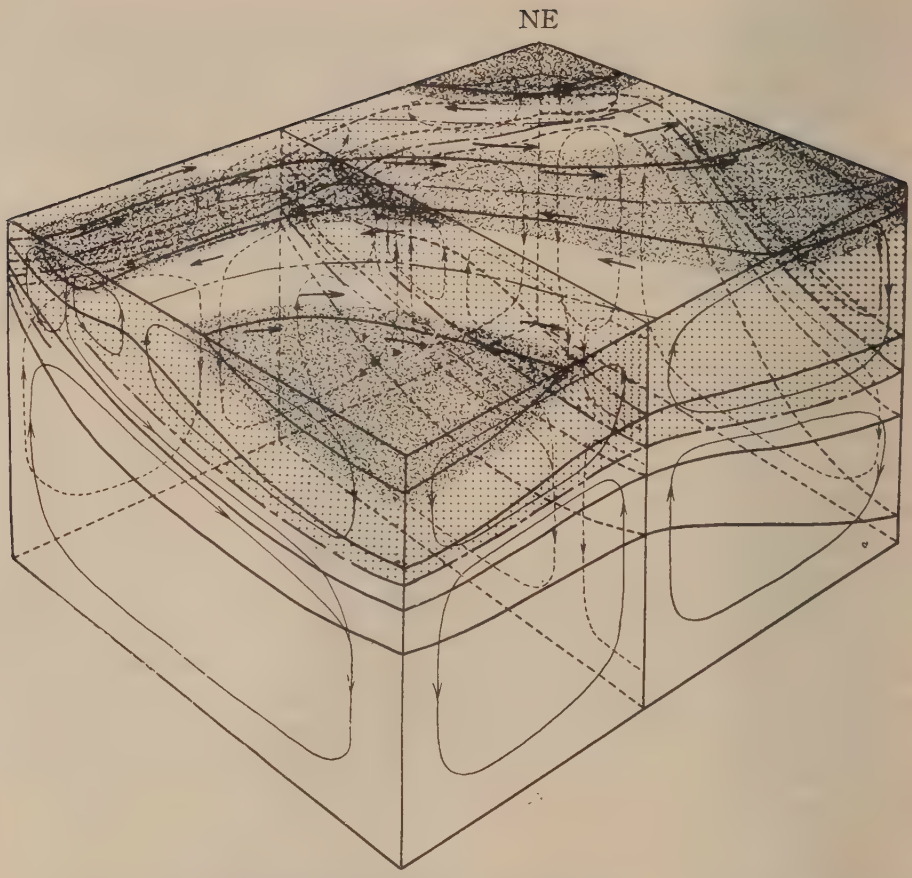

Fig. 11. Schematic structure of the ocean in the region under consideration. (Inferred vertical circulations are shown.)

Putting all of these results together, the upwelling and descending current in this region may be considered to have some relation with the Zunan ridge and may be explained by a theory analogous to that of the mountain lee waves in meteorology.

Whether the cold water mass is limited to the coast or spreads out far to the south according to the year may depend on the width of the flow of the subpolar intermediate water. The prosperity and decline of the cold water may also depend on the stability of the water.

Because the main upwelling areas are bounded by the land and the velocity of ascending current may be larger than that of the descending current, the upwelling may be compensated mainly by a narrow zone of convergence along the boundaries of the upwelling regions on the surface. As we have already seen, the descending

current at the convergence forms small vertical circulations together with the diffused ascending currents of compensation on both sides of it. Therefore, even in the descending area, a slow ascending current comes about in the upper thin layer. This can be seen in Fig. 8. In this figure we can see that, in the intermediate water, the isopycnals descend on the whole, but in the upper water they ascend locally just as that of 25.00.

Fig. 11 showing the schematic structure of the ocean in this region is obtained by summarizing the results obtained above.

Reference

(1) Saito, Yukimasa (1952): On the Oyashio Current (Part I). *Journal of the Institute of Polytechnics*, Osaka City University, Series B, Vol. 3, No. 2.

On the Subsidence of Ground Level at Amagasaki Region, especially with the Relation to the Tidal Level

By

Kozo Hishida

Kobe Marine Observatory

1. Introduction

The subsidence of ground level at Amagasaki Region, Hyogo Prefecture in the innermost part of Osaka Bay has been studied for many years by the agencies concerned and also some investigators.[(1)-(4)] In this report, we intend to attack this problem at Amagasaki, with the relation of the tidal level to the subsidence. The level survey and the observation by the subsidence meter has been hitherto carried out, but the relation to the tidal level has not yet been studied, because it was only a few years ago when the accurate tidal observation enough to discuss this problem was to be conducted. Thus, after showing a brief outline of the results by the level survey and the subsidence meter, the tidal effect on the subsidence will be pointed out here.

2. Outline of the subsidence

The subsidence of ground level has been recognized for a long time in this region. But the study was left until about 30 years ago, when the municipal authorities of Amagasaki conducted firstly the level survey to consider a counterplan to keep out of its menace. The precise level survey has been continued once every year at several tens selected stations over the whole city. The results are summarized as shown in Fig. 1, where we see the mean values of the subsidence, their changes with year and so forth. At first, the yearly means during 1932—1953 may be found several centimeters, smaller in the northern part and larger in the coastal region as in Fig. 1 (1). Since the ground level is generally low as shown in Fig. 1 (5), its subsidence has the serious influence upon the various industrial fields in this region, where many equipments are being operated in many factories. The subsidence, however, has not occurred with an uniform speed during this period. The amount of subsidence exceeded 10cm during 1939—1941, as shown in Fig. 1 (2), while decreased during 1943~1948, when the disaster of the World War fell the industry into decay as shown in Fig. 1 (3) and the ground level subsided only in the extremes of 5cm even in the coastal region, and it was rather elevated elsewhere (as denoted by the negative values).

In the recent five years (1953~1958), the phenomena of the subsidence was

(1) 1932 ~ 1933
(Mean)
(2) 1939 ~ 1941
(Mean)
(3) 1943 ~ 1948
(Mean)
(4) 1949 ~ 1958
(Mean)
(5) Contour
(6) 1953 ~ 1954

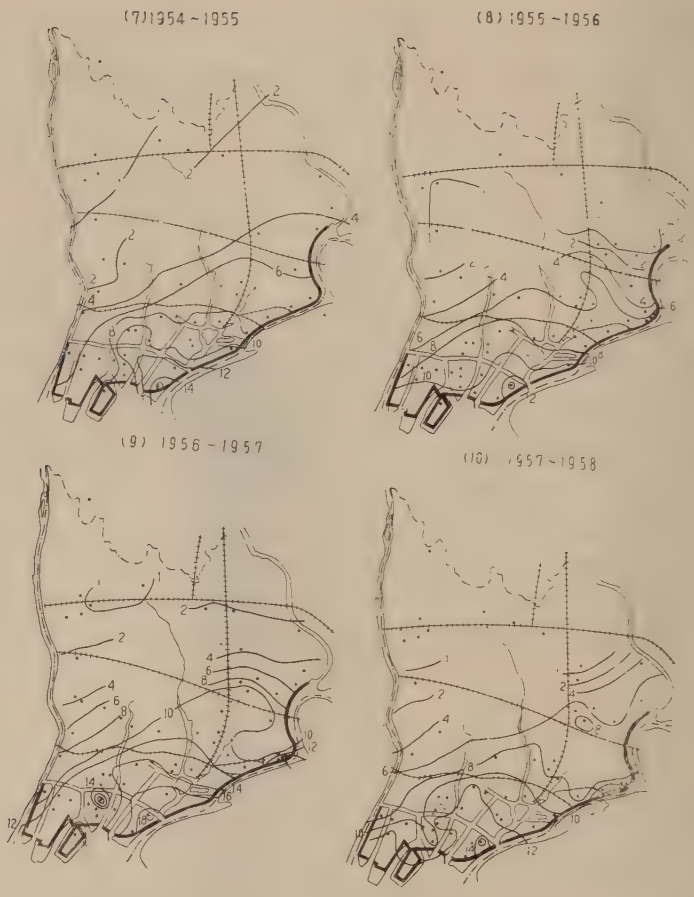

Fig. 1. The amount of subsidence by the leveling survey conducted every year.

again stood out conspicuous as shown in Fig. 1 (4), where we see that the yearly mean values exceed 10cm at many stations in the coastal zone with the maximum of 14cm at Osaka Soda Company. In Fig. 1 (6)—(10), the values are shown in every year during these five years for the sake of the precise knowledge about their changes with year. The accumulated values of subsidence during the same period are also represented in graphic form (Fig. 2) for some observed stations, which seem to be classified in a few groups due to the features of curves, though they differ from each other in every station.

According to the results from the subsidence meter at two stations Higashihama and Nishikaigan (hereafter to be abbreviated as "H" and "N" station respectively) shown by A and B in Fig. 1 (5) respectively, the total amounts of subsidence in every month are plotted since the beginning of the observation in Fig. 3 and

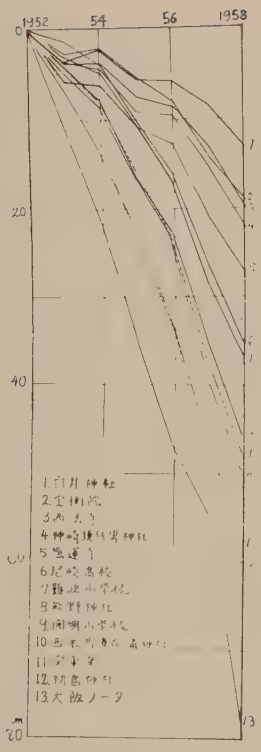

Fig. 2. The change of the amount of subsidence at several stations.

the means of those values are also tabulated during these recent six years in the following.

In order to find the change of ground level with time in detals, we must be led to this subsidence meter which is self-recorded, since the level survey is only to be carried out once a year. Due to the structure of this instrument, however, it serves only to determine the amount of subsidence at surface layer, relative to a certain depth, which is taken 182m at the station "H" and 57m at "N" in these subsidence meters respectively.

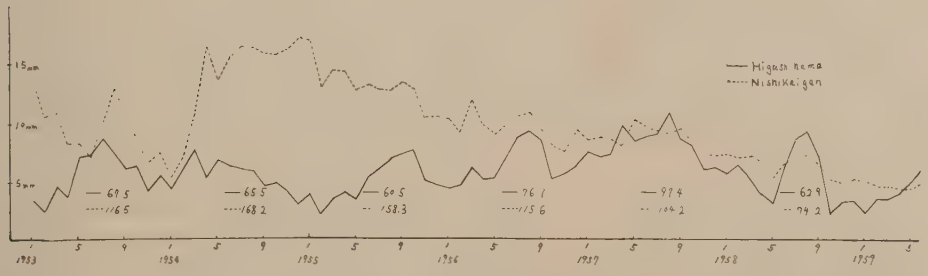

Fig. 3. The monthly amount of subsidence by the subsidence meter. (Numbers indicate the yearly amout)

	1	2	3	4	5	6	7	8	9	10	11	12	mean
Nishikaigan	10.4	9.3	10.7	10.6	9.9	10.3	11.0	11.6	11.0	9.8	8.8	9.5	10.2
Higashihama	4.8	4.8	5.7	5.3	5.7	6.8	7.9	8.3	7.1	5.7	4.7	4.8	6.0

3. The mean tidal level

Tidal observations have been conducted by authorities of Hyogo prefecture for a long time, but it was only a few years ago that the data from this tidal station, the position of which is designated at C in Fig. 1 (5), have been available for the guide to a knowledge of rise and fall in ground level. Then, the monthly mean tidal level may be shown only during recent three years as in Fig. 4 where those at Kobe are plotted at the same interval of time for reference. However, we may consider it preferable to represent the deviation of these monthly tidal levels from their means over during three years in order to get rid of the annual variation of tidal level, as shown by the full line in this figure. Though the values of deviation fluctuate randomly at both stations, they show an upward tendency, and then the increasing speed may be evaluated as 14.8 cm/year at Amagasaki, which is far larger than that of 2.8 cm/year at Kobe. Then, the main part of the rise in tidal level at Amagasaki may be considered as the result of the subsidence of ground level.

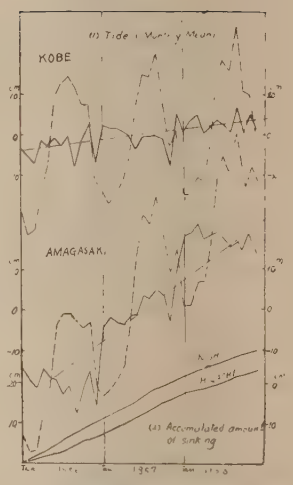

Fig. 4. The monthly mean tidal level and the accumulated amount of subsidence.

For the comparison of the result by the subsidence meter measurement, the accumulated amounts of subsidence are plotted in this figure at the same time. Though these curves tend to rise without a constant speed, the mean speed may be taken as 7.9 cm/year at the station "H" and 9.8 cm/year at "N" and so the magnitudes of the subsiding speed are in a good accordance among by the tidal observation, by the subsidence meter measurement, and by the level survey stated above. The further discussion seems to be limited in the validity, since the mean rise of tidal level is computed to have a range of 12—17 cm/year within the confidence limit of 5%.

For reference, however, it is still preferable to enter into the differences between them in a certain extent. The tidal station itself is found to be settling with the embankment in which it was installed with the speed of about 4 cm/year from the level survey recently conducted, and so the rise of tidal levels may be considered 14.8−4.0=10.8 cm/year at Amagasaki. On the other hand, the deeper pipe of the subsidence meter, which is taken as the standard of relative rise or fall at the surface layer of the ground, is found to sink by 11.4cm at the station "H" during the same interval of three years by the level survey. And then, we may consider that the speed of subsidence is 7.9+11.4/3=11.7 cm/year and this value equals nearly to the value of rise in tidal level mentioned above, and also to the value

of 10.7 cm/year which is obtained at the neighbouring level station "Kansai Electric Power Co" by the level survey during the same period. It is regrettable that the sinking of the deeper pipe can not be given at the station "N" due to the lack of survey. However, if the speed of its sinking is assumed to be 1 cm/year, we obtain the settling speed of ground level as 9.8+1.0=10.8 cm/year by the subsidence meter. This amount accords to that from tidal observations mentioned above.

4. The state of fluctuations in the ground level

In seeking for an explanation of the fluctuating state of ground level it is necessary, as a first step, to see how the underground water may affect this phenomena. Graphically the monthly mean underground water level in every month are represented since 1956, with the monthly amount of underground water pumped out for the industrial purpose in Fig. 5, where the amounts of subsidence by the

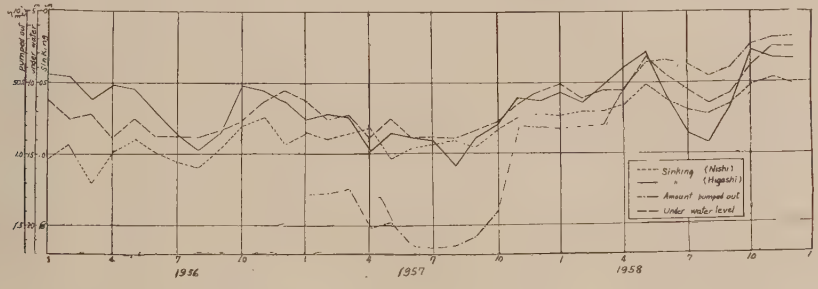

Fig. 5. The monthly amount of the subsidence, the water pumped out, and the underground water level.

subsidence meter in both stations are also shown. The ground level seems to vary from month to month in the irregular manner, but it may be found that the amount of subsidence is larger in summer, especially in August and smaller in winter at the station "H" in every year, though at the station "N" only in 1958. And the correlation between the amount of subsidence and the underground water level may be manifested in some extent till November of 1957, when the water service for industry began to be used, while it is recognized in a clearer way since this time at the station "H", though this features may be seen in lesser degree at the station "N".

Next, the mean values of the amount of subsidence in every day of the week are computed over the whole year of 1957, and plotted in Fig. 6, from which we see that the amount

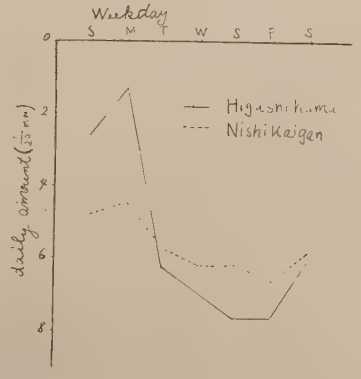

Fig. 6. The change of subsidence by the week day.

of subsidence decreases in a great degree on Sunday and Monday, while it increases on Thursday and Friday at both stations, and that this feature is more noteworthy at the station "H" than at "N". The fact compells us to consider that the amount of water pumped out for the industrial use decreases in the holidays and then, the underground water level being raised, the ground level may recover with some lag of time.

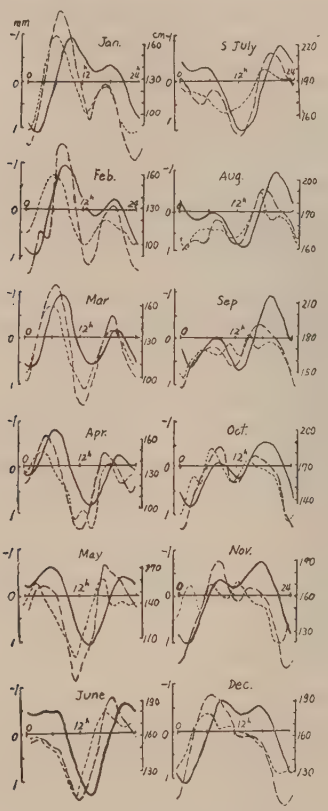

Fig. 7. The daily changes of the tidal level (full line) and the speed of subsidence (broken-Nishikaigan and dotted Higashihama) in every month.

Now we seek for the influence of change in tides upon the subsidence. The values of tidal level at every hour are given from the tidal curve in the routine work and then, the monthly mean values of them are graphed at every two hours, to-gether with the monthly mean values of subsidence at the same interval of time computed from the self-record readings during 1957 at both stations in Fig. 7, where the tidal level is in the arbitary scale. Strikingly, these figures show the dependence of the tidal level on the subsidence, though with the phase difference. Naturally, the effect of tidal level on the subsidence should be considered in those coastal region. The quantitative representaton, howerver, has not been reported yet in this region, so that this result may be valuable to be introduced here. Besides this, we want to indicate the tidal curve with the continuous record of subsidence from December 23, 1958 to January 7, 1959 as shown in Fig. 8, It is noted that the ground level seems to move up not in a steady speed, but in a repeated manner of rise and fall and that the manner of fluctuation in the subsidence is keenly correlated to the change of tidal level. This period adopted here includes the holidays before and after New year, and thus, the underound water may be pumped out in the least amount over the year. The result appears in the curve of subsidence at the station "H, where the ground level falls in a slight degree since December 28, while it tends to rise until January 4. This fact it not able to be found on ordinary days, and also at the station "N".

From those results pointed out, it may be suggested that when we attack the cause of the subsidence in ground level, the effect of tidal phenomena has an important part and must not be neglected. The various factors such as underground

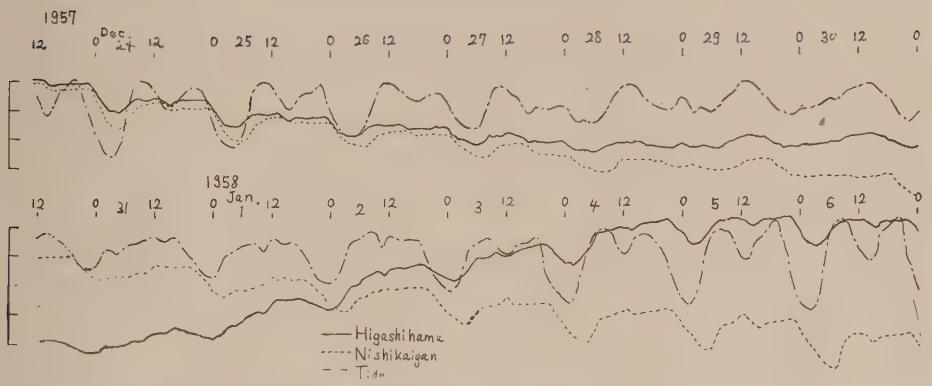

Fig. 8. The sequence of the tidal level and the ground level in the end of 1957 and the beginning of 1958.

water level, and the amount of pumped out water are so important that many studies have already been carried out and reported to point out the relation of these factors to the subsidence. However, the way to the knowledge about the mechanism of the subsidence of ground level may be found in seeking for the effect of tidal level together combined with that of those factors. Of course, the amount of the precipitation and that of the river water may affect indirectly the subsidence through the underground water, but it is not to be discussed here by the absence of reliable data.

5. Summary

From the data of the level survey once every year carried out by Amagasaki municipal authorities, the yearly amount of the subsidence in ground level has a order of a few centimeters in the mean during the past twenty years. It varies year by year and recently, it seems to increase so fairly that the locality over 10cm/year of subsidence is being enlarged.

The result of tidal observations there indicates that the rise of tidal level attains a speed of about 10cm/year, which is in a good accordance with the result from the subsidence meter and the level survey.

The level of underground water and the amout of the water pumped out for industrial uses may be represnted to have the relation to the subsidence in an appreciable degree at the station "H" and in some degree at the station "N". Besides this, the tidal phenomena at the coast must be taken into considerations in the study on the fluctuated state of the ground level, because the comparison of the self records between tidal level and ground level gives us the conspicuons relation between them.

References

(1) Soejima, M. (1956): On the subsidence of ground level at Osaka and Amagasaki. *Trans. Soc. Civil Eng.*, Vol. 41, No. 8, p. 67.

(2) Matsudaira, Y. and Kawamoto, T. (1954): On the subsidence of Ground level at Amagasaki Region. (I) *Umi to Sora*, Vol. 30, No. 1—2, and (II) Vol. 30, No. 3.

(3) Comittee of the harbour engineering along the bay of Osaka (1952—1955): *The report of the works by members of the comittee.*

(4) Municipal authorities of Amagasaki city (1959): *The state of the subsidence of ground level and its counterplan.*

On the Fluctuation and Prediction of Ocean Temperature in the North Pacific

By

Michitaka Uda

Tokyo University of Fisheries

Introduction

Basing on the data from the "Mean Atomospheric Pressure, Cloudiness, and Sea Surface Temperature of the North pacific Ocean and the Neighbouring Seas" (1911—1941) published by the Imperial Marine Observatory at Kōbe, the author studied the fluctuation of the sea surface temperature in the northern part of the North Pacific along the zone of (35°—55°N.), with wishes to commemorate Dr. Y. Horiguti who contributed much to the pacific meteorlogy.

Thanks are due to Dr. J. Masuzawa of the Meteorological Agency (Oceanographic Section) who has kindly shown the publications cited above.

1. Analysis and results

At first isopleth charts of sea surface temperature distributed in the 5 degree (latitude, longitude) grids between 140°E. and 120°W. in the North Pacific Waters during the years of 1911—1941 for each zones of (35°—40°N.), (40°—45°N.), (45°—50°N.), (50°—55°N.), and for each month (season) of February (winter), May (spring), and August (summer) respectively. (Refer to Fig. 1 a, b, c, d, e.)

Fig. 1 a. 45°—50°N. Zone, Aug. Sea Surface Temp.

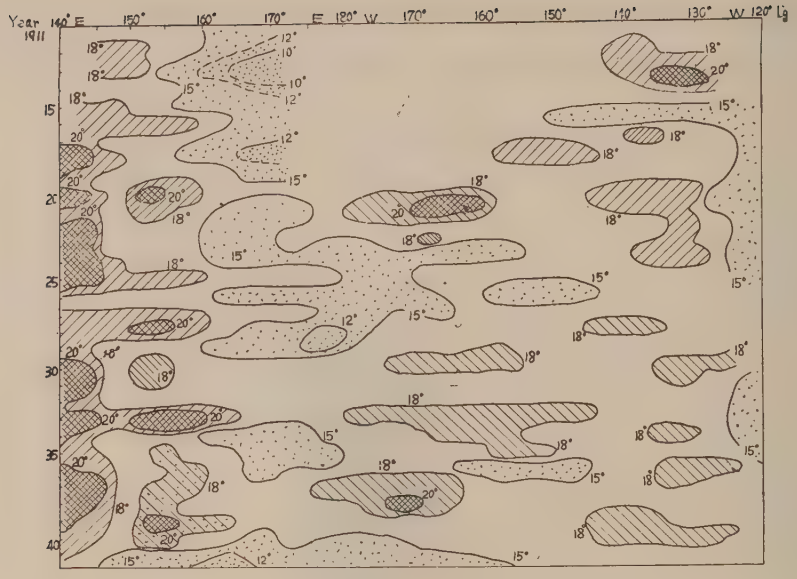

Fig. 1 b. 40°—45°N. Zone, Aug. Sea Surface Temp.

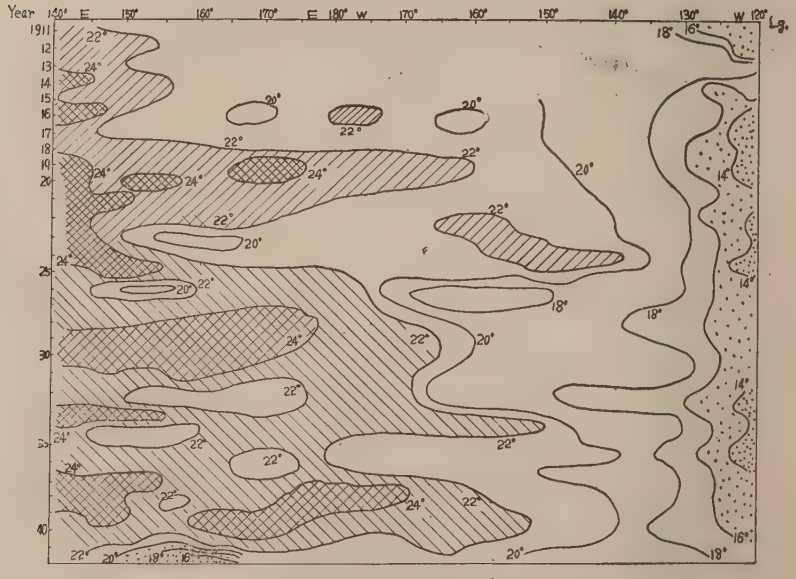

Fig. 1 c. 35°—40°N. Zone, Aug. Sea Surface Temp.

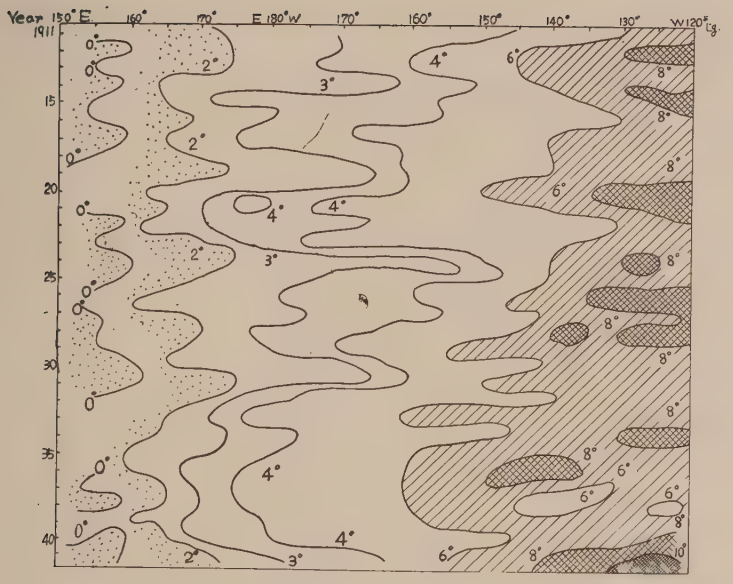

Fig. 1 d. 45°—50°N. Zone, Feb. Sea Surface Temp.

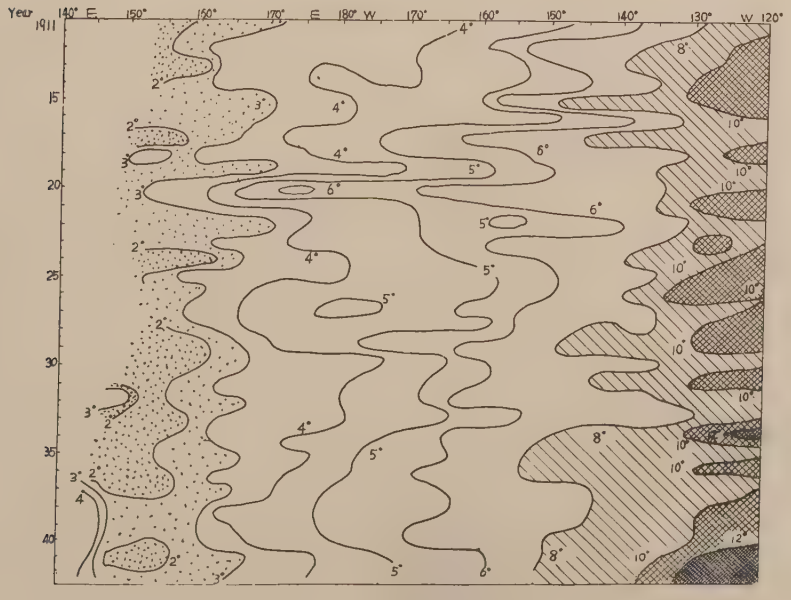

Fig. 1 e. 45°—50°N. Zone, May Sea Surface Temp.

Temperature means taken in the meridional belts are shown in Table 1 a, b, which were illustrated in Fig. 2 a, b, c, d.

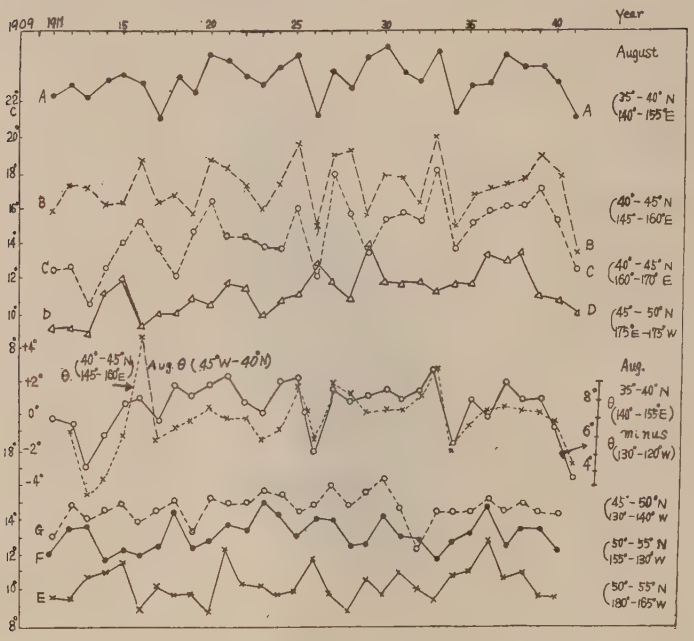

Fig. 2a.

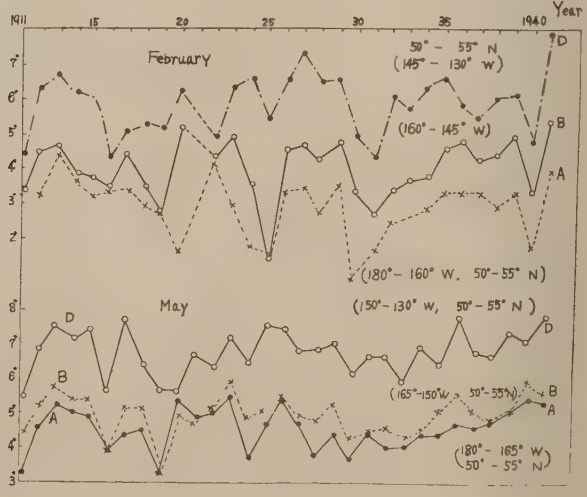

Fig. 2b.

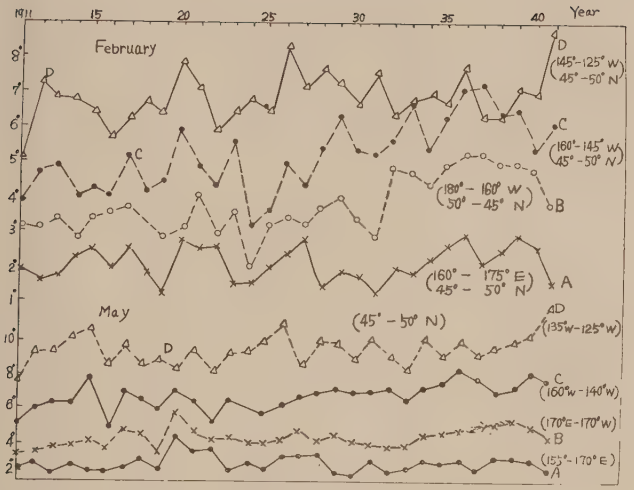
1911
15
20
25
30
35
40
Year
February
D
(145°-125° W)
45°-50° N)
C
(160°-145° W)
45°-50° N)
(180°-160° W
50°-45° N)
B
(160°-175° E)
45°-50° N)
A
May
(45°-50° N)
AD
(135°W-125°W)
C
(160°W-140°W)
(170°E-170°W)
B
(155°-170° E)
A

Fig. 2c.

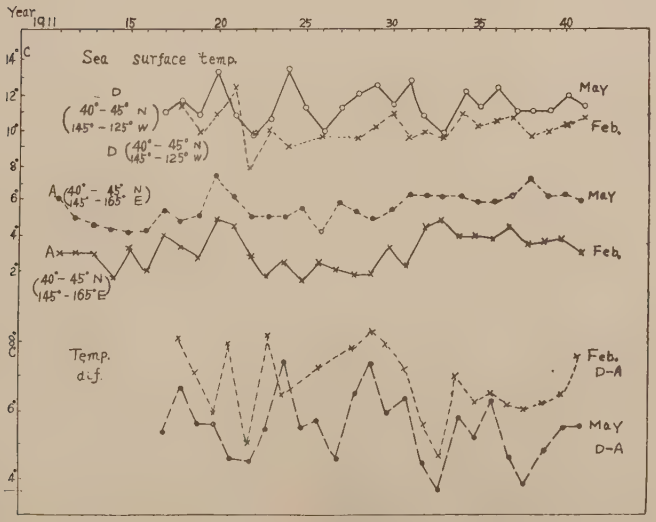
Year
1911
15
20
25
30
35
40
C
Sea surface temp.
D
(40°-45° N
145°-125° W)
D (40°-45° N
145°-125° W)
May
Feb.
A (40°-45° N
145°-165° E)
May
A
(40°-45° N
145°-165° E)
Feb.
Temp.
d.f.
Feb.
D-A
May
D-A

Fig. 2d.

Table 1 a. Sea Surface Temperature (°C) in August.

Mean Lat.(N) Lg.(E) / Year	A 35° – 40°N 140° – 155°E	B 40° – 45°N 145° – 160°E	C_1 45° – 50° 155° – 160°E	C_2 40° – 45° 160°N – 170°E	D 45° – 50°N 175°E – 175°W	E 50° – 55°N 180° – 165°W
1911	22.3	15.8	10.6	(12.4)	9.1	9.3
12	22.9	17.3	11.9	12.6	9.1	9.2
13	22.3	17.1	10.4	10.3	8.8	10.6
14	23.2	16.2	12.2	12.5	11.0	10.8
15	23.5	16.2	11.5	13.9	12.0	11.4
16	23.0	18.7	12.9	(15.2)	9.1	8.4
17	21.0	16.3	11.2	13.7	9.8	10.0
18	23.5	16.8	12.2	12.0	9.8	9.5
19	22.4	15.8	11.7	14.6	10.7	9.6
20	24.7	18.8	14.1	16.2	10.3	8.6
21	24.3	18.3	13.7	14.4	11.6	(12.1)
22	23.4	17.3	12.0	14.3	11.4	10.2
23	22.9	15.9	10.3	13.7	9.6	10.0
24	23.9	17.3	10.6	13.5	10.6	9.6
25	24.5	19.7	12.4	15.9	10.9	9.8
26	21.0	14.9	10.7	12.0	12.7	11.5
27	(23.9)	19.1	12.4	17.9	11.7	9.8
28	(22.6)	19.2	13.6	15.5	10.6	(8.6)
29	(24.5)	15.7	11.0	13.3	13.8	10.4
30	(25.0)	17.9	12.5	15.3	11.6	9.6
31	23.5	17.7	11.7	15.6	11.6	10.9
32	23.2	16.3	11.0	15.2	11.7	9.9
33	24.8	20.0	13.5	18.0	11.0	9.2
34	21.3	15.1	10.6	13.5	11.5	10.7
35	22.9	16.7	11.2	14.9	11.6	10.9
36	22.9	17.2	12.4	15.6	13.2	12.7
37	24.7	17.4	11.0	15.9	11.8	10.5
38	23.9	17.6	12.2	16.0	12.5	10.7
39	23.9	18.9	12.4	17.0	10.9	9.6
40	22.9	17.8	11.4	15.2	10.6	9.3
1941	21.1	13.4	10.0	12.3	9.9	—
Max.	25.0	20.0	14.1	18.0	13.8	12.7
Min.	21.0	13.4	10.0	10.3	8.8	8.4
Dif.	4.0	6.6	4.1	7.7	5.0	4.3

F 50° | 55°N 150° | 135°W	G 45° | 50°N 140° | 130°W	H 35° | 40°N 130° | 120°W	G′ 40° | 45°N 145° | 140°W	A—H	B—G′	G - C_1
12.1	13.0	15.5	—	6.8	—	2.4
13.5	14.9	16.5	(18.1)	6.4	(−0.8)	3.0
13.5	14.0	18.6	—	3.7	—	3.6
11.5	14.6	17.3	(20.0)	5.9	(−3.8)	2.4
12.0	15.0	16.0	17.3	7.5	−1.1	3.5
11.8	13.8	15.0	14.0	8.0	+4.7	0.9
12.3	14.5	14.5	(17.8)	6.5	(−1.5)	3.3
14.3	15.1	14.8	17.5	8.7	−0.7	2.9
12.1	13.1	14.4	16.1	8.0	−0.3	1.4
12.6	15.2	16.0	18.4	8.7	+0.4	1.1
(13.6)	14.9	15.2	18.5	9.1	−0.2	1.2
13.2	14.9	15.8	17.5	7.6	−0.2	2.9
14.9	15.5	16.1	17.5	6.8	−1.6	5.2
14.2	15.4	15.1	18.2	8.8	−0.9	4.8
12.8	14.4	15.5	18.0	9.0	+1.7	2.0
13.9	14.8	16.1	16.4	4.9	−1.5	4.1
13.9	16.0	15.4	17.3	8.5	+1.8	3.6
12.4	14.7	14.9	18.1	7.7	+1.1	1.1
12.5	15.6	16.5	15.7	8.0	0	4.6
14.1	16.3	16.6	17.6	8.4	+0.3	3.8
13.0	14.6	15.7	17.5	7.8	+0.2	2.9
12.7	12.3	14.9	15.4	8.3	+0.9	1.3
11.6	14.5	15.3	17.5	9.5	+2.5	1.0
12.6	14.5	16.2	17.4	5.2	−2.4	3.9
13.1	14.5	15.0	17.4	7.9	−0.7	3.3
14.8	15.0	15.9	17.1	7.0	+0.1	2.6
12.3	14.4	15.9	17.0	8.8	+0.4	1.1
13.5	15.0	16.1	17.4	7.8	+0.2	2.8
12.3	14.4	16.1	17.9	7.8	+1.1	2.0
12.2	14.3	16.7	18.2	6.2	−0.4	2.9
—	—	17.9	16.4	3.3	−3.0	—
14.9	16.3	18.6	20.0			
11.5	12.3	14.4	14.0			
3.4	4.0	4.2	6.0			

Table 1 b. Sea Surface Temperature in Feb. and May.

Year	February			February			
	50°—55°N			45°—50°N			
	180°W–160°W	160°W–145°W	145°W–130°W	160° E–175° E	180°W–160°W	160°W–145°W	145°W–125°W
1911	3.3	3.3	4.3	1.9	3.1	3.8	5.1
12	3.2	4.5	6.3	1.6	3.0	4.7	7.3
13	4.4	4.7	6.7	1.7	3.3	4.9	6.9
14	3.6	3.9	6.2	2.3	2.7	4.0	6.8
15	3.2	3.8	6.1	2.5	3.4	4.2	6.4
16	3.4	3.5	4.4	1.9	3.5	4.0	5.7
17	3.4	4.6	5.1	2.6	3.7	5.2	6.2
18	3.0	3.5	5.3	1.8	3.2	4.1	6.7
19	2.8	2.7	5.2	1.2	2.9	4.4	6.4
20	1.7	5.2	6.3	2.8	3.0	6.0	7.9
21	—	—	—	2.5	4.1	4.8	7.1
22	(4.2)	4.4	4.9	2.6	3.9	4.3	5.9
23	(3.0)	5.0	6.4	1.5	4.6	5.6	6.4
24	1.8	3.6	6.6	1.5	1.9	3.2	6.8
25	1.6	1.5	5.5	2.0	3.2	(3.6)	6.4
26	3.4	4.6	6.6	2.4	3.4	5.0	8.3
27	3.5	4.7	7.4	2.9	3.2	4.3	7.1
28	2.8	4.3	6.6	1.4	3.7	5.4	7.7
29	3.6	4.8	6.6	1.9	4.0	6.3	7.3
30	0.9	3.3	5.0	1.8	3.4	5.4	6.6
31	1.7	2.8	4.4	1.3	2.8	5.2	7.6
32	2.5	3.4	6.2	2.0	4.7	5.6	6.3
33	—	3.7	5.8	1.9	4.4	6.7	6.7
34	2.9	3.8	6.4	2.3	4.9	5.4	7.0
35	3.4	4.7	6.7	2.7	5.2	6.3	6.7
36	3.4	4.9	5.9	3.0	5.2	7.2	7.8
37	3.4	4.3	5.6	2.2	5.0	7.3	(6.4)
38	3.0	4.5	(6.1)	2.5	5.0	6.4	6.3
39	(3.4)	5.0	6.2	3.0	5.0	6.5	7.2
40	1.8	3.3	(4.8)	2.7	4.8	5.4	7.0
1941	4.0	5.4	7.9	1.6	3.8	6.1	8.8

February		May			May			May	
40°—45°N		50°—55°N			45°—50°N			40°—45°N	
145° E	145°W	180°W	165°W	150°W	155° E	170° E	135°W	145° E	145°W
165° E	125°W	155°W	150°W	135°W	170° E	170°W	125°W	165° E	125°W
3.1	—	3.2	4.3	5.4	2.6	3.4	7.7	6.3	—
3.2	—	4.5	5.1	6.8	3.0	3.5	9.3	6.1	—
3.2	—	5.2	5.7	7.5	2.5	3.8	9.3	4.7	—
1.8	—	5.0	5.3	7.1	2.9	3.9	10.1	4.5	—
3.7	—	4.8	3.3	7.3	2.7	4.2	10.4	4.2	—
2.1	—	3.9	3.9	5.6	2.5	3.8	8.4	4.4	—
4.2	—	4.3	5.1	7.6	2.7	4.8	9.5	5.5	(11.0)
3.5	(11.7)	4.5	5.1	6.4	3.3	4.5	8.5	5.0	11.7
2.8	10.0	3.2	3.1	5.7	2.6	3.4	8.8	5.2	10.9
5.2	(11.1)	5.3	4.9	5.6	4.6	5.9	8.4	7.7	13.3
4.7	(12.8)	4.8	4.7	6.7	3.9	4.7	9.5	6.4	11.1
3.0	(8.0)	4.9	5.1	6.2	2.7	4.2	8.1	5.2	9.8
1.9	10.2	5.5	5.9	(7.1)	3.0	4.5	9.2	5.2	(10.7)
2.8	(9.3)	3.6	4.8	6.3	2.4	4.1	9.3	5.2	(12.7)
1.6	—	4.6	5.0	7.5	3.3	4.1	9.9	5.8	11.4
2.6	9.9	5.4	5.4	7.4	3.5	4.3	10.9	4.3	10.1
2.3	—	4.7	4.9	6.8	3.7	4.9	8.6	6.1	11.4
1.9	9.8	3.7	4.7	6.8	3.2	4.3	10.0	5.7	12.3
2.0	10.4	4.4	5.2	7.0	2.6	4.7	9.9	5.2	12.6
3.5	11.5	3.6	4.2	6.1	2.4	4.3	8.9	5.6	11.6
2.4	(9.7)	4.4	4.4	6.6	3.2	4.1	10.1	6.5	12.9
4.6	10.2	3.9	4.5	6.6	2.7	4.0	9.1	6.5	11.0
5.1	9.8	4.0	4.3	5.8	2.7	4.0	8.3	6.4	10.1
4.1	11.2	4.4	4.5	6.9	3.3	4.7	10.3	6.5	12.4
4.2	10.5	4.3	5.0	6.4	3.1	4.8	9.1	6.2	11.5
4.2	10.8	4.7	5.6	7.8	3.2	5.0	10.1	6.1	12.6
4.8	11.0	4.5	5.1	6.8	2.8	5.2	9.3	6.4	11.1
3.8	9.9	—	4.8	6.7	3.6	5.6	9.7	7.5	11.4
3.9	10.2	5.2	5.1	7.3	3.5	5.6	10.0	6.5	11.4
4.1	10.6	5.4	5.9	7.1	3.4	5.2	10.4	6.6	12.2
3.4	11.0	5.3	5.6	7.8	2.8	4.6	(12.1)	6.1	11.7

The results are shown in the following:

(1) Basing on Figs. 1, 2 and Table 1, in summer (August) sea temperature in the western part of the North Pacific (west to 160°E.) has indicated minima in the years 1913, 1923, 1926, 1934, and 1941 which correspond to the bad year of rice crop due to cool summer. Moreover, in such years, waters in the eastern part of the North Pacific Ocean are warmer remarkably than normal. Conversely, we can notice the warmer years (rich rice crop years) in the western region of the ocean contrasted to the colder years in the eastern region of the ocean. The temperature difference between the western and eastern parts of the ocean shows the trends of fluctuation such as greater minus value in the cooler years and greater plus values in the warmer years.

(2) Basing on Fig. 2, we can easily recognize the trends of the reciprocal variation between the temperature in the western part (west to 160°E.) and in the eastern part (east to 160°W.) of the ocean along the Polar Frontal Zone (35°—50°N.). In particular, such a trend is obvious along the zones of 40°—45°N. and 45°—50°N. by the mean sea temperature in the western part contrasted to that of the eastern part (e. g. between two meridional belts of A and D) in the months of February, May and August respectively. In the zone of 50°—55°N., in the eastern Bering Sea (east to 180° Lg.) the temperature trend is similar to the variation in the eastern part of the North Pacific Ocean (east to 160°W.).

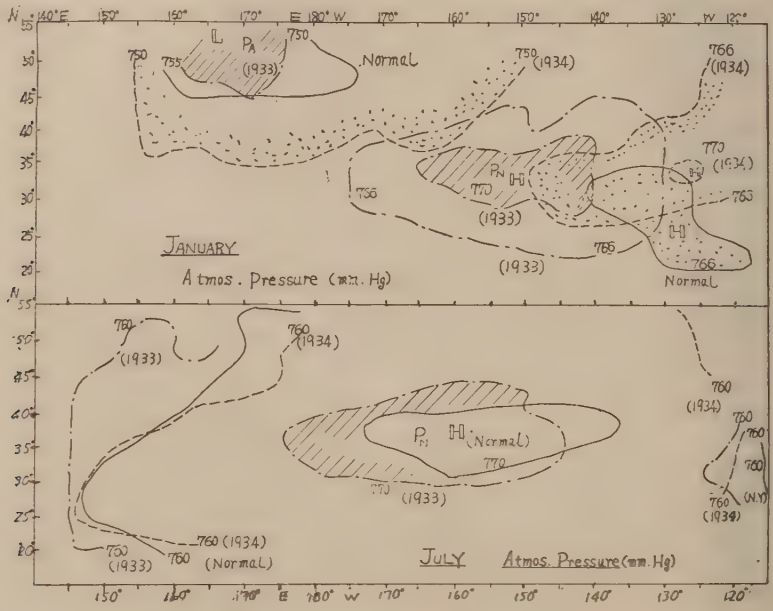

Fig. 3. Atmos. Pressure Pattern.

(3) The above mentioned results may be interpreted by the yearly fluctuation of atmospheric pressure system such as "Siberian High" (P_S), "Aleutian Low" (P_A), "North Pacific High" (P_N) depressions.

For example the pressure patterns in February (winter) and August (summer) of 1934 (western cool year and lower pressure generally) are quite different from those of 1933 (western warm year, higher pressure generally) compared to the normal year (Fig. 3).

In winter higher pressure on the continent and lower pressure on the sea arouses stronger monsoon (between P_S and P_A) in the western sea regions (carrying colder water to south) brings cooler climate and transports more warmer waters by westerly or southwesterly drift current due to prevailing wind between P_N and P_A into the eastern part of the ocean.

(4) During the period (1911—1941) in question we can remark the general warming (+1°—4°C) of the northern waters in the Pacific, especially notable in winter and in spring (conspicuous in the eastern and western part), also in summer (conspicuous in the middle and eastern part of the ocean) in the Polar Frontal Zone (40°—45°N.). We may explain them on the maritime meteorological basis as before. (See Figs. 1, 2 and Table 1.)

(5) In general the distribution patterns of sea temperature in the North Pacific (Fig. 1) indicate the western warmer, eastern cooler pattern in the)35°—45°N.) zone and the western cooler, eastern warmer pattern in the (45°—50°—55°N.). zones i. e. as the contact zones of two independent great circulations (subtropical and

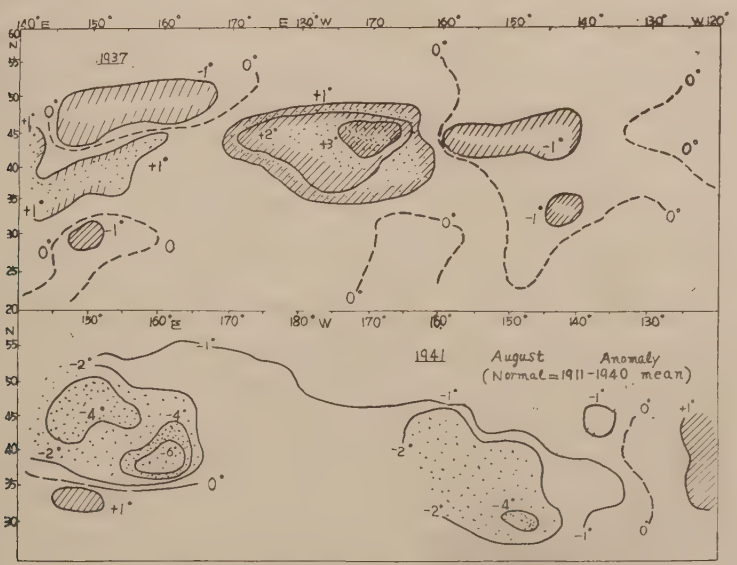

Fig. 4. In 1937 and 1941, August Anomaly.

subarctic circulations).

(6) The anomaly distribution of sea temperature ($\Delta\theta$) during the period of 1930—1941 is shown in Fig. 4. From them we can find:

(i) The zonal maximum of the year by year fluctuation concerning sea temperature locates in the zone of 40° to 50°N. i. e. around the Poalr Frontal Zone.

(ii) The meridional fluctuation of the year by year fluctuation centres around (A) 140°—165°E., (B) 170°E—160°W., (C) 155°—120°W., (A_1 140°—155°E., A_2 160°—165°E.) as seemingly independent areal blocks which correspond to the warm water intrusion areas. (See the following 2.)

(7) Fig. 5a, b show the transpacific pattern (from west to east) of temperature anomaly in the years (1930—1941).

We can recognize the variation from the western higher, eastern lower type, through the middle higher type unto the western lower, eastern higher type successively and cyclically (cycle of about more than seven years).

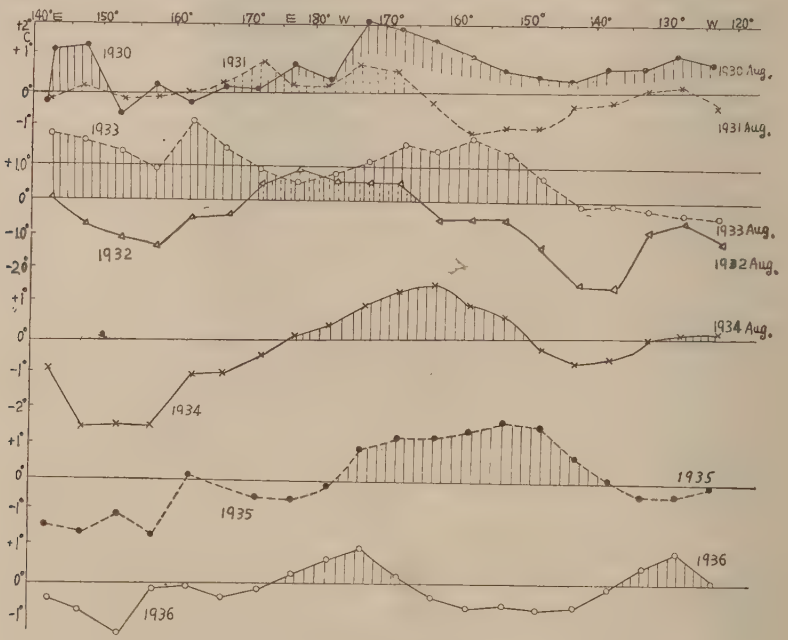

Fig. 5 a. Mean of Anomaly in the Zone of 50°—35°N. (Sea Temp).

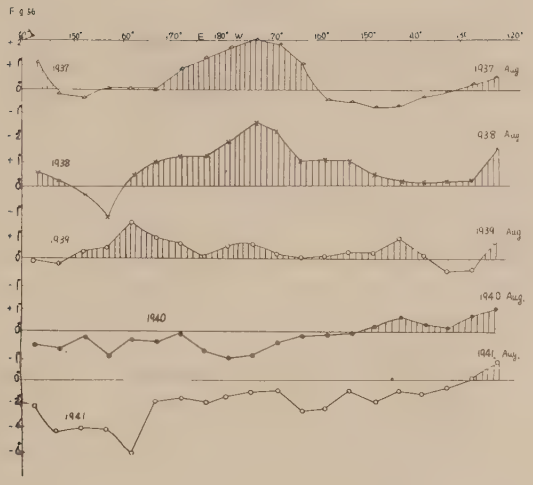

Fig. 5b. Mean of Anomaly in the Zone of 50°—35°N. (Sea Temp.)

2. Considerations

First we will discuss on the mechanism of reciprocal variation of east to west in the North Pacific Ocean. We have already compiled the data covering the whole North Pacific Ocean during 1955 to 1958 and also those in the western and middle parts of the Ocean during 1952 to 1958, and have constructed the distribution charts of water temerature, salinity, transparency, dissolved oxygen, density *in situ*, dynamic topography (ΔD), dichothermal water, methothermal water and intermediate water topographies.

Thousands of observed stations were classified into 3 types, (I) subarctic (SA), (II) Subtropical (ST), and Polar Frontal (PF) (Transitional) types on the basis of TS-curves as well as vertical distribution maps of temperature, salinity, density and dissolved oxygen. Fig. 6 is the summarized distribution maps of those types corresponding to the quasi-stationary gyrals (each peculiar circulations).

The author examined the year by year fluctuation by superposing those isolines in the same season (e. g. ΔD 0db/1000db, in summer) during 1952—1958 and found the most conspicuous fluctuation occuring at the head of the warm water intrusions of Polar Frontal Zone (4 or 5 waves) which accompanies mass transfer and fluctuation of fisheries (stronger intrusion, richer fisheries conditions).

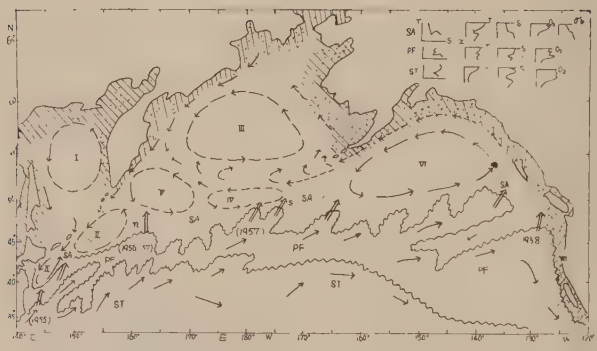

Fig. 6. Summarized Subarctic Circulations, Gyrals and Intrusions (by Uda).
I Okhotsk Gyral, II′ Oyashio Gyral, II Kurile Gyral
III Bering Gyral, IV Aleutian Gyral, V Kamchatka Gyral,
VI Alaska Gyral, VII Calif. Gyral,
n. North Kurile Warm Current, s. South Aleutian Warm Current
Warm Water Intrusion, a. Alaska Stream, hatched area.....
Low Salinity Water

Table 2. Shift of the Peak of Intrusion in the Pacific Ocean.

Year	Western part	Middle part 1.	Middle part 2.	Eastern part
1952	⊙	—	—	—
1953	⊙	●	—	—
1954	○	⊙	—	—
1955	◎	○	⊙	▲
1956	○	◎	○	⊙
1957	●	○	◎	○
1958	▲	⊙	○	◎

The amplitudes of intrusion shifted its peak successively from west to east such as shown in Table 2, i. e. warmest in 1955 in the adjacent waters in east to Japan, in 1957 in the middle Aleutian waters and in 1958 in the neighbouring waters off American Pacific coasts, seemingly the peak of oceanographic intrusion (temperature rise etc.) shifted from west to east. In 1958, compared to the western cooling the eastern warming was remarkable.

In the past the peak in 1937—1938 (warming maximum with sardine fisheries prosperity) and the following decline since 1941 moved from oriental waters to American waters after the delay of 3—4 years.

Peaks (±) appeared in the course of temperature variation along American

coast studied by M. Robinson seems reciprocal to our experienced one along the Japanese coastal waters. Formerly J. Fukuoka (1957) has noticed the reciprocal relation between the sea temperature along the northeast coast of Japan and those along the B. C. coast of Canada reported by Pacific Oceanographic Group. M. Okada (1941) also remarked the reciprocal relation concerning daily temperatures observed along the Japanese coast and the Canadian Pacific coast. Really these are very encouraging evidences for the future prediction of the ocean temperature in the Pacific.

Further, the author studied the mechanism of fluctuation mentioned above on the bases of the Northern Hemisphere Weather Maps of monthly mean atomospheric pressure (from Jan. 1955 to April 1959) published by the U. S. Weather Bureau and discovered the amplitude of the pressure difference between "Siberian High" and "Aleutian Low" $P_S - P_A$ or $\sqrt{P_S - P_A}$ (and also the pressure difference between "North Pacific High" and "Aleutian Low" $P_N - P_A$ or $\sqrt{P_N - P_A}$, (similar trend of the difference between North American High and Icelandic Low), suggesting the common fluctuation in the northern hemisphere circulation) in winter increased year by year during 1955—1958. Therefore, the winter monsoon $W_1 = K_1\sqrt{P_S - P_A}$, $W_2 = K_2\sqrt{P_N - P_A}$ corresponding to intensified gradient and duely also wind stress $\tau = D_\rho V^2$ (Reid, 1948) increased. Following H. Stommel (1958, Gulf Stream, p. 155) βM_y = curl τ and accordingly vorticity may be increased. Consequently we can infer that in quasi-stationary state gyrals were intensified successively from west to east by such mechanism aroused intrusion.

However, this wave is not due to the mere planetary wave, but the quasi-stationary pulsational wave with fluctuating amplitude due to topographically confined or boundary conditioned gyrals. (Pulsation theory proposed.)

P. S.

Remembering Mr. G. Roden's suggestion to the interpretation of reciprocal trends of temperature anomaly on the west and east sides of North Pacific Ocean in relation to the location of Aleutian Low and North American High on 22 April, 1959 at Biological Station (Nanaimo), the author states his hearty acknowledgement. Also the author wishes to state his thanks to Mr. M. Hanzawa who kindly reminded me his excellent work on reciprocal relation of water temperature on both sides of the North Pacific Ocean in 1955. Referring to Rodewald's paper (1957) the trends of temperature variation along the west coasts of the North Pacific and North Atlantic Oceans appear concurrently.

References

(1) Uda, M. (1960): Researches on the subarctic oceanography in the North Pacific Ocean. (In press.)

(2) Robinson, M. (1957): Sea temperature in the Gulf of Alaska and in the northeast Pacific Ocean, 1941—1952. *Bull. of SIO*, Vol.7, No. 1.

(3) Fukuoka, J. (1957): The variation of the oceanic conditions in the seas adjacent to Japan. *Oceanogr. Mag.*, Vol. 9, No. 1.

(4) Okada, M. (1941): The correlated variation of water temperature in summer on the west and east coasts of the North Pacific Ocean. *Kaiyō no Kagaku* (*Marine Science*), Vol. 1, No. 2.

(5) Uda, M. (1955): Researches on the fluctuation of the North Pacific circulation I. *Records of Oceanogr. Works in Japan*, Vol. 2, No. 2.

(6) Stommel, H. (1958): *Gulf Stream*, p. 155.

(7) Reid, R. O. (1948): The equatorial currents of the eastern pacific as maintained by the stress of the wind. *Jour. Mar. Res.*, Vol. 7, 74-99.

(8) Hanzawa, M. (1958): Studies of the interrelationship between the sea and the atomosphere. Ⅲ. *Oceanogr. Mag.*, Vol. 10, No. 1.

(9) Roden, G. and Reid, J. L. MS. On a relation between atmospheric pressure and sea surface temperature in the North Pacific Ocean.

(10) Rodewald, M. (1957): Beiträge zur Klimaschwankung im Meer. Die Temperatur der pazifischen Küstengewässer Nordamerikas von 1920 bis 1955. *D.H.Z.*, Bd. 10, Hf. 4, 151—157.

Vertical Distribution of Living and Dead Diatoms down to One Thousand Meters off Sanriku, Northern Japan

By

Mamoru Ohwada

Hakodate Marine Observatory

From the viewpoint of the economic cycle in the sea it is desirable to observe the occurrence of living and dead diatoms separately, since dead diatoms no longer contribute to the production, sinking and eventually decaying of themselves. A brief observation on this line was performed at seven different stations in the sea off Sanriku, East Coast of Northern Honshū, on the occasion of the oceanographic cruise of the M. S. "Yūshio Maru" from May 22 to June 2, 1954 (Fig. 1).

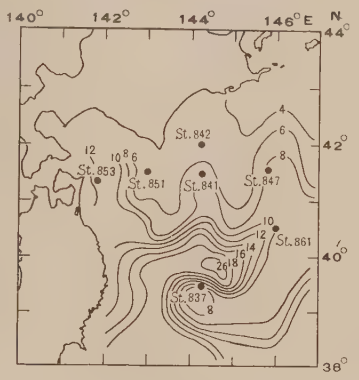

Fig. 1. Stations of sampling and surface isotherms (°C).

Samples were taken in Nansen bottles from ten different levels of water down to the 1000 meter depth, with the exception of the surface water which was dipped with a bucket. Diatoms contained in 330 cc of sample water into which formalin was added immediately after sampling, were concentrated by the settling method, and microscopic observations on these samples were made at the laboratory within a fortnight after returning from the cruise.

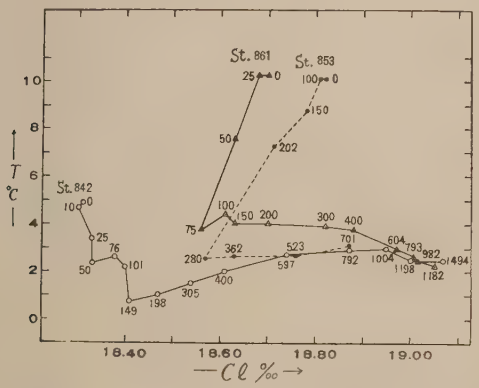

Fig. 2. T-Cl diagram at representative stations in the neritic Oyashio Current (St. 842), oceanic Oyashio Current (St. 861), and Tsugaru Warm Current (St. 853). The numerals in the diagram denote depths of observation.

The cruise covered three different sea areas in regard to the nature of water mass. The surface isotherms (Fig. 1), T-Cl diagram (Fig. 2) and also other hydrographic conditions (Centr. Meteorol. Obs., 1955) indicate that the stations of sampling were located in the following respective waters;

Neritic Oyashio Current: St. 837, St. 841, St. 842, St. 851,

Oceanic Oyashio Current: St. 847, St. 861,
Tsugaru Warm Current: St. 853,

Most of the diatoms observed from the shallow levels had normal chromatophores. In some others from deeper levels chromatophores were abnormally concentrated (systrophe) or had almost been entirely lost. Cells having normal chromatophores are considered to be alive when sampled, while those showing systrophe or lost chromatophores are considered to be dead. Fig. 3 shows the vertical distribution of the number of cells of these living and dead diatoms regardless of the species composition.

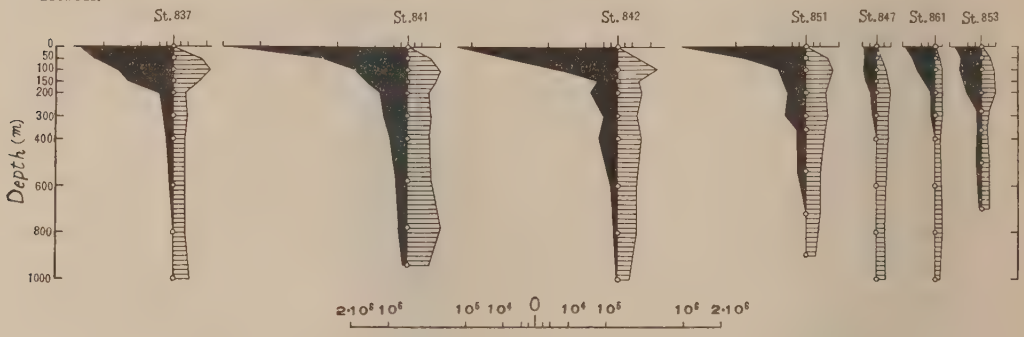

Fig. 3. Vertical distribution of living and dead diatoms (cell number per liter).
Left (black): Living cells,
Right (hatched): Dead cells.

It is shown that in the neritic Oyashio Current in which there was a large concentration of diatoms ($10^6-2\times10^6$ cells/L) at the surface, active production, as indicated by the presence of abundant living cells, occurred in the levels above 100 meters. In the oceanic Oyashio Current which was not densely populated by diatoms (10^4 cells/L) compared with neritic Oyashio Current, the productive zone was also confined in similar upper levels, i. e., roughly above 100 meters. In the Tsugaru Warm Current in which diatoms were present as much as in the oceanic Oyashio Current, the lower limit of the productive zone seemed to be down to 150 meters.

The percentage in number of living cells and dead cells of diatoms to the total number of living and dead cells together in the upper productive zone at each station is calculated as follows:

		Living cells	Dead cells
Neritic Oyashio Current	St. 837	95.4%	4.6%
(Productive zone: 0—100 m)	St. 841	99.0	1.0
	St. 842	98.6	1.4
	St. 851	98.8	1.2
	Average	98.4	1.6
Oceanic Oyashio Current	St. 847	93.0	7.0
(Productive zone: 0—100 m)	St. 861	98.4	1.6
	Average	96.9	3.1
Tsugaru Warm Current	St. 853	95.1	4.9
(Productive zone: 0—150 m)			

In each case no dead diatom cells were found in the surface water, while at 50 meter depth about 7—20 per cent of the total diatoms were dead. The number of dead cells definitely increased with depth even in the productive zone. It is calculated that about 1—5 per cent of the diatoms were not active in their photosynthesis in the productive zone.

Analyses were made on the species composition in the vertical distribution of living and dead diatoms (Fig. 4). At the stations in the neritic Oyashio Current living cells of subgenus *Hyalochaete* (*Chaetoceros debilis*, *C. furcellatus*, *C. compressus*, *C. radicans*) were so prevalent that they constituted the major part of living community in shallow water, while in the deep zone *Thalassiosira decipiens* prevailed as dead diatoms.

At St. 847 in the oceanic Oyashio Current subgenus *Phaeoceros* (*Chaetoceros atlanticus*, *C. concavicornis*, *C. convolutus*), *Coscinodiscus* spp. and *Denticula marina* were predominantly distributed as living cells in the upper productive zone, and also similarly abundant in the deeper layers but as dead cells. At St. 861 living cells of *Chaetoceros radicans* occupied the major part of the community at the surface, while below the 50 meter layer different living flora including *Thalassionema nitzschioides*, *Nitzschia seriata*, *Corethron hystrix* and *Coscinodiscus* spp. were dominant. In the non-productive zone below 200 meters dead *Coscinodiscus* spp., *Denticula marina*, *Stephanopyxis nipponica* and *Chaetoceros furcellatus* were common.

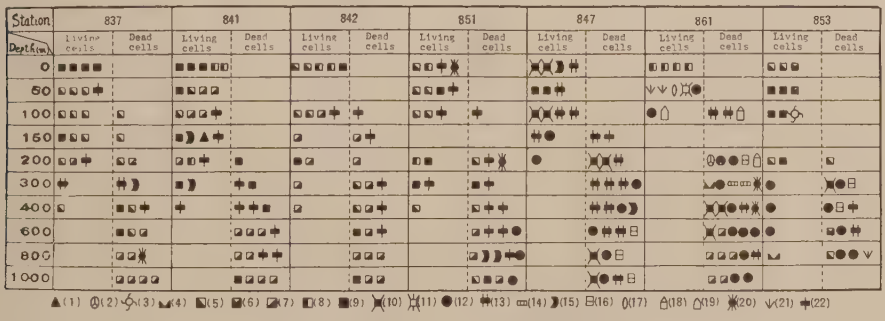

Fig. 4. Composition of diatom communities at various depths. One symbol represents the occurrence in about 20 per cent of total number of cells; forms occurring less than 20 per cent are ommited.

Symbol in the figure:

(1) *Asterionlla japonica*, (2) *Asteromphalus heptactis*, (3) *Bacteriastrum delicatulum*, (4) *Biddulphia aurita*, (5) *Chaetoceros debilis*, (6) *C. decipiens*, (7) *C. furcellatus*, (8) *C. radicans*, (9) *Chaetoceros-Hyalochaete* misc., (10) *Chaetoceros atlanticus*, *C. convolutus*, (11) *Corethron hystrix*, (12) *Coscinodiscus* spp., (13) *Denticula marina*, (14) *Eucampia zoodiacus*. (15) *Fragilaria oceanica*, (16) *Navicula membranacea*, (17) *Nitzschia seriata*, (18) *Rizosolenia alata*, (19) *R. stolterfothii*, (20) *Stephanopyxis nipponica*, (21) *Thalassionema nitzschioides*, (22) *Thalassiosira decipiens*.

In the Tsugaru Warm Current living *Chaetoceros debilis*, *C. decipiens* and *C. curvicetus* were prevalent in the upper layer, and living *Coscinodiscus* spp. appeared in the deeper layers. In this station, differing from the other stations, living diatoms composed of *Coscinodiscus* spp. or *Biddulphia aurita* were found to the depth of about 700 meters, as much as or more than 20 per cent of total diatoms.

From the above analyses it was noticed that the dead diatom flora found in the deep non-productive zone was usually different from the living flora distributed in the shallow productive zone. The similarity of both flora was only observed at St. 847 in the oceanic Oyashio Current. There is no available data in the present study to explain that the dead flora in the deep zone was originated from other geographical region, not from the upper zone at the same locality. It is supposed that the dead flora found in the deep zone at the time of observations, might have thrived in the upper zone before a certain time, and later sank to the depths. Then new flora came to grow in the shallow water, substituting the former flora.

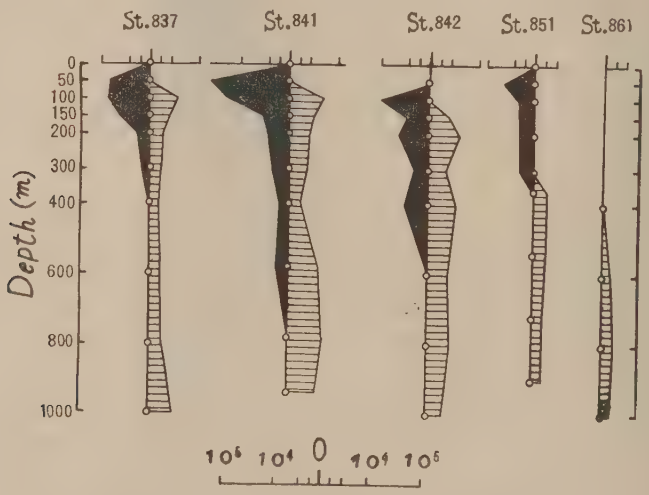

Fig. 5. Vertical distribution of living and dead cells of *Chaetoceros furcellatus* (cell number per liter).
Left (black): Living cells,
Right (hatched): Dead cells.

The vertical distribution of *Chaetoceros furcellatus* which occurred in the neritic Oyashio Current gives an example of subsurface preference, differing from the other species mentioned above (Fig. 5). Neither living cell nor dead cell appeared at the surface. The maximum distribution of living cells was found in 50—100 meters where the water temperature was 2—3°C. Living cells disappeared at the depth of 800 meters (St. 841). Dead cells which sank from the productive zone commonly appeared in the deep zone and often increased with depth.

Summary

From the vertical distribution of living cells of diatoms the productive zone is supposed to be confined in the upper 100 meters in the neritic Oyashio Current (Sts. 837, 841, 842, 851), in the upper 100 meters in the oceanic Oyashio Current (Sts. 847, 861) and in the upper 150 meters in the Tsugaru Warm Current (St. 853). The percentage in number of dead cells to the total cells in these upper productive zones is calculated as two per cent in the neritic Oyashio Current, three per cent in the oceanic Oyeahio Current and five per cent in the Tsugaru Warm Current. Dead flora in the deep zone is often different from the living flora in the upper productive zone, suggesting that subsequent growth of different flora might have happened after sinking of flora which is found in the deep zone.

The author is gratefully obliged to Dr. S. MOTODA, Hokkaido University, for his kindness in giving many valuable advices during the studies and to Messrs. Z. YASUI and J. SUGIURA, Hakodate Marine Observatory, for their kind advice and encouragement during the present studies.

Reference

(1) Oceanographical Section, Central Meteorological Observatory. (1955): Report of oceanographical observations east off Honshū in 1954. *Oceanpgr. Rep. Centr. Meteorol. Obs.*, Vol. 4, No. 1, 1—24, (in Japanese).

A Contribution of Microplankton Observations to the Hydrography of the Northern North Pacific and Adjacent Seas - III
Plankton Diatoms of the Western Okhotsk Sea in the Period from June to August 1957

By

Yutaka Kawarada

Japan Meteorological Agency

1. Introduction

On the occasion of the cruises of the "Hokusei Maru", training ship of Hokkaidō University, to and from the Siberian coast during the period from June to August 1957, the research staff and crew members of that vessel gathered the diatom samples by dipping the water, and kindly provided the samples to the author at his disposal. The cruises of "Hokusei Maru" were carried out monthly in the three months. The hydrographical data and other details of these cruises were published in the Data Record of Oceanographic Observations and Exploratory Fishing, No. 2 (Fac. Fish., Hokkaidō Univ., 1958).

There was generally no great difference in location between the outward and homeward courses of the vessel, except the outward voyage of the second cruise in July, and, therefore, these samples may be said to represent the fluctuations of the diatom properties at intervals of about a month or less in the sea areas from Hokkaidō to northern Siberian coast in the Okhotsk Sea within the longtitudes 144°E to 153°E. Laboratory procedure is detailed in the previous paper (Kawarada and Ohwada, 1957); shortly, the diatom samples contained in 330 cc surface water are concentrated by decanting and later by centrifugalizing; identification and counting are made under microscope by aid of counting slide glass.

2. Monthly variaton of diatom communities

(1). The former term of June (from 16th to 20th)

The total population of diatoms is fairly large, counted to be 2×10^6 cells per liter of water at the maximum and mostly from 3×10^4 to 4×10^5. Such a dense population may be closely related to the low water temperatures below 6°C.

The diatom communities in this term are represented by *Phaeoceros* group (*Chaetoceros concavicornis* and *Ch. convolutus*), *Hyalochaete* group (*Ch. constrictus* and *Ch. debilis*), *Denticula marina*, *Detonula confervacea*, *Fragilaria* group (*F. oceanica*), *Rhizosolenia* group (*Rh. fragilissima*) and *Thalassiosira* group (*Th. nordenskioldii*), among which *Thal'ra* group is most important. In addition to these species, *Bacteriosira fragilis* is also found, but in a rather small quantity.

(2) The latter term of June (from 22nd to 27th)

In consequence of the rise of water temperature in a range from 4°C to 7°C, the total number of diatoms comes to decrease, but still keeps more than 3×10^3 cells. The diatom communities during this term, as a whole, are characterized by the increase of *Phaeo.* (*Ch. atlanticus, Ch. concavicornis* and *Ch. convolutus*) and *Rhiz.* groups accompanied with remarkable decreases of *Thal'ra* group, *Dent. marina* and the other diatom species which were important in the former term of June. Near the Siberian coast, *Hyal.* group (*Ch. compressus* and *Ch. debilis*) is abundant just like as observed in the former term of June.

(3) July (from 22nd to 27th)

The population of diatoms is diminished to less than 5×10^2 cells, except in a region near lat. 50'N where the count of diatoms is 3×10^3 cells. The mean temperature of surface water in this month is slightly high, ranging from 9°C to

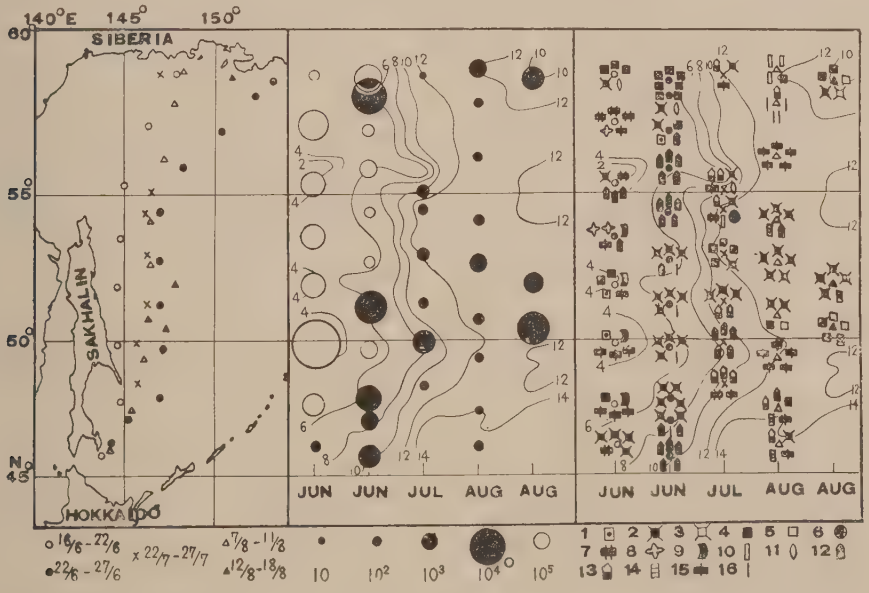

Fig. 1. The total number of diatoms per liter, major components of diatom communities and surface water temperature along the observation lines. Symbolized figures represent the important diatom species. Each figure approximately corresponds to 20 per cent of total diatoms in occurrence. Specific names represented by the figures are given:

(1) *Bacteriosira fragilis*, (2) *Chaetoceros atlanticus, C. concavicornis, C. covolutus*, (3) *C. danicus*, (4) *C. compressus, C. constrictus, C. debilis, C. decipiens*, (5) *C. distans, C. paradoxus*, (6) *Coscinodiscus marginatus*, (7) *Denticula marina*, (8) *Detonula confervacea*, (9) *Fragilaria oceanica, F. ocea.* f. *circularis*, (10) *Leptocylindrus danicus*, (11) *Nitzschia closterium, N. seriata*, (12) *Rhizosolenia fragilissima*, (13) *R. hebetata* f. *semispina*, (14) *Skeletonema costatum*, (15) *Thalassiosira decipiens, T. hyalina, T. nordenskiöldii*, (16) *Thalassiothrix longissima.*

13°C. The most dense population as observed in the above-mentioned region, near lat. 50°N, corresponds to the lowest water temperature, 8.7°C. *Rhiz.* group is predominant as was before, but its components are represented by *Rh. fragilissima* and *Rh. hebetata* f. *semispina*; the former species has been found in June, and the latter never abundant before. On the contrary, *Phaeo.* group decreases in occurrence. *Hyal.* group prevails also in a restricted location near lat. 53°N. Although *Hyal.* group has been present monotonously in the Siberian coast in the former and latter terms of June, it is entirely absent there in July. Together with them, *Ch. atlanticus*, *Ch. convolutus*, *Coscinodiscus* spp., *Dent. marina*, *Leptocylindrus danicus*, *Nitzschia* spp. and *Thal'ra decipiens* are also relatively important, among which the occurrence of *Lept. danicus*, considered to be the north temperate species, is noteworthy.

(4) The former term of August (from 8th to 11th)

The total population of diatoms is also small, less than 3×10^2 cells as in the previous month. At the two stations near lat. 53°N and 59°N, however, the number of diatom cells is fairly large, showing 10^3 cells. The water temperature is about 13°C, which is not so different from that in July. The diatom communities are characterized by the predominant occurrence of *Phaeo.* and *Thal'ra* groups (*Th. decipiens* and *Th. hyalina*) which have been prevalent in June, while *Rhiz.* group, prevailing in the preceding month, decreases remarkably. Although *Thal'ra* group has been observed also in the former term of June, the components of the group are different with months. *Hyal.* group (*Ch. decipiens* and *Ch. distans*), *Lept. danicus* and *Thalassiothrix longissima* are abundant in some restricted locations. Though the amount is not

Table 1. Abridged table showing characteristics of diatom communities from June to August

Period		Former term of June	Latter term of June	July	Former term of August	Latter term of August
Number of stations		8	11	7	9	3
Mean surface water temperature		4.2	6.2	11.2	13.3	12.4
Total number of diatom cells		5×10^5	9×10^4	6×10^2	4×10^2	3×10^3
Percentage of important diatom groups	*Bacteriosira fragilis*	4	2	—	—	—
	Chaetoceros Phaeoceros total	15	33	17	25	42
	Ch. Hyalochaete total	13	13	14	13	41
	Coscinodiscus total	0.0	0.5	4	0.8	2
	Denticula marina	11	5	5	2	—
	Detonula confervacea	9	—	—	—	—
	Fragilaria total	9	0.4	—	—	—
	Leptocylindrus danicus	0.2	—	2	7	—
	Nitzschia total	2	4	5	2	—
	Rhizosolenia total	13	32	40	12	4
	Skeletonema costatum	—	0.5	—	6	11
	Thalassiosira total	21	2	6	24	—
	Thalassiothrix longissima	0.0	5	6	9	0.3

so large, the occurrence of *Skeletonema costatum* which has been entirely absent in the previous months is most distinctive.

(5) The latter term of August (from 12th to 18th)

Although the difference of the water temperature between the former and the latter terms of August is very small, the total population of diatoms comes to increase gradually and it counts more than 2×10^3 cells. The observation stations in this term are only three, so the general features of diatom communities remain unexplained. The leading forms are *Phaeo.* group (*Ch. convolutus* and *Ch. danicus*) and *Hyal.* group (*Ch. debilis, Ch. decipiens, Ch. distans* and *Ch. paradoxus*). Thus the appearance of rather warm water species, viz. *Ch. danicus, Ch. distans* and *Ch. paradoxus*, is characteristic.

The monthly variations of the total population of diatoms and the diatom communities are illustrated in figure 1. In table 1, the mean number of the total diatom cells and the percentage of chief species in each month are shown, abridged from the original planktological data.

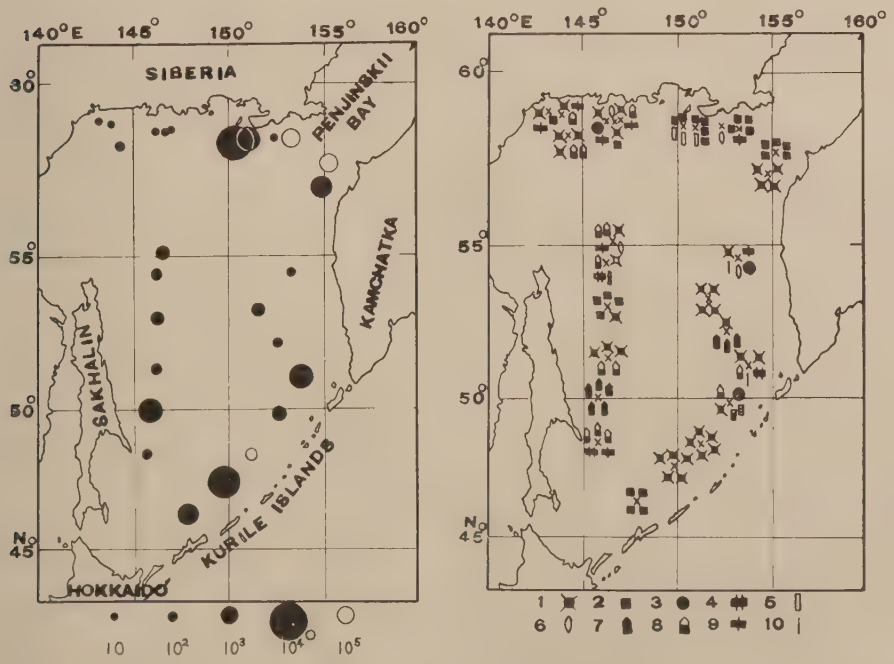

Fig. 2. Cell number of diatoms per liter and diatom communities in July.
(1) *Chaetoceros atlanticus, C. borealis, C. convolutus,* (2) *C. compressus, C. constrictus, C. debilis C. radicans,* (3) *Coscinodiscus marginatus,* (4) *Denticula marina,* (5) *Leptocylindrus danicus,* (6) *Nitzschia closterium, N. seriata,* (7) *Rhizosolenia fragilissima,* (8) *R. hebetata* f. *semispina,* (9) *Thalassiosira decipiens,* (10) *Thalassiothrix longissima.*

3. Horizontal distribution of diatoms in the coastal areas of the Okhotsk Sea in July

The areas near the Kurile Islands and near the mouth of Penjinskii Bay are rich in diatoms, counting 2×10^3 to 4×10^4 cells per liter of water and 3×10^3 to 2×10^5 cells, respectively. On the contrary, along the west coast of Kamchatka, Sakhalin and the Siberian coast between long. 143°E and 150°E, the total population of diatoms is considerably small, less than 5×10^2 cells, and especially in the Siberian coastal waters it shows only 10^2 cells. The chief diatom species are *Phaeo.* group (*Ch. atlanticus*, *Ch. borealis* and *Ch. convolutus*), *Hyal.* group (*Ch. compressus*, *Ch. constrictus*, *Ch. debilis* and *Ch. radicans*) and *Rhiz.* group (*Rh. fragilissima* and *Rh. heb.* f. *semispina*). Among them, *Phaeo.* group is most important in its wide distribution and predominant occurrence, while *Hyal.* and *Rhiz.* groups are also sometimes rather abundant, though in restricted locations. Besides these groups, *Leptocylindrus danicus*, *Skeletonema costatum*, *Thal'ra decipiens* and *Thal'thrix longissima* are more or less numerous.

4. Discussion

The total population of diatoms is large in June, and then it decreases remarkably from July to the former term of August. In the latter term of August, however, it tends to increase gradually. The water temperature is low in June, varying from 2°C to 7°C and, thereafter, from 10°C to 15°C. So, there may be an inverse mutuality between the fluctuation of population and the surface water temperature. Owing to the planktological observations in the west Kamchatka in 1955 (Ohwada, 1957), the densest population of diatoms is observed from May to the first ten days of June, while the water temperature during the same period is quite low, showing from 1°C to 5°C. It is suggested from the above-mentioned facts that the vernal growth in the Okhotsk Sea is observed until the middle of June, when the water temperature is below 6°C.

Among the chief diatoms, *Phaeoceros* group composed of *Ch. atlanticus*, *Ch. concavicornis* and *Ch. convolutus* is most important, from the view point of the wide distribution and abundant occurrence throughout the entire area and period. Both *Hyalochaete* group comprising *Ch. compressus*, *Ch. constrictus*, *Ch. debilis* and *Ch. radicans*, and the *Rhizosolenia* group mainly composed of *Rh. fragilissima* and *Rh. hebetata* f. *semispina* are always present in company with *Phaeo.* group; the distribution of the former is restricted within a certain location and the occurrence of the latter is limited to the period from the latter term of June to July. Excepting these three groups, others can not be found usually throughout all of the months observed. Among them, *Thal'ra* group composed of *Th. decipiens*, *Th. hyalina* and *Th. nordenskiöldii* is relatively important in respect of its predominant presence in the former terms of June and August, respectively. In the case of the observations in the coastal

waters of west Kamchatka in 1955 (Ohwada, 1957), *Thal'ra* group is prevalent from April to May, accompanied by *Fragilaria* group which prevails from April to June. Moreover, owing to the planktological observations near Hokkaidō in the Okhotsk Sea which were made by the Hakodate Marine Observatory (Oceanogr. Rep., 1956, 1957; Kaiyō—Sokuhō 1955), *Thal'ra* and *Fragilaria* groups are never seen in summer, but predominant in spring. As compared with the above-mentioned past observations, the occurrence of *Thal'ra* group in August is considerably characteristic in this observation, while *Frag.* group is not so abundant as in the case of the past observations. In addition to these important species, *Denticula marina*, *Skeletonema costatum* and *Thal'thrix longissima* are fairly abundant in this observation. Although the amount is more or less small, the occurrence of relatively warm water species, viz. *Ch. danicus*, *Ch. distans*, *Ch. paradoxus* and *Leptocylindrus danicus*, is noteworthy after July.

The diatom communities in the adjacent seas of the Okhotsk Sea, which have been reported in the previous paper (Kawarada and Ohwada, 1957: Kawarada, 1957), are not so different from those in the areas of this observation. Nearly all of the kinds of diatom species appearing in these northern seas are of almost the same nature. Only the relative amounts among these representative species are partially different from each other.

5. Summary

There is a remarkably dense population of diatoms in the western areas of the Okhotsk Sea in June, but it greatly decreases in other months, excepting the latter term of August when it tends to increase gradually. The dense population is found in the waters of low temperature, while the paucity of diatoms is closely related to the high water temperature.

The diatom communities in the investigated areas are characterized by the abundance of the following cold water species throughout the whole periods: *Phaeoceros* group (*Ch. atlanticus*, *Ch. concavicornis* and *Ch. convolutus*), *Hyalochaete* group (*Ch. compressus*, *Ch. constrictus*, *Ch. debilis* and *Ch. radicans*) and *Rhizosolenia* group (*Rh. fragilissima* and *Rh. heb.* f. *semispina*). While *Thal'ra* group (*Th. decipiens*, *Th. hyalina* and *Th. nordenskioldii*) is also predominant in June and August, and especially the occurrence in the latter month is characteristic.

The difference of diatom communities among the Okhotsk Sea, Bering Sea and Tōhoku District can not be said to be essentially distinct.

The author is gratefully obliged to Dr. R. Marumo of the Japan Meteorological Agency for his kind guidance in the present study. He is also much obliged to the research staff and crew members of "Hokusei Maru" of the Hokkaidō University for their cooperation in obtaining the plankton samples on which this report is based.

References

(1) Kawarada, Y. and Ohwada, M. (1957): A contribution of microplankton observations to the hydrography of the northern North Pacific and adjacent seas–I. Observations in the western North Pacific and Aleutian waters during the period from April to July 1954. *Oceanogr. Mag.*, Vol. 9, 149-158.

(2) Kawarada, Y. (1957): Ibid.–II. Plankton diatoms in the Bering Sea in the summer of 1955. *Journ. Oceanogr. Soc. Jap.*, Vol. 13, 151-155.

(3) Oceanographical Section and Marine Meteorological Section, Hakodate Marine Observatory (1955): Report of the oceanographic observations in the Okhotsk Sea from June to July, 1955 (In Jap. Mimeogr.). *Kaiyō-Sokuhō*, No. 48, 13-19.

(4) Ibid. (1956): Report of the oceanographic observations of the Okhotsk Sea from April to May, 1956 (In Jap.). *Oceanogr. Rep. Jap. Meteor. Agency*, Vol. 5, 107-112.

(5) Ibid. (1957): Report of the oceanographic observations in the Okhotsk Sea in April, 1957 (In Jap.). *Oceanogr. Rep. Jap. Meteor. Agency*, Vol. 6, 141-145.

(6) Oceanographical Section, Hakodate Marine Observatory (1957): Report of the oceanographic observations in the sea east of Tōhoku District and the Okhotsk Sea from August to September, 1957 (In Jap.). *Oceanogr. Rep. Jap. Meteor. Agency*, Vol. 6, 160-149.

(7) Ohwada, M. (1957): Diatom communties in the Okhotsk Sea, principally on the west coast of Kamchatka, spring to summer, 1955. *Journ. Oceanogr. Soc. Jap.*, Vol. 13, 29-34.

On the Vertical Distribution of Pelagic Copepoda Collected from the Kuroshio Region South of Honshū

By

Kenzo Furuhashi and **Yasuo Matsudaira**

Kobe Marine Observatory *Hiroshima Univerity*

1. Introduction

A series of regular zoeplankton investigations have been carried out by the Kobe Marine Observatory in the warm Kuroshio Current region south of Honshū since May, 1954 to the present time. In the meantime, biological surveys of this area were undertaken by the Tokai Regional Fisheries Research Laboratory (1957), the Japan Meteorological Agency (1951-1954) and others. In all these investigations and surveys, plankton collections were limited to layers above 150 m except in a few cases. Previously, the authors (Matsudaira & Furuhashi: 1955) had made some fragmental vertical collections of zoeplankton in the depths greater than 1000 m with the result of finding a remarkable distribution of planktonic animals and obtaining several rare species of copepods. Then Matsudaira planned collection of deep-sea plankton by divided hauls, and Furuhashi realized this plan in the summer of 1955 on board the R. M. S. Shnupū Maru of the Kobe Marine Observatory.

The present paper presents the results of this collection with special reference to some interesting features of vertical distribution of plankton animals, particularly pelagic copepods.

The authors wish to express their hearty thanks to the members of Oceanographical Section of the Kobe Marine Observatory for the aid rendered for the progress of this study. They are indebted also to the crew of the Shunpū Maru for the assistance in the collection at sea.

2. Methods

Collection of deep-living plankton was carried out at the two stations, K8 and U3, where the characteristics of the warm Kuroshio Current and those of the cold water region were typically represented respectively. A small closing net (51 cm in mouth diameter and made of GG54 bolting silk) was towed vertically in the layers above the depth of 1000 m according to the method of divided hauling. The samples collected were fixed in 5% formalin on the spot and identified later by Furuhashi at the laboratory on land.

During this particular cruise of the Shunpū Maru, zooplankton of the upper layers were collected at the 44 stations distributed over the general area where Stations K8 and U3 were located by towing the O-net (36 cm in mouth diameter

and made of GG54 bolting silk) vertically from the depth of 100 m up to the surface. The results of quantitative determination and taxonomic identification of the obtained samples have already been reported (K. M. O.: 1956).

Fig. 1 shows the positions of collecting stations and the horizontal distribution of water temperature at 400 m at the time of collection.

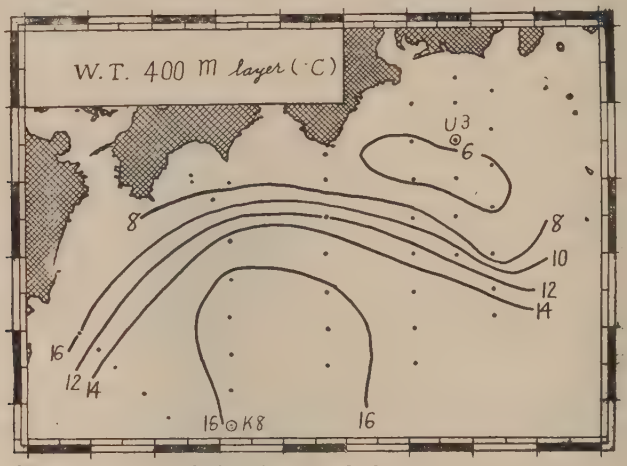

Fig. 1. Horizontal distribution of the water temperature at 400 metres layer. ⊙ sampling stations.

3. Oceanographic conditions

The results of the hydrographic observations conducted by the Kobe Marine Observatory (1956) indicate that there was a cold water region in the Enshū-nada in the summer of 1955, that a counter-clockwise eddy developed in it, and that the stream axis of the Kuroshio was located south of this cold water region (Fig. 1). They indicate also that vertical gradients of water temperature and chlorinity were pronounced over the whole area investigated with the vertical stability being stable near the surface, and that such tendency was particularly conspicuous in the cold water region. Table 1 shows the water temperature and chlorinity observed at different depths at Stations K8 and U3.

Table 1. Water temperature and chlorinity at the stations.

Station	Depth (m)	0	50	100	200	300	400	500	600	1000
K8	W.T. °C	28.4	24.60	21.04	19.43	17.94	16.10	13.48	10.99	3.57
	Cl ‰	19.08	19.12	19.30	19.29	19.25	19.21	19.11	19.02	19.01
U3	W.T. °C	26.0	17.21	14.66	10.49	7.99	6.39	5.30	4.44	3.14
	Cl ‰	18.77	19.14	19.12	19.02	18.97	18.95	18.97	18.98	19.05

4. Results obtained

a) Qualitative analysis.

The plankton animals represented in the samples are divided into three groups; namely, copepods, chaetognaths and other animals. The numbers of the species belonging to each group are shown in Table 2 for different stations and collecting layers.

Table 2. Numbers of the species of copepods, chaetognaths and other animal plankton.

Collecting layers (m)	Station K8			Station U3		
	Copepods	Chaetog.	Others	Copepods	Chaetog.	Others
0 — 100	37	6	16	39	5	17
100 — 250	30	8	11	26	0	9
250 — 500	24	4	7	32	2	7
500 — 750	29	1	6	26	3	7
750 — 1000	30	1	7	34	0	8
Whole layers	95	12	—	95	7	—

One hundred and four species belonging to 40 genera of Gymnoplea and 35 species belonging to 10 genera of Podoplea of Copepoda were identified in the samples. The list of these species appears in the Appendix Table, in which boreal or abyssal forms are marked with an asterisk (*) and those species collected exclusively from the layer above 100 m, with double asterisks (**).

While almost all the surface- and deep-living species of Gymnoplea hitherto collected from the seas near Japan are included in Tanaka's works (1956-'58), there have been only few studies on the Podoplea in the deeper layers of Japanese waters. The present authors previously recorded *Mormonilla phasma*, *Aegisthus aculeatus* and *Conaea rapax* (all belonging to Podoplea) for the first time from the Kuroshio region south of Japan (Matsudaira & Furuhashi: 1955). To add to these, 50 females of *Mormonilla minor* and one female of *Aegisthus mucronatus* are found in the present samples collected at depths over 100 m; neither of these species had ever been recorded from the neighboring waters of Japan.

Calanus cristatus, *Cal. plumchrus*, *Pareuchaeta japonica*, *Metridia lucens*, etc. are common in both upper and deeper layers of the Oyashio (subarctic cold water) region, and are distributed also in the deeper layers of the Japan Sea (Anraku: 1954, Motoda & Anraku: 1954, Bogorov: 1958, Furuhashi: 1953, etc.). It is interesting, therefore, that these species are totally absent in the present samples. Actually, it seems probable that the cold water mass, which originates from the Oyashio and extends

under the Kuroshio Current south of Honshū, did not occur in the summer of 1955.

It is also noteworthy that whereas oceanographic conditions differ considerably between the upper and deeper layers, the number of the copepod species that occur in each layer varies very little. Furthermore, the species which are taken in a given layer account for only a small fraction of all the species that are taken at the respective station. These facts lead one to speculate that many of the species probably occurred only in one of the collecting layers, with small number of species being distributed over wider bathymetric ranges. From this viewpoint, the copepod species are grouped according to the types of vertical distribution, and the numbers of the species belonging to each group are shown in Table 3. In this table, the first five groups occurred in one collecting layer only, and the following groups showed wider bathymetric distribution.

Table 3. Number of copepod species by types of vertical distribution.

Collecting layer (m)					Stations	
0 | 100	100 | 250	250 | 500	500 | 750	750 | 1000	K 8	U 3
○	•	•	•	•	19	20
•	○	•	•	•	8	9
•	•	○	•	•	4	10
•	•	•	○	•	11	7
•	•	•	•	○	13	11
		(Total)			(55)	(57)
○	○	•	•	•	8	2
•	○	○	•	•	4	1
•	•	○	○	•	3	2
•	•	•	○	○	5	5
○	○	○	•	•	3	1
•	○	○	○	•	2	2
•	•	○	○	○	3	1
○	○	○	○	•	0	1
•	○	○	○	○	0	3
○	○	○	○	○	0	2
		Other types			12	18
		Total numbers			95	95

○ indicates the layer where the respective species occurred.

It is clear from this table that those species which occurred only in one collecting layer account for a greater portion (about 60%) of the whole species. Two species, namely, *Calanus helgolandicus* and *Oncaea venusta*, occurred in all layers at Station U3, but no species showed such distribution at Station K8. It is also indicated in this table that the numbers of the species which occurred in two or more layers differ slightly between the two stations.

It should be borne in mind that, with reference to water temperature, the 2nd and 3rd layers of Station K8 correspond nearly to the surface layer of Station U3, the 4th layer of the former to the 2nd layer of the latter, and the 5th layer of the former to the 3rd and 4th layers of the latter (see Table 1). Then, it seems that the difference between the vertical distributions of copepods at Stations K8 and U3 is not of intrinsic nature, but was caused by the upwelling of deeper water at Station U3.

It was shown in our previous paper that the catch was of monotonous composition, constituted mainly by *Calanus helgolandicus---Eucalanus bungii californicus*, in a vertical haul made from the depth of 2000 m up to 1300 m in the same general region where the present samples were taken. In contrast, none of the present samples showed such monotonous composition. This is probably due to the greater gradients of physical and chemical environmental factors in the layers above 1000 m than in the layers below.

b) Quantitative analyis.

The plankton animals appearing in the samples are divided into three groups as in the preceding section, and the population density (i. e., the number of individuals per 10 m^3 of sea water) of each group is shown in Table 4 for each station and collecting layer.

Table 4. Population density of copepods, chaetognaths and other zooplankton.

Station	K 8					U 3				
Location Lat. (N)	29-40					33-30				
Long. (E)	134-10					137-38				
Date	August 21, 1955					September 2, 1955				
Time	01-53	02-45	03-00	03-20	03-45	18- 45	20-00	21-45	20-35	20-50
Hauled distance (m)	0-100	88-250	264-500	460-720	690-1030	0-100	145-250	245-500	522-700	810-1100
Wire angle (degree)	10	10	13	17	17	17	10	15	30	40
Hauld depth (m)	0-98	87-246	257-487	444-696	666-995	0- 96	143-246	237-483	452-606	620-842
Total plankton /10m^3	3444	356	174	102	80	3548	475	318	201	90
Copepods /10m^3	2448	260	115	70	61	2084	340	201	126	58
Chaetognaths /10m^3	96	19	7	1	1	164	4	6	4	1
Other zooplankton/10m^3	900	77	52	31	18	1300	131	111	71	31

It appears that copepods lived in the majority near the surface layer, and decreased suddenly in number to the order of one tenth or less below the depth of 100 m at each station. It is noteworthy, however, that the rate of decrease became rather small in the deeper layers. The same tendency was seen in other groups. In the layers above 250 m the dominant species of Copepoda were *Oithona plumifera* and *Oncaea venusta* of Podoplea, which accounted for more than 10% of the whole copepods. In deeper layers, *Mormonilla minor* and *Conaea rapax* were dominant in number, but their ratio to the whole copepods did not reach 10%.

5. Summary

1. Description is made of the vertical distribution of pelagic copepods which was observed in the collections made with divided hauls in the summer of 1955 in the warm Kuroshio Current region south of Honshū.

2. One hundred and thirty five species of copepods are identified. The majority of these species occurred in one collecting layer only, while the rest of them occurred over wider bathymetric ranges.

3. *Mormonilla minor* and *Aegisthus mucronatus* are recorded for the first time in this region.

4. The cold water species which are usually dominant in the Oyashio region are not found in the present samples, even in the ones from deeper layers.

5. Population density of copepods is high in the upper layers (i. e., above 100m), and decreased to about one tenth or less in deeper layers.

Monotonous composition of copepods is not encountered in any layer.

6. Exploration of the deep living plankton will hereafter explain many useful unknown phenomena on deep water systems and environmental conditions of deep living organisms.

References

(1) Anraku, M. (1954): Gymnoplea Copepoda collected in Aleutian waters in 1953. *Bull. Facul. Fish., Hokkaido Univ.*, Vol. 5, No. 2.

(2) Bogorov, B. G. (1958): Biogeographical regions of the plankton of the North-Western Pacific Ocean and their influence on the deep sea. *Deep-Sea Research*, Vol. 5, No. 2.

(3) Furuhashi, K. (1953): On the vertical distribution of animal plankton in the Sea of Japan off San'in-District in summer of 1952. *Publ. Seto Mar. Biol. Lab.*, Vol. 3, No. 1.

(4) Giesbrecht, W. (1892): Systematik und Faunistik der pelagischen Copepoden des Golfes von Neapel. *Fauna und Flora des Golfes von Neapel*, XIX.

(5) Honjo, K. et al (1957): Distribution of Copepoda in the "Kuroshio" area, south of Honshū, May 1955. *Records of Oceanographic works in Japan*, Special Number.

(6) Japan Meteorological Agency (1951-'54): *The Results of Marine Meteorological and Oceanographical Observations*, Nos. 6-13.

(7) Kobe Marine Observatory (Oceanog. Sec.) (1956a): *Ibid.*, No. 17.
(8) Kobe Marine Observatory (Oceanog. Sec.) (1956b): Report of the oceanographic observations in the sea south off Honshū in August, 1955. *Ocean. Rep. Central Meteorological Observatory*, Vol. 4, No. 4.
(9) Matsudaira, Y. & Furuhashi, K. (1955): Notes on some animal plankton collected from the deep layers of the Pacific waters off southern Japan, *Umi To Sora*, Vol. 31, No. 5 & 6. (In Japanese, with English abstract.)
(10) Motoda, S. & Anraku, M. (1955): Further observation on the daily change in amount of catches of plankton animals in vertical hauls. *Bull. Facul. Fish., Hokkaido Univ.*, Vol. 6, No. 1.
(11) Tanaka, O. (1956-'58): The pelagic copepods of the Izu Region, middle Japan, systematic account I-V, *Pub. Seto Mar. Biol. Lab.*, Vol. V, No. 2–Vol. VI, No. 3.

Appendix Table

List of Copepods. (*shows abyssal or boreal forms, **shows surface water forms.)

Suborder Gymnoplea

Fam. Calanidae
- *Calanus helgolandicus* (Claus)
- *Cal. tenuicornis* (Dana)
- *Cal. minor* (Claus)
- *Canthocalanus pauper* (Giesbrecht)
- *Undinula darwini* (Lubbock)
- *U. vulgaris* (Dana)

Fam. Eucalanidae
- *Eucalanus attenuatus* (Dana)
- *Eu. elongatus* (Dana)
- *Eu. bungii californicus* Johnson
- *Eu. crassus* Giesbrecht
- *Eu. mucronatus* Giesbrecht
- *Eu. pileatus* Giesbrecht
- *Eucalanus subtenuis* Giesbrecht
- *Rhincalanus cornutus* Dana
- *Rh. nasutus* Giesbrecht
- *Mecynocera clausi* Thompson**

Fam. Paracalanidae
- *Paracalanus aculeatus* (Giesbrecht)
- *Par. parvus* Giesbrecht
- *Par.* sp.*
- *Acrocalanus gracilis* Giesbrecht
- *Calocalanus pavo* (Dana)

Fam. Pseudocalanidae
- *Clausocalanus arcuicornis* (Dana)
- *Cl. pergens* Farran
- *Cl. furcatus* (Brady)**
- *Ctenocalanus vanus* Giesbrecht
- *Pseudocalanus* sp.*
- *Spinocalanus spinosus* Farran*
- *S. magnus* Wolfenden*
- *S. angusticeps* Sars*
- *Monacilla typica* Sars*
- *Drepanopsis orbus* Tanaka*

Fam. Aetideidae
- *Aetideus acutus* Farran
- *A. giesbrechti* Cleve
- *A. bradyi* A. Scott
- *Aetideopsis multiserrata* Wolfenden*
- *Chiridius carnosus* Tanaka*
- *Ch. poppei* Giesbrecht
- *Gaetanus* sp.*
- *Euchirella curticauda* Giesbrecht
- *E. bitumida* With
- *Chirundina streetsi* Giesbrecht
- *Undeuchaeta plumosa* (Lubbock)
- *Euchaeta marina* Prestandrea
- *E. wolfendeni* A. Scott**
- *E. longicornis* Giesbrecht
- *E. media* Giesbrecht
- *E. spinosa* Giesbrecht
- *Pareuchaeta russeli* (Farran)
- *Par. simplex* Tanaka*
- *Amallophora* sp.*
- *Scottocalanus helenae* (Lubbock)
- *S.* sp.*
- *Scaphocalanus magnus* (T. Scott)

S. elongatus A. Scott*
S. longifurca (Giesbrecht)*
S. temporalis Tanaka*
S. sub-brevicornis (Wolfenden)
S. sp.*
Scolecithrix danae (Lubbock)
Scolecithricella propinqua Sars*
S. vittata (Giesbrecht)
S. emarginata Farran
S. dentata (Giesbrecht)
S. arcuta Sars*
S. longipes (Giesbrecht)*
S. ctenopus (Giesbrecht)
S. ovata (Farran)
S. sp.*

Fam. Temoridae
Temora discaudata Giesbrecht**

Fam. Metriidae
Metridia curticauda Giesbrecht*
M. brevicauda Giesbrecht*
M. venusta Giesbrecht*
M. princeps Giesbrecht*
Pleuromamma abdominalis (Lubbock)
P. xiphias Giesbrecht
P. gracilis Claus
P. robusta Giesbrecht

Fam. Lucicutiidae
Lucicutia flavicornis (Claus)
L. ovalis Wolfenden
L. longiserrata Giesbrecht*
L. curta Farran*
L. clausi Giesbrecht*

Fam. Heterorhabdidae
Heterorhabdus papilliger (Claus)
H. dubius Tanaka*
H. robustus Farran*

Fam. Augaptilidae
Euaugaptilus magnus Wolfenden*
E. nudus Tanaka*
E. hecticus (Giesbrecht)*
Haloptilus longicornis (Claus)
Hal. acutifrons (Giesbrecht)
Hal. ornatus (Giesbrecht)
Hal. spiniceps (Giesbrecht)

Fam. Arietellidae
Phyllopus helgae Farran*
Ph. mutatus Tanaka*

Fam. Candaciidae
Candacia bipinnata (Giesbrecht)
Can. aethiopica (Dana)**
Can. catula (Giesbrecht)
Can. truncata (Dana)**
Can. bispinosa (Claus)
Can. longimana (Claus)

Fam. Pontellidae
Labidocera acutifrons (Dana)
Lab. detruncata (Dana)

Fam. Acartiidae
Acartia danae Giesbrecht
A. negligens Dana

Suborder Podoplea

Fam. Mormonillidae
Mormonilla phasma Giesbrecht*
Mor. minor Giesbrecht*
Oithona plumifera Baird
O. setigera Dana
O. robusta Giesbrecht
O. similis Claus

Fam. Harpacticidae
Microsetella rosea (Dana)
Setella gracilis Dana
Aegisthus mucronatus Giesbrecht
A. aculeatus Giesbrecht*

Fam. Oncaeidae
Oncaea venusta Philippi
On. mediterranea Claus
On. media Giesbrecht
On. conifera Giesbrecht
On. sp.*
Conaea rapax Giesbrecht
Lubbockia squillimana Claus
Lub. marukawai Mori

Fim. Corycaeidae
Copilia mirabilis Dana**
Cop. denticulata Claus
Corycaeus flaccus Giesbrecht
Cor. furcifer Claus
Cor. speciosus Dana
Cor. longistylis Dana
Cor. concinnus Dana**
Cor. gibbulus Giesbrecht**
Cor. clausi F. Dahl
Cor. crassiusculus Dana
Cor. limbatus Brady
Cor. typicus Kröyer
Cor. pacificus M. Dahl

Summer Temperature in North Japan Related to the Tropospheric Zonal Wind Profile

By

Ken Suda

Japan Meteorological Agency

ABSTRACT

The relationship between summer temperature in north Japan and the distribution of zonalwind on 500mb level is studied on the basis of 5-day mean maps for 5 years of 1949 — 1953. It is found that the latitudinal position of the mean jet is a decisive factor for temperature anomaly: its northward and southward shift from its normal position bring about respectively persistent warmth and coolness in north Japan.

The relationship between surface temperature distribution in the Far East and the zonal index was noticed soon after the start of regular construction of 500mb maps in JMA. Since then, the zonal index has been used by long-range and extended-range forecasters as an indicator of temperature trend, but its study has been confined to the treatment of special weather conditions [1, 2, 3] or of restricted latitudinal range [4] and no systematic survey on the subject has yet been made. In the present report, it is attempted to make clear the distribution of tropospheric zonal wind which characterizes high and low temperatures in north Japan in summer.

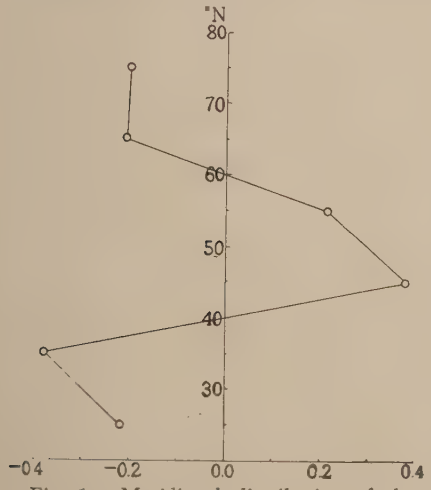

Fig. 1. Meridional distribution of the correlation coefficients between zonal index for consecutive latitudes 10° apart and temperature at Miyako, both in anomaly of 5-day mean.

As is done in the similar study on winter season [5], the temperature regime of north Japan is represented by the 5-day mean temperature anomaly at Miyako (585), and the latter is correlated with the difference from each other of 5-day mean 500mb height anomalies averaged along latitudinal circles, ten degrees apart, for the range of 90°E eastward to 180°. Such height anomaly difference may be considered the indicator of zonal westerlies and is called here the zonal index for the respective latitudinal range. As the basic material, 5-day mean 500mb charts covering four summer months of May to August in 1949–1953 prepared by the Meteorological Research Intitute are used; they are $25 \times 5 = 125$ in number.

The result is represented by the meridional distribution of correlation coefficients as shown in Table 1 and Fig. 1. As will be seen in

Table 1.

latitude range	20—30°	30—40°	40—50°	50—60°	60—70°	70—80° N
correl. coef.	−0.218	−0.378	0.382	0.214	−0.209	−0.200

these, summer temperature at Miyako is correlated positively in the latitudinal range of 40°-60°N and negatively to the north and south. This is the same result as we found for winter season [5] suggesting that southward shift of the axis of the strongest westerlies is favorable to low temperature in north Japan, whereas its northward shift to high temperature.

Here, it may be worth special mention that the sign of the correlation coefficient changes abruptly at 40°N. In consequence of this, while the zonal index computed for the range of 40°-60°N is fairly high being 0.491, that for 30°-50°N is -0.038 and is practically useless as an indicator of temperature. Therefore, the zonal index for the former range should be used in the forecasting practice as far as the temperature of north Japan is concerned.

In order to visualize the relation between the zonal index for 40°-60°N and the temperature at Miyako, 3-pentad running averages of the both quantities in 5-day mean anomaly are computed for three summers of 1949 - 1951 and shown graphically in Fig. 2. As can be seen readily from this, parallelism of the general trend of temperature (solid line) and of zonal index (broken line) is evident, although

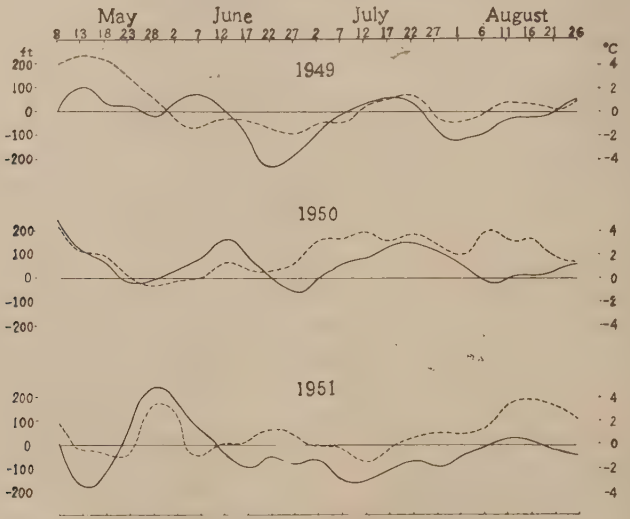

Fig. 2. 3-pentad running averages of zonal index anomaly for 40° — 60°N (full) and of temperature anomaly (dashed) at Miyako. Ordinate in hundreds of foot and degrees centigrade, abscissa in day of month.

there are some minor discrepancies.

Having established the relationship between temperature in north Japan and the zonal index for 40°–60°N, we may proceed to make clear the broadscale mechanism leading to persistent coolness or warmth. First of all, to find the longitude contributing most to the above relationship, 5-day mean height difference anomalies between 40°N and 60°N are computed for each meridian and correlated with the temperature anomaly at Miyako. From the result thus obtained as shown in Table 2, we see that the correlation coefficient is the highest for the 150th meridian (a little to the east of north Japan) and drops on both sides of it.

Table 2.

longitudinal range	90°	100°	110°	120°	130°	140°
correl. coef.	0.143	−0.120	−0.012	0.131	0.278	0.444
longitudinal range	150°	160°	170°	180° E		
correl. coef.	0.579	0.395	0.239	0.141		

Then, to see the actual wind distribution over Japan characteristic for high and low temperatures, 17 cases of extreme coolness and 19 cases of extreme warmth at Miyako are selected from the 5-day mean temperature records for the summer seasons of five years 1949–1953, and for each of them, a composite profile of geostrophic zonal wind speed along 140th meridian is constructed as shown in Fig. 3. A glance at it may be sufficient to see that both of the curves for high temperature (full) and low temperature (dashed) show respectively a sharp maximum in middle latitudes.

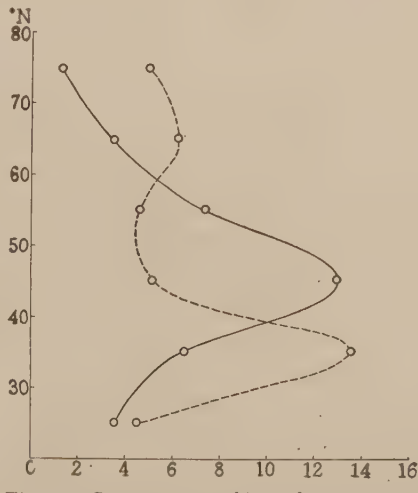

Fig. 3. Composite profiles of geostrophic zonal wind along 140° E for 19 cases of extreme high (full) and 17 cases of extreme low (dashed) 5-day mean temperature at Miyako. Abscissa in m/sec, ordinate in degrees of latitude.

Undoubtedly, this indicates the position of the mean jet stream or the tropospheric frontal zone. However, its position shows a marked difference for high and low temperature cases: in the former it is located in the range of 40°–50°N, whereas in the latter it is in 30°–40°N. In view of this marked difference in the

wind profile, it is evident that the position of the jet is a decisive factor for the temperature in north Japan: its northward and southward shift from normal position around 40°N leads respectively to warmth and coolness. The peculiar feature of the distribution of the correlation coefficients illustrated in Fig. 1 and Table 1 with a positive maximum in 40°-50°N and a negative maximum in 30°-40°N confirms the generality of the relationship.

Next, in order to see what upper-air pattern corresponds to such abnormality in the position of the jet stream, eight cases are chosen from each of the 19 warm and 17 cool cases mentioned above and, based on them, composite maps of 500mb contours and anomalies are constructed as shown in Fig. 4. In the selection of component maps, meridional distribution of zonal wind speed is considered and cases with especially high and low zonal index taken along 150°E for the range of 40°-60°N are chosen, in order to amplify the difference in the latitude of the jet.

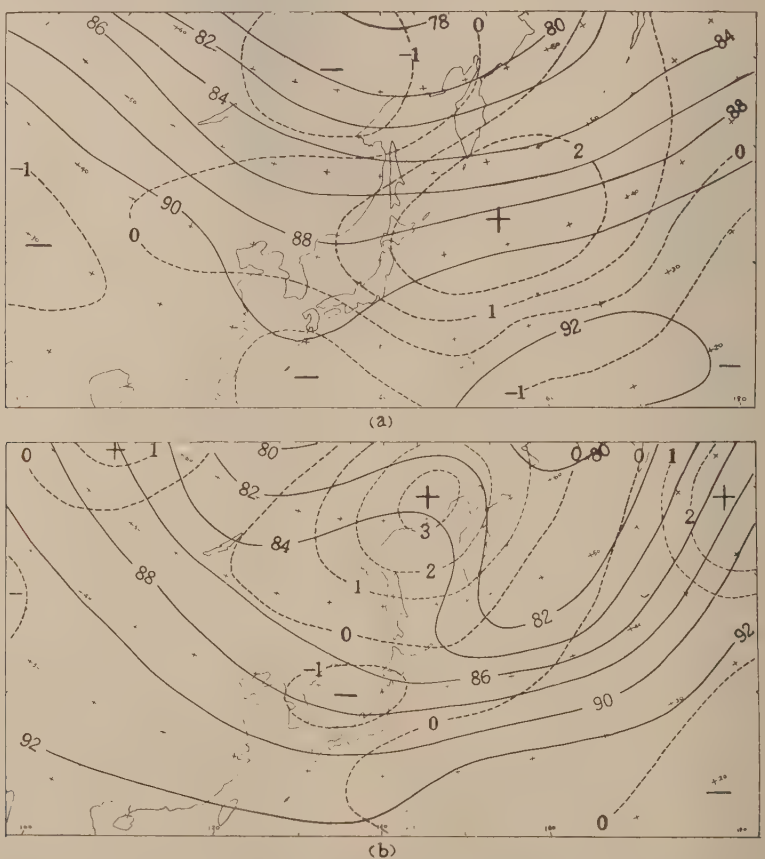

Fig. 4. Composite 5-day mean 500mb maps for eight high temperature cases (a) and eight low temperature cases (b) at Miyako. Contours in full and anomalies in dashed lines are drawn 200ft and 100ft apart respectively.

Comparing the maps for high temperature (Fig, 4-a) and low temperature (Fig. 4-b) with each other, we see that there is a fundamental difference between them. In the case of high temperature, the vast area extending from Aleutian Is. toward Manchuria is covered by positive anomaly centered in the northeast of Japan, whereas Siberia and the lower latitudes of the north Pacific is covered by negative anomaly. Contours are zonal and the mean jet, identified with the zone of crowded contours, is located to the north of Japan as we mentioned already. In contrast, in the case of low temperature, an intense positive anomaly covers northeast Siberia and the Sea of Okhotsk, and the area which showed positive anomaly in (a) is now covered by negative anomaly. Corresponding to this, contours show a marked undulation forming an intense ridge over the Sea of Okhotsk and an intense trough over the area extending from the middle of Bering Sea toward the south of the Kurile Is.

From what we have found through the study of zonal wind profile and upper-air pattern described so far, we may explain the mechanism of persistent warmth and coolness in north Japan in the following way.

As has been already mentioned, the axis of the strongest westerlies or the mean jet on the 500mb level represents the tropcspheric frontal zone, along which the meridional temperature gradient in the lower tropcsphore is greatest [6]. Accordingly, this is also the zone of frequent formation of surface fronts and frontal cyclones.

Now if the jet is displaced to the north of its seasonal normal (Fig. 4-a), surface frontal zone will also be shifted northward and the cyclonic activity will be confined to the north of Japan. The country will then be covered by the tropical air to the south of the frontal zone and warm weather will prevail there. In contrast to this, if the jet is displaced to the south (Fig. 4-b), surface frontal zone will be shifted southward too and the cyclogenesis will be activated along the southern coast of Japan. The cold air originating from the sea area to the northeast of Japan, where the center of cold is located in this season (see e. g. [7], pp. 35-38), will then invade north Japan as northeasterly wind, bringing there cool weather.

Hereby, the significance of the blocking situation with a ridge over the eastern Siberia and a trough extending along the Kurile Is. (see Fig. 4-b) should not be minimized in its effect of steering cold air southward. As has been pointed out previously [8], such configuration of trough and ridge is liable to appear in the Far East in accompaniment with the southward shift of the jet and must be studied in detail for the understanding of the mechanism of persistent coolness. However, for lack of space, this is left for a separate report.

To see the validity of the above reasoning on actual data, frequency of the passage of surface fronts across each $10° \times 10°$ quadrangle is read off from the component daily charts of the two sets of eight 5 day periods, for which the composite maps in Fig. 4-a and 4-b are constructed. The frequency, after a proper correction

of latitude, is then plotted in the middle of the respective quadrangle and isolines are drawn (Figs. 5-a and 5-b).

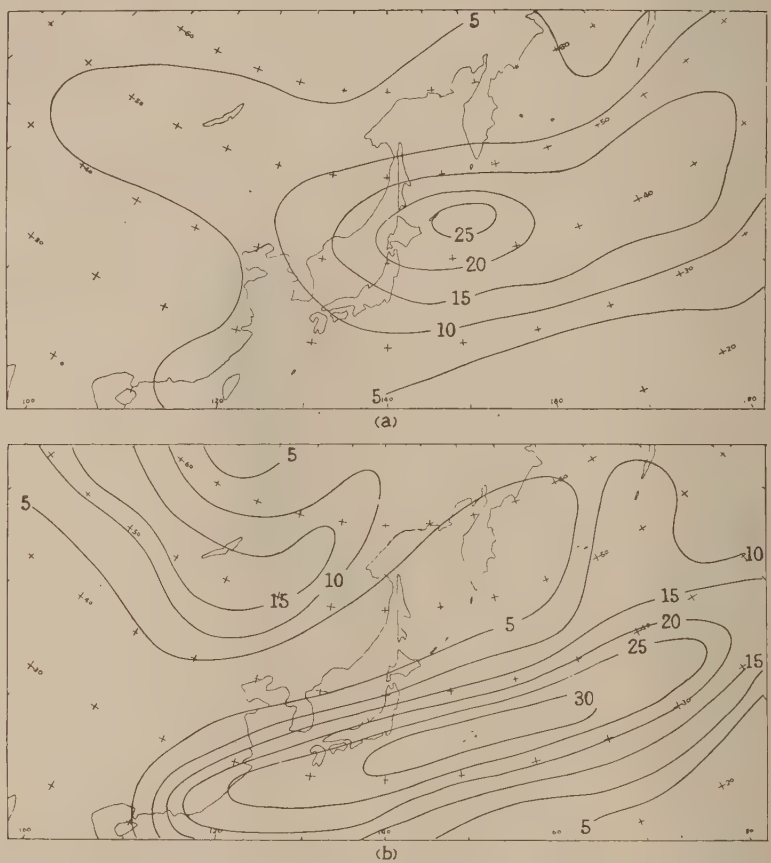

Fig. 5. Frequency distribution of surface fronts for eight 5-day periods of high temperature (a) and eight 5-day periods of low temperature (b) at Miyako. Number of frequency is counted on 40 component daily charts for each 10°×10° quadrangle and reduced to the range of 30°—40°N.

Comparing these with each other, we see that the upper-air pattern characteristic to high and low temperature in north Japan is reflected clearly on the distribution of surface fronts. In the case of warmth (Fig. 5-a), the surface frontal zone, which may be identified with the axis of maximum frequency, runs from the Kurile Is. eastward, in the zone of 40°-50°N, whereas in the case of coolness (Fig. 5-b), it is located farther south and extends from the southern coast of Japan to the middle of the North Pacific in the zone of 30°-40°N showing a maximum of frontal actity to the east of Japan. Such features of the distribution of surface fronts clearly point

to the fact that the latitudinal position of the mean jet or the tropospheric frontal zone (see Fig. 3) is a governing factor of the temperature anomaly in north Japan as we have postulated already.

Conclusion

The results obtained from the present study may be summarized as follows:

(1) Temperature in north Japan is correlated with the zonal index on 500mb level positively for 40°-60°N and negatively for the latitudinal ranges to the north and south, with a positive and a negative maximum in 40°-50°N and 30°-40°N, respectively.

(2) Persistent warmth and coolness in north Japan may be understood as the result of northward and southward shift of the mean jet stream or the tropospheric frontal zone. This relationship is due to the movement of surface frontal zone in accompaniment of the latter.

(3) Abnormally high and low temperatures in north Japan are characterized by peculiar upper-air patterns: zonal contours with positive anomaly over the area extending from Aleutian Is. toward Manchuria for the case of high temperature; a ridge with positive anomaly over northeast Siberia and the Sea of Okhotsk and a trough with negative anomaly over the sea area to the northeast of Japan for the case of low temperature.

References

(1) Suda, K. (1955): On the cold wave of January 1954 in the Far East. *Geofisica pura e Applicata*, Vol. 32, 159 — 169.

(2) Suda, K. (1956): A persistent cold-outbreak in the Far East related to the blocking situation. *Journal of the Met. Soc. of Japan*, Ser. II, Vol. 34, 13 — 22.

(3) Suda, K. (1956): On the unusual hot summer of 1955. *Journal of Met. Research*, Vol. 8, 463 — 472 (in Japanese).

(4) Asakura, T. (1956): Studies on the seasonal weather forecasting (V, b). *Papers in Meteorol. and Geophys.* Vol. 6, 221 — 227.

(5) Suda, K. (1959): A study on the dynamic climatology of cold outbreaks in the Far East. *Geophys. Magazine*, Vol. 29, 413 — 461

(6) Pogosyan, Kh. P. (1959): *Obshchaya Tsirkulyatsiya Atmosfery*. Gidrometeoizdat, Leningrad.

(7) *Normal Weather Charts for the Northern Hemisphere*, U.S. Weather Bureau, Washington, 1952.

(8) Suda, K. and T. Asakura (1955): A study on the unusual Baiu season in 1954 by means of northern hemisphere upper-air mean charts. *Journal of the Met. Soc. of Japan*, Ser. II. Vol. 33, 233 — 244.

On the Evolution of a Tropical Cyclone in Relation to Its Life Cycle

By

Hiroshi Matano

*Osaka District Central Meteorological Observatory**

ABSTRACT

An evolutional hypothesis of tropical cyclone in relation to its life cycle is presented. The hypothesis mentions that a tropical cyclone does not develop into a severe typhoon by itself but evolves into a severe typhoon by the outbreak of a severe whirl wind system, which is the origin of severity of typhoon, within the inner core of a tropical cyclone, and that this composite system drops out the severe whirl wind system during the passage over the Japanese Islands, to survive the tropical cyclone which makes a complex system with an extratropical cyclone induced on the pre-existing front with which the survived tropical cyclone contacts after invading into the middle latitudes.

1. It has been experienced that the severe typhoon hittng the Japanese Islands indicates some characteristics on the sequence weather maps during the passage over the Japanese Islands, which are described as follows;

(1) The outer isobaric pattern, say outside the 990mb isobar, almost conserves its shape and dimension, though the inner isobaric pattern near the center of typhoon changes greatly, therewith the central pressure fills up rapidly, say from 930mb to 970mb.

(2) The center of typhoon lies eccentrically to the whole isobaric pattern when the central pressure is deep.

(3) The central eccentricity of typhoon disappears after the central pressure reaches a nearly steady value, the double centers being used to appear before the period of the quasi-constancy of the central pressure.

(4) One of the double centers lies on the path of the center of the outer isobaric pattern to stand for the center of typhoon after the double centers disappear. On the other hand, the rest of the double centers stands for the previously recognized center of typhoon before the double centers appear.

(5) Thus the center of typhoon seems to transfer its path from the previously recognized central path before the double centers appear to the dormant path of the center of the outer isobaric pattern after the double centers disappear.

2. These characteristic behaviors of typhoon leads to the conception that the severe typhoon hitting the Japanese Islands is not a single cyclonic system as it pretends in appearence, but is composed of two cyclonic systems, one of which is the severe

* Present affiliation: Osaka Air Weather Station.

cyclonic system of smaller scale in rapidly decaying nature over the Islands, and the rest is the cyclonic system of larger scale in almost conserved nature. This conception being introduced into the synoptic analysis, the above mentioned behaviors are fairly well explained in the light of the meteorograms and the observed records taken at the stations within the area of typhoon. This is the synoptic background of the Theory of Main and Secondary Typhoons presented by Namekawa and Aoki.[1] [2]

Analytical results based upon this conception applied to many cases are summarized as follows,

(1) The isobaric pattern after the double centers disappear is the manifestation of the quasi-conserved cyclonic system of larger scale to be considered the mature tropical cyclone and is named the main typhoon (or vortex). The center of typhoon in this period is therefore nothing but the center of this vortex.

(2) The dormant isobaric pattern of the main vortex before the double centers appear is replaced by the above mentioned isobaric pattern of the main vortex in accordance with the previously peeping outer isobaric pattern. Thus the actual isobaric pattern in this period is decomposed of two cyclonic systems and the isobaric pattern of the severe whirl wind system of smaller scale in rapidly decaying nature over the Japanese Islands is obtained on the sequence weather maps. This smaller but severe whirl wind system is considered the origin of severity of typhoon and is named the secondary typhoon (or vortex). The apparent center of typhoon in this period stands for the center of this vortex.

(3) Bjerknes' vortex is adopted to the isobaric patterns of each systems, to treat semi-quantitatively the analysis. Thus the actual isobaric pattern is represented by

$$P = P_\infty - \underbrace{\frac{\pi'}{1+\left(\frac{r'}{b'}\right)^2}}_{\text{(main)}} - \underbrace{\frac{\pi}{1+\left(\frac{r}{b}\right)^2}}_{\text{(secondary)}}$$

where P: the pressure at the point in the distances r' and r from the centers of main and sceondary vortices,

P_∞: the surrounding pressure,

π' and π; the lowerings of central pressures of each vortex from the surroundings, representing the rotation intensity of the vortex,

b' and b: the radii of the inner cores of each vortex, representing the horizontal dimension of the vortex, in accordance with the radius of the maximum wind zone of the vortex.

The synoptic behaviors of each vortex are physically defined by these two sets of parameters, namely π' and b', and π and b. The analytical results through the investigation of many cases show that π', b' and b are almost conserved though

π varies greatly during the passage over the Japanese Islands. Further investigation by the present writer[3] clears the damping behavior of the vortex theoreticcally to explain the analytical results and also he shows the fact that the main vortex has the universally constant vorticity in its inner core during the passage over the Japanese Islands.

3. It is very interesting to study the situation that a tropical cyclone comes into a severe typhoon over the tropical ocean prior to the arrival at the Japanese Islands for the continuation of the above mentioned conception as well as for the practical purpose. As a matter of course, it is considered that a tropical cyclone does not develop into a severe typhoon by itself, but evolves into a severe typhoon by the birth of secondary vortex, the essential origin of the severity of typhoon, and that a tropical cyclone itself is maintained as the main vortex. This postulation is synoptically and statistically confirmed by the present writer[4] [5] to obtain the systematic behaviors of typhoon over the tropical ocean through the investigation of many cases. The results are summarized as follows;

(1) b' and b are almost conserved throughout the whole life of the main and secondary vortex.

(2) The main vortex develops gradually until it posseses the universally constant vorticity at the mature stage.

(3) The secondary vortex forms in the inner core of the main vortex, southeast of the center of main vortex, and the relative positon of both centers are almost conserved until the secondary vortex decays out over the Japanese Islands.

4. It is often experienced that a typhoon pretends to transform into an extratropical cyclone after entering into the middle latitudes, and that this cyclone redevelops sometimes even after decaying inclination. It is also experienced that the double centers appear in these situations. It is very natural to consider that the main vortex survives holding considerable intensity even though it decays slowly after the passage over the Japanese Islnds, and that the main vortex is difficult to transform so rapidly into a different nature, especially into a redevelopment nature. Based upon this postulation, the actual isobaric pattern is analyzed in use of the known field of the main vortex, through the investigation of many examples successfully carried out by Sekioka.[6] [7] [8] The results of investigation give the dormant field typical to the frontal wave cyclone development on the sequence weather maps. The double centers are explained that one of them is the center of the main vortex and the rest is the center of the separated extratropical cyclone which is dormant when the cyclone is nascent. Thus the typhoon entering into the middle latitudes in the appearence of the extratropical cyclone does not transform directly into the extratropical cyclone but induce the formation of the extratropical cyclone on the preexisting front with which the inner core of the main vortex contacts and the main

vortex survives with considerable intensity though in the decaying stage to make a complex of the main vortex and the newly formed extratropical cyclone. This conception explains fairly well the complicated features on the weather maps and on the meteorograms at the stations passed by the typhoon in this phase.

5. Thus the evolution of a tropical cyclone in relation to its life cycle is described by the present writer[9] as follows;

(1) Shortly after the formation of a tropical cyclone, it exhibits a weak circulation pattern with the inner core of about 200km radius. This is termed "Nascent Main Vortex (or Typhoon).

(2) This formative main vortex develops, conseving the radius of its inner core, to the circulation pattern with the central pressure drop of about 30mb. The tropical cyclone at this stage is termed "Mature Main Vortex (or Typhoon).

(3) A secondary vortex is, at times, formed in the inner core of the main vortex in the developing or mature stage. The tropical cyclone thus evolves into a first-class typhoon when the violent secondary vortex forms.

(4) This two-vortex typhoon rapidly loses its secondary vortex during its passage over the Japanese Islands.

(5) The tropical cyclone or main vortex, which invades the middle latitudes, sometimes makes for the formation of the extratropical cyclone on the pre-existing front to make a complex system of the main vortex and the extratropical cyclone.

6. The hypothes's described here is found to be well applied to the hurricane hitting the United States, the similitude of the typhoon hitting the Japanese Islands, and it is shown that hurricane has the same synoptic structure as that of typhoon.[10]

References

(1) Namekawa, T. and Aoki, S. (1936): A view of the structure of Muroto Typhoon. *Mem. Coll. Sci. Kyoto Imp. Univ.* Ser. A, Vol. 19, No. 2.

(2) Namekawa, T. and Aoki, S. (1954): On the structure of the disastrous typhoon hitting the Japanese Islands. *Proc. UNESCO symp. on Typhoons.* Nov. 9–12, 1954. Tokyo.

(3) Matano, H. (1956): On the role of the lateral mixing in the cyclostrophic flow pattern in the atmosphere. *Jour. Met. Soc. Japan,* Ser. II, Vol. 34, No. 3.

(4) Matano, H. (1957): A synoptic study of the formation of severe typhoon over the tropical ocean. *Jour. Met. Soc. Japan,* Ser. II, Vol. 35, No. 2.

(5) Matano, H. (1957): A statistical study of the formation of severe typhoon over the tropical ocean. *Jour. Met. Soc. Japan.* Ser. II, Vol. 35, No. 4.

(6) Sekioka, M. (1956): A hypohesis on complex of tropical and extratropical cyclone for typhoons in the middle latitudes (I) Synoptic structure of typhoon Marie passing over the Japan Sea. *Jour. Met. Soc. Japan,* Ser. II, Vol. 34, No. 5.

(7) Sekioka, M. (1956): A hypothesis on complex of tropical and extratropical cyclones for typhoons in the middle latitues (II) Synoptic structure of typhoons Louise, Kezia and Jane

passing over the Japan Sea. *Jour. Met. Soc. Japan*, Ser. II, Vol. 34, No. 6.
(8) Sekioka, M. (1957): A hypothesis on complex of tropical and extratropical cyclones for typhoons in the middle latitudes. (III) Examples of typhoon not accompanied by extratropical cyclone in the middle latitudes. *Jour. Met. Soc. Japan*, Ser. II. Vol. 35, No. 3.
(9) Matano, H. (1958): A synoptic verification of the development of a tropical cyclone into a severe typhoon. *Jour. Met. Soc. Japan*, Ser, II, Vol. 36, No. 1.
(10) Matano, H. (1958): On the synoptic structure of Hurricane Hazel, 1953, over the Eastern United States. *Jour Met. Soc. Japan*, Ser. II. Vol. 36, No. 2.

On an Example of Cyclone Development

By

Kozo Kanaya

Kobe Marine Observatory

1. Introduction

Of the many attempts in dealing with the problem of cyclone development, the works of Sutcliffe (1947) and Petterssen (1955) deserve the special mention. Sutcliffe discussed the relations between the difference of divergence for the two layers and the cyclone development by making use of the vorticity equation. Petterssen reviewed the Sutcliff's theory and obtained an expression for the cyclone development at the sea level. From his theory is concluded that the cyclogenesis at the sea level occurs as an unbalance between the vorticity advection at the level of nondivergence and the laplacian of the thermal components.

An example of the cyclone development was reviewed according to Petterssen's theory.

2. Example

The writer dealed with an example of the development of the extra-tropical cyclone, which passed through the Japan Sea on the 13th of December in 1957 and accompanied with the gale all over the Japan proper.

This cyclone formed at 15. J.S.T. on the 11th of December on the stationary front extending from east to west south of the Yangtze River. The cyclone deepened rapidly passing through the southern part of the Japan Sea and when it reached near the southwest sea of Kamchatka by 09 J.S.T. of the 14th, the pressure of its center was observed 950-mb. Thereafter, the cyclone is gradually decaying and it crossed the southern part of Kamchatka to the Bering Sea as shown in Fig. 1.

Fig. 1. Track of 6 hr. positions of the cyclone center, during the period from 11th to 15th. December 1957.

On the other hand Fig. 2 shows the 6-hr change of the pressure at the cyclone center. From this figure we can see that the rate of the deepening is large over

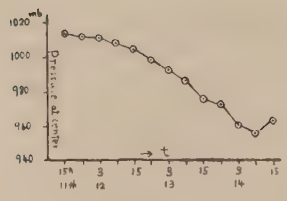

Eig. 2. 6-hr. change of the pressure at the cyclone centerfrom 11th to 14th Cecember 1957.

the region, (1) : from Yellow Sea to Japan Sea and (2) : near the southeast sea of Hokkaido. Though the strong development of the cyclone occured, the characteristics derived from the synoptic analysis was that after the cyclone passage the northwesterly monsoon did not prevail over the Japan and its near sea owing to the weak continental high. Therefore, as shown in Table 1 the air temperature all over the Japan did not lower and on the contrary it was higher than normal temperature

Table 1. The observed air temperature °C at 1800z aud the departure of temperature from the normal value at each station.

time	Sapporo	Sendai	Tokyo	Nagoya	Kobe	Takamatsu	Hiroshima	Fukuoka
1957. Dec. 12.3h	3 +7	6 +2	3 0	3 0	7 + 2	3 − 1	4 0	8 + 2
13. //	1 +5	7 +3	8 +5	14 +11	16 +11	13 + 9	17 +13	17 +11
14. //	−2 +2	4 0	7 +4	6 + 3	8 + 3	6 + 2	6 + 2	9 + 3
15. //	−3 +1	5 +1	8 +5	7 + 4	6 + 1	8 + 4	7 + 3	10 + 4

by the southerly warm wind. The fact is evident from the movement of the isotherm. 0°C on the surface charts in Fig. 3.

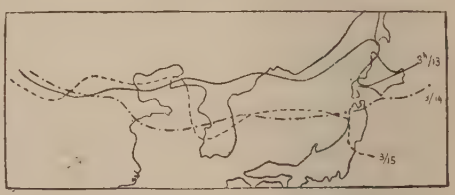

Fig. 3. Movement of 0°C isotherms on the surface chart.

3. Dynamics of the development

According to Petterssen's theory

$$\frac{\partial Q_0}{\partial t} = A_Q - \frac{R}{f}\nabla^2\left(\frac{g}{R}A_T + S + H\right)$$

$$= A_Q - \frac{g}{f}\nabla^2 A_T - \frac{R}{f}\nabla^2 S - \frac{R}{f}\nabla^2 H \qquad (1)$$

Where

A_Q: vorticity advection at level of nondivergence

A_T: thickness advection from 1000mb to level of nondivergence.

S: $log\left(\frac{P_0}{P}\right)\overline{\omega(\Gamma_a - \Gamma)}$ = adiabatic influence.

H: $log\left(\frac{P_0}{P}\right)\frac{1}{C_P}\frac{\overline{dW}}{dt}$ = nonadiabatic influence

As the thermal components represented by S and H is neglected, Eq. (1) is

$$\frac{\partial Q_0}{\partial t} \fallingdotseq A_Q - \frac{g}{f}\nabla^2 A_T \qquad (2)$$

In Eq. (2) Petterssen have decribed the thermal advection is very small in the initial stage of the cyclone development.

Of course, the writer does not deny Petterssen's theory. But since now the writer will discuss the case which in the initial stage of the cyclone development the thermal advection is not so small and its magnitude is same order as that of vorticity advection.

Ⅰ) The movement of the warm air.

The wind system over the south china on the 850-mb isobaric surface are as follows.

1957. Dec.	8.	9h	NW-ly or N-ly wind
	9	9h	S-ly wind
	10	9h	
	11	9h	SW-ly wind

Over the region NW-ly or N-ly wind prevailed on the 8th, but S-ly wind began to blow since 9th. As shown in Fig. 4 the isothem 8°C on the 850-mb chart moved northward since 10th.

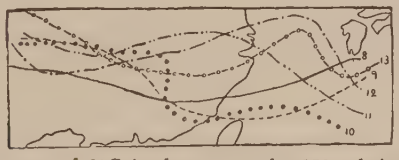

Fig. 4. Movement of 8°C isotherms on the 850 mb isobaric surface.

Judging from the thickness changes in Fig. 5, the strong warm air advection was seen over the basin of the Yangtze River before the cyclone formed. The region was cloudy with scattered rain and the activity of the front was more active since 11th.

Ⅱ) A_Q

Here we made use of the height change in place of the vorticity on the 500mb. Fig. 6 give the successive 24-hr sections of the 500mb level with the 12-hr height changes and the track of the negative regions located near the upper course of the Yangtze River.

The moving speed of the negative region is as follows.

1957. Dec.	10th~11th	40km/hr
	11th~12th	60km/hr
	12th~13th	50km/hr

The negative region caused by the trough formed near 30°N, 100°E about 10th.

Ⅲ) The process of the cyclogenesis.

The cyclone occured on the stationary front extended from east to west along the Yangtze River. From the Fig. 5 and Fig. 6 it is posible to estimate that the confluence of the positive area of thickness and the negative region of the height change will occurs near the upper or middle course of the Yangtze River and over

(a) 1957. Dec. 10, 21 h

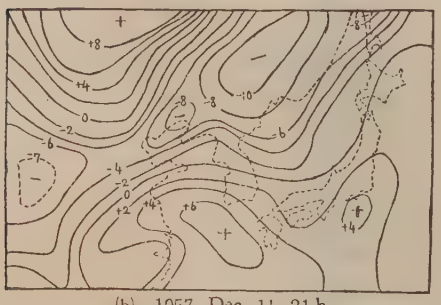

(b) 1957. Dec. 11, 21 h

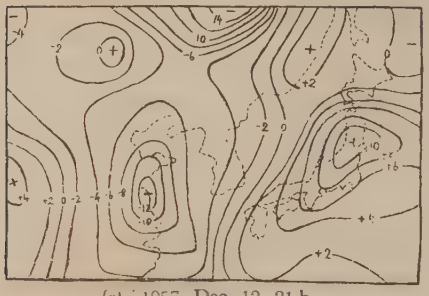

(c) 1957 Dec. 12, 21 h

Fig. 5. Successive 24-hr sections with the 12-hr. thickness (1000mb-500mb) changes.
unit of thickness change: 10m

(a) 1957 Dec. 10, 21 h

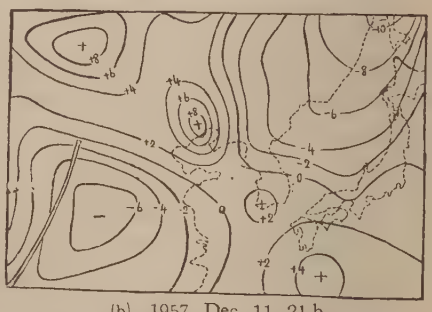

(b) 1957. Dec. 11, 21 h

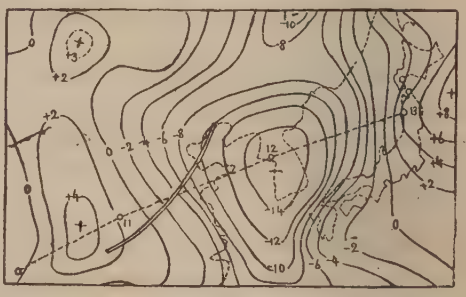

(c) 1957. Dec. 12, 21 h

Fig. 6. Successive 24-hr. sections at the 500mb level with the 12-hr. height changes. In each figure the double-line shows trough-line. In figure (c) the dashed-line is a track of the negative height change center.
unit of height change: 10m

that region the cyclone forms. As pointed out by Petterssen, it is needless to say that the existing front plays the important role in this cyclogenesis.

IV) The process of the development.

The development of the surface cyclone was studied from the relations between the location of the surface cyclone and the negative region of the 500-mb height

change in Fig. 7.

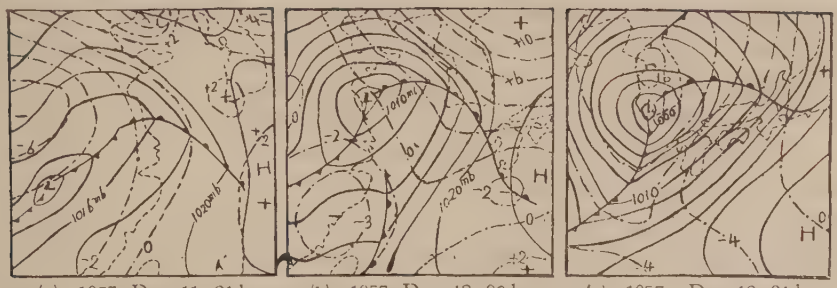

(a) 1957. Dec. 11, 21 h (b) 1957. Dec. 12, 09 h (c) 1957. Dec. 12, 21 h

Fig. 7. Successive 12-hr. sections of the sea level chart with the height tendency on the 500-mb level (the dash-dot) superimposed.

Petterssen's theory that the development commenced when the area of the positive vorticity advection superimposed upon the sea-level disturbance, is applied to that case.

The cyclone gradually developed from about 09 J.S.T. of 12th as shown in Fig. 2.

4. Summary

The writer reviewed the thermal advection in the initial stage of the cyclone development. The situation of the cyclone from 21 J.S.T. of 11th to 03 J.S.T. of 12th and finally at 03 J.S.T. of 12th established a simple circulation. Thereafter the cyclone moved to the Yellow Sea and gradually began to develop from that time. In the comparison the vorticity advection and the thickness advection in the initial stage of its development, it is better to do both advections corresponded to the location of the cyclone at 03 J.S.T. of 12th. Fig. 8 (a) and (b) indicate respectively the height change and the successive 12-hr thickness change on the 500-mb level.

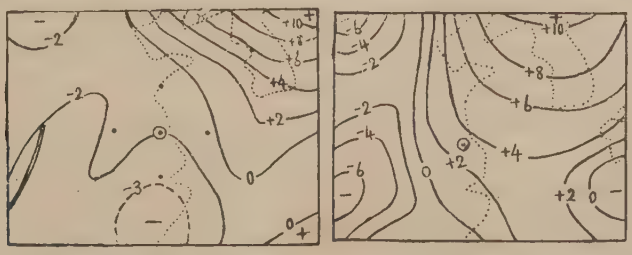

(a) 1957. Dec. 12, 09h height change (b) 1957. Dec. 12, 09h thickness change

Fig. 8. ⊙: (33 N. 120E) position of cyclone at surface chart at 1800z. Dec. 12 1957.
• : mesh size : distance : 300km

In this case we make use of surface chart at 03 J.S.T. of 12th as the time lag is neglected. Because these figures show the 12-hr average situation.

Now, if the vorticity and thickness advections at center of the surface cyclone are evaluated by Fig. 8 (a) and (b), These values are as follows.

1) vorticity advection $A_Q = +1 \times 10^{-9}\ \mathrm{sec}^{-2}$

2) thickness advection $A_T = -1 \times 10^{-9}\ \mathrm{sec}^{-2}$

Its magnitude is almost same order.

The author emphasize that the thickness advection in the initial stage of the cyclone development is not so small as Petterssen is pointed out.

The writer wish to express his hearty thanks to Mr. K. Kadoya for the guidance throughout this work and Mr. Y. Kawanabe and Mr. M. Ota for their discussions kindly exchanged with him.

References

(1) Petterssen, S. (1955): A general survey of factors influencing development at sea level. *Jour. Met*, Vol. 12, 36～42.

(2) Sutcliffe, R. C. and A. G, Forsdyke (1950): The theory and use of upper air thickness patterns in forecasting. *Quart. J. R. Met Soc.*, Vol. 76, 189～217.

(3) Petterssen, S.: *Weather Analysis* and *Forecasting*, Vol. 1. 2nd edition.

The Ice-Nucleating Property of Some Substances and its Dependence on Particle Size

By

I. Sano, Y. Fujitani and Y. Maena

Chemical Institute, Faculty of Science, Nagoya University

ABSTRACT

More than 100 substances, inorganic and organic, were observed, after they had been converted into smoke, on their effectiveness as ice nuclei employing a cold-box of the diffusion-cloud-chamber type. Nickel oxide, cadmium chloride, bismuth iodide and magnesiumoxide, etc. were found to be effective following silver iodide.

A train of the experiments on the particle-size dependence of the ice-nucleating activity was, also, made with iodides of silver, mercury and lead; oxides of nickel, magnesium, aluminium and zinc; and further, urea. The result was that the activity decreases notably as the size of particle goes smaller than 0.2μ in diameter. A formula describing the situation was proposed on the basis of thermodynamic consideration.

1. Introduction

For some years the authors have been conducting the research, both from basic and technical points of view, on the artificial rain-making practice; in the course of the laboratory work undertaken as part of it, the authors (1956) inquired into the influence of ultraviolet irradiation on the ability of silver iodide smoke to nucleate a supercooled water cloud, and in consequence, found that the addition of vaporous water, ammonia or hydrogen sulfide prior to irradiation renders the smoke insensitve to a great extent to the deteriorating action of ultraviolet light; originating from this, a series of experimental investigations directed toward the solution of the mechanism of heterogeneous ice-nucleation by foreign solid materials as well as the finding of any effective seed substances other than silver iodide are now in progress. This paper deals primarily with the results of nucleation experiment so far obtained with chemicals and mineral substances, which the authors believe to be of sufficient significance to justify their publication at this occasion.

Although a good deal of knowledge has already been secured concerning the ice-nucleating property of substances, it appears that the position is far from being settled and much remains to be done in completing and systematizing the mass of experimental data before general conclusions may be drawn from it (cf., for example, Sano and Fukuta, 1956; Fukuta, 1958; Sano, Fujitani and Kawase, 1958; Mason, 1959). In a recent paper Birstein and Anderson (1955) report an experiment which was carried out, with the intention of gaining insight into certain of the

processes in the formation of ice crystals in the atmosphere, by making use of a cryostat held at −20°C. A number of materials were, after being dispersed in nitrogen to smoke of the particle size ranging from 0.04 to 0.4μ in diameter, examined for the ice-forming ability.

2. Experimental

The apparatus used is of the diffusion-cloud-chamber type and diagrammed in Fig. 1. The inner box was composed of 4 side glass-plates (B) sealed together each of which is 35 cm long, 20 cm wide and 0.5 cm thick, and a bottom copper-plate (A) of 3 cm thickness.* This box was, with its wooden stand (J), set in a wooden case (H) having walls stuffed with sawdust. Between these was charged 25–30 kg of dry ice (I) as a cooling agent. Fig. 2 shows how the temperature in the inner box varies with the height measured from the bottom when thermal equilibrium is attained in the presence of supercooled cloud; the experimental uncertainty in the temperature determinations was within ±1°C.

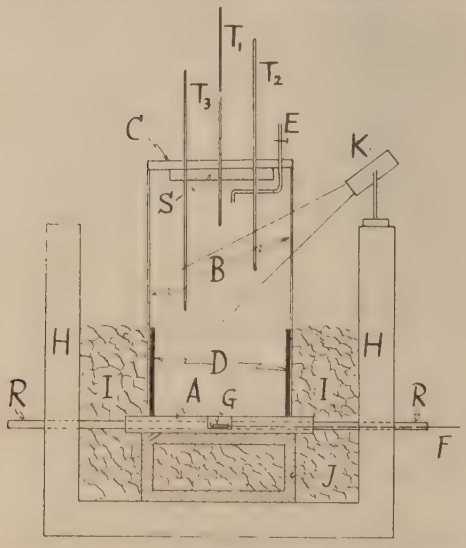

Fig. 1. Schematic diagram of the cold chamber
A: bottom copper-plate (27×27×3cm³)
B: glass-plate walls (35×20×0.5cm³)
C: top copper-plate (20×20×0.5cm³)
D: side copper wall (18×15×0.5cm³)
E: smoke-inlet tube
F: wooden rod carrying sample-holder
G: sample-holder
H: heat-insulating wooden box
I: dry ice
J: wooden stand
K: illuminator
R: brass-pipe(1 cm diameter)
S: water-impregnated sponge
T: thermometer

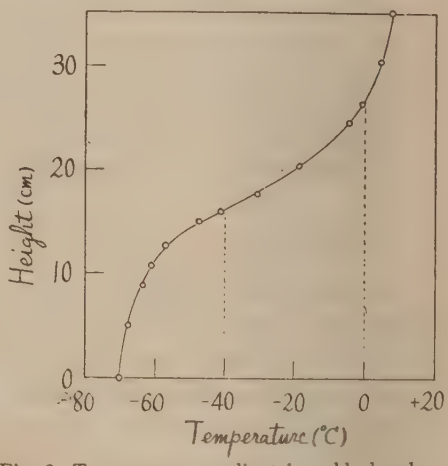

Fig. 2. Temperature gradient in cold chamber

The material under test regarding the effectiveness as an ice nucleus was, after it had been made smoke, injected through an inlet tube (E) into the box, and, illuminating its interior with a beam of light, the ice formation was monitored by the

* The hole (1×3 cm²) in the plate is intended to be utilized for capturing ice-crystals formed and recording them as replicas.

naked eye and the highest-temperature zone where the glitter of ice crystals burst into view was located visually. Let the temperature of this zone be called the temperature of nucleation and denote it by t_c. In the present article, the main purpose is to describe the results of its measurement with a variety of substances.

The smoke of the material being examined was produced by either the condensation or dispersion method; in the former method, the material was burnt or heated in air, vaporized, mixed with air and condensed to form a smoke, the particle size of which was commonly found to range from 0.1 to 0.8μ in diameter. There is, in this case, the possibility, particularly for halides and organic substances, of chemical reactions such as decomposition, oxidation and so forth occurring thermally through the process, making it difficult to say what is really effecting the nucleation.

In the latter method, the material was placed, after desiccation and pulverization, in a smoke chamber and dispersed mechanically by means of a jet of compressed air; the particles were usually found to be of a wider distribution in size so that they were fractionated by sedimentation process in which larger particles were allowed settle under gravity and smaller ones floating indefinitely were discarded, and the smoke carrying particles in the size limits of 0.5 to 2.0μ diameter was put to test. In so doing, the smoke was taken into a syringe, diluted with smoke-free air to the concentration of 10^5 particles per cm^3, and 10 cm^3 of it was introduced into the supercooled cloud.

The particle size as well as the smoke concentration were observed microscopically and ultramicroscopically; some of the results thus obtained are depicted in Fig. 3.*

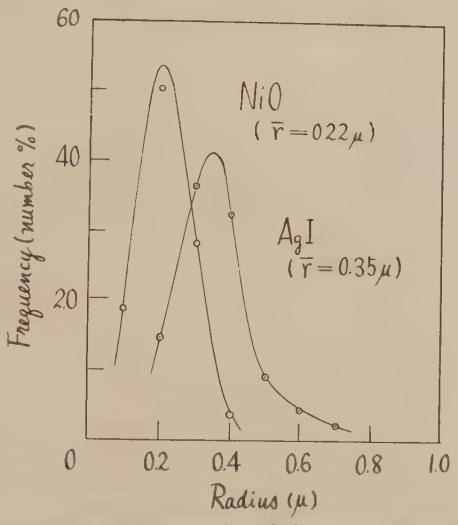

Fig. 3. Illustrative examples of the particle size distribution in case of smokes prepared by condensation method. $\bar{r}$: mean radius

3. Results and its discussion

About 115 substances, inorganic and organic, have been examined in their effectiveness as ice nuclei, and their temperatures of nucleation determined in the above-mentioned manner. The results are presented in Table 1. Many of these materials were obtained from chemical supply-houses and, in most cases, used after purification; the others, such as hydroxides, sulfides and a number of oxides and

* For particulars of the method of preparation of the nickel oxide smoke, see below.

Table 1. Nucleation temperature (shown in °C., with omission of − sign) and vividness of ice crystal formation (denoted by + or − symbol), together with method of smoke-making (c: condensation method, d: dispersion method) and crystal symmetry (C: cubic, H: hexagonal, M: monoclinic, R: rhombic. T: tetragonal)

Oxide				
CuO	M	d		−
Ag_2O	C	d		−
MgO	C	c	10	+++
MgO_2		d		−
BaO_2	T	d	25	+
ZnO	H	c	16	+++
CdO	C	d	20	+
Al_2O_3	C, H	d	12	+++
CeO_2	C	d		−
SiO_2	H	d	25	++
SiO_2-gel		d		−
SiO_2-gel (ignited)		d		−
PbO (yellow)	R	d		−
Pb_2O_3	M	d		−
Pb_3O_4	T	d		−
PbO_2	T	d		−
As_2O_3	C	d		−
Cr_2O_3	H	d		−
MnO_2	T	d		−
MoO_2	T	d		−
Fe_2O_3	H	d		−
NiO	C	d	7	++++
Co_2O_3	C	d	25	++
$Na_2O \cdot Bi_2O_5$		d		−
Hydroxide				
$Ca(OH)_2$	H	d		−
$Fe(OH)_3$		d		−
$Ni(OH)_2$	H	d	25	+
Iodide				
KI	C	c		−
NH_4I	C	c		−
AgI	H	c	5	++++
ZnI_2		c		−
CdI_2	H	c	18	++
HgI_2	R, T	c	14	++
PbI_2	H	c	18	+++
BiI_3	H	c	10	++
CHI_3	H	c		−
Chloride				
NaCl	C	c		−
NH_4Cl	C	c	17	++
Cu_2Cl_2	C	d		−
$CdCl_2$	H	c	9	+++
Hg_2Cl_2	T	c	24	++
$HgCl_2$	R	c	20	++
$SnCl_4$		c		−
$PbCl_2$	R	c	13	+++
$CrCl_3$	H	c	15	+
CaF_2	C	d		−
Sulfide				
BaS	C	d		−
ZnS	C, H	d		−
CdS	C	d		−
PbS	C	d		−
NiS	H	d		−

Table 1—2.

Sulfate				
$CaSO_4$ (ignited)	R,M	d		−
$BaSO_4$	R	d		−
$Al_2(SO_4)_3$ (ignited)	M	c		−
$PbSO_4$	R	d	16	++
Chromate				
$BaCrO_4$	R	d	13	++
$ZnCrO_4$		d		−
$PbCrO_4$	R	d		−
Carbonate				
Li_2CO_3	M	d	18	++
Na_2CO_3 (anhydrous)		d	20	+
$(NH_4)_2CO_3$ (hydrous)	R	d	15	+
$CuCO_3$ (basic)	M	d		−
$CaCO_3$	H,R	d		−
$BaCO_3$	R	d	25	+
$ZnCO_3$	H	d		−
$Ce_2(CO_3)_3$		d		−
$PbCO_3$	R	d	12	+
$PbCO_3$ (basic)	H	d		−
$Bi_2(CO_3)_3$		d	35	+
$NiCO_3$	R	d	18	+

Simple Substance				
Zn	H	d		−
Al	C	d		−
Active C		d		−
Ti	H	d		−
Sb	H	d		−
S	R	d		−
I_2	R	c	35	+
Mineral Substance				
Diatomaceous earth				−
Japanese acid clay				−
Ball clay				−
Agalmatolite				−
Tile-chamotte				−
Korean kaoline				−
Zettritz kaoline				−
Hongkong kaoline				−
Lava (Mt. Mihara, Ōshima)				−
Sublimate (Mt. Shin-Shōwa, Hokkaidō)				−

Table 1—3.

Organic Substance				
Urea	T	c	14	+++
Thiourea	R	c		−
Camphor	H	c	14	++
Naphthalene	M	c	17	++
Picric acid	M	c	19	+
Salicylic acid	M	c	35	+
Phthalic anhydride	R	c	32	+
Sulfanilic acid		d		−
p-Nitrobenzoic acid	M	d		−
Stearic acid		c		−
Phenol	R	c		−
m-Aminophenol	R	c		−
p-Hydroquinone	H	c		−

Aminoazobenzene	M	c	16	++
m-Nitrobenzene	R	c		−
Hydrobenzene	R	c		−
Urethane		c		−
β-Naphthol	M	d		−
Vinyl chloride		d		−
Isatin	M	d		−
Indigo	M	c	35	+
Indigocarmine		c		−
Fuchsin	R	d		−
Crystal violet	H	c		−
Congo red		d		−
Arizarin red	R	d	25	+
$Ni(COO)_2$		d		−

organic compounds, were prepared in the laboratory. In the table, the second column gives the crystal system of crystallization quoted from literature (Wyckoff, 1948, 1951, 1953; Robertson, 1953), the third the method of making smoke, the fourth the temperature of nucleation, tc, and the fifth the look of the shower of ice crystals observed visually, - symbol meaning ineffective as a nucleus at temperatures down to −40°C. It is obvious that considerable difficulty is encountered in interpreting the vividness of the appearance of ice crystals, since the size and its distribution of particles or, what comes to the same thing, the number of effective nuclei, the rate of further growth of the ice crystals produced and other factors have to be taken into account; there will remain room for question in this respect until fuller investigation has been brought to effect.

It can be seen from the table that some of the oxides, iodides and chlorides are most effective whereas organic substances are generally ineffective; in particular, silver iodide (−5°), nickel oxide (−7°), cadmium chloride (−9°), bismuth iodide (−10°), magnesium oxide (−10°), aluminium oxide (−12°), lead carbonate (−12°), lead chloride (−13°), barium chromate (−13°), urea (−14°), camphor (−14°), mercuric iodide (−14°), etc. should be marked both because they are of high activity and because the greater part of them are not of hexagonal form. In addition, the fact that nickel oxide is nearly as active as silver iodide might be of interest in connection with the practical side of artifical rain-making.*

Birstein and Anderson (1955) claim in their report that iodine has a positive

* In order to test the practical applicability of nickel oxide as a seed substance for rain-making, the authors have performed a field experiment in the period of January 27 to February 4, 1956 and succeeded in deriving snow from the atmosphere at temperatures below than −7°C. The details of the experiment have been published in *Jour. Met. Soc. Japan*, Vol. 34 (1956), 185—189.

ice-nucleating ability at −20°C, and moreover, they suggest as an explanation of the result that whereas some iodides are found inactive when they are prepared as smoke by heating in nitrogen, these exhibit a certain activity if treated suchwise in air. According to them, these iodides yield iodine through reactions such as

$$NH_4I = NH_3 + HI, \qquad 2\ HI = H_2 + I_2$$

$$2\ CdI_2 + O_2 = 2\ CdO + 2\ I_2$$

when heated in air, and once iodine is produced, it may react further with minute traces of unknowns to give ice nuclei.

By contrast, however, the table indicates that iodine has a poor activity so that its temperature of nucleation is as low as −35°C and ammonium iodide is inactive down to the lowest temperature available. As for potassium iodide, it is not subject to thermal decomposition, and, though it has been reported to be active by Vonnegut (1947), Hosler (1951) and Birstein and Anderson (1955), no matter which atmosphere, air or nitrogen, was employed in turning the iodide into smoke, the reverse was found true; the position is the same for lead oxide. Sulfides are, in general, ineffective as shown in the table; nevertheless, silver sulfide has been proved to be effective by the same researchers. It is worth noting, furthermore, that there is an apparent agreement, though qualitative, between these researchers and the present authors in the results for iodides of silver, mercury, cadmium and lead, chlorides of lead, mercury and sodium. Lastly, mention must be made of the tests done with mineral substances; these were obtained in powdery form and applied after being reduced to dust by force of an air-jet. As recorded in the table, they ended only in negative outcomes, though it had been, at times, pointed out by some investigators (Schaefer, 1953; Isono and Komabayashi, 1954) that volcanic ashes and clays act effectively as ice nuclei. The reasons for the inconsistency are not, at present, clear; it might be for one thing that the materials were contaminated, during their storage in laboratory, with greasy matter, moisture and so on precipitaed from air. The results may be taken as tentative and should be subject to confirmation by better experiments in future.

Since nothing definite has been found so far, though some scattered evidence exists in literature (see, for instance, Vonnegut, 1947, 1949), of how the nucleating effecfiveness of substances is dependent upon their particle size, an exploratory approach to this subject has been conducted here by resorting to the measurement of the temperature of nucleation of iodides of silver, mercury and lead, oxides of nickel, magnesium, zinc and aluminium, and further, urea. Of these, aluminium oxide was made smoke by the dispersion method. The others, except nickel oxide, by the condensation method; nickel oxide was prepared as smoke either by the dispersion method according to which the powder of hydroxide, oxalate or carbonate of nickel was, in the presence of air, heated at 300° to 400°C for 1 hour and the oxide produced was blown up by a jet of air or by the condensation method in which

case the vapor of nickel carbonyl was, after being mixed with air, passed through

Table 2. Particle size of nickel-oxide smoke produced through thermal decomposition (300°C) of nickel-carbonyl vapor mixed with air.

Concn. of $Ni(CO)_4$ vapor (mg./l.)	Particle size of NiO-smoke (Mean diameter, μ)
10	0.04
50	0.08
100	0.15
200	0.22

a glass-tube maintained at 300°C and converted into a smoke of nickel oxide. The particle size of the smokes so formed is shown in Tables 2 and 3. The results of the nucleation experiment are graphically represented in Fig. 4 by taking particle

Table 3. Particle size of nickel-oxide smoke obtained by dispersing the thermal decomposition product of nickel compounds in air.

Ni-compound	Conditions of thermal decompn.		Particle size of NiO-smoke (Mean diam., μ)
	temperature (°C)	time (hr.)	
$Ni(OH)_2$	400	1	1.7
$Ni(COO)_2$	300	1	0.70, 0.95
$NiCO_3$	300	1	0.83, 2.0

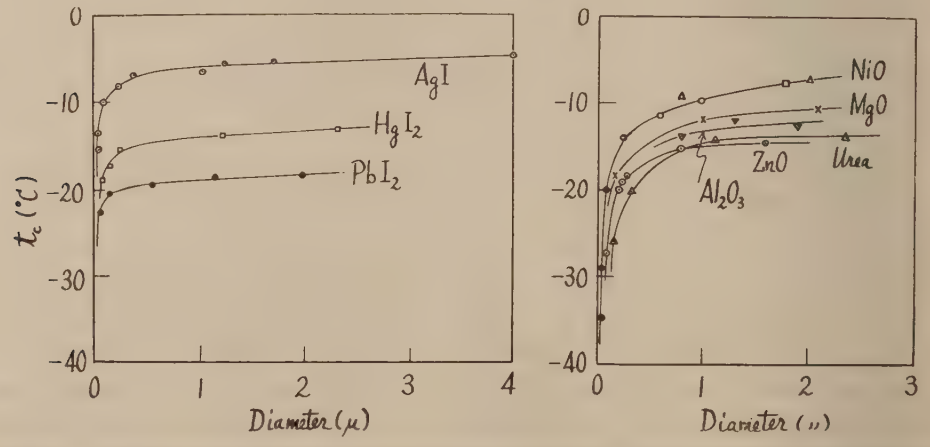

Fig. 4. Relation between nucleation temperature and particle size for various ice-nucleating substances

● : obtained from nickel carbonyl △ : obtained from nickel carbonate
○ : obtained from nickel oxalate □ : obtained from nickel hydroxide

size as abscissa and choosing a vertical scale for temperature of nucleation. It is seen from the figure that the nucleability falls off in rapid succession as the particle becomes finer than 0.2 μ in diameter. This finding is in close agreement with the estimate, recently made by Fletccher (1958), which reveals that the size effect contributes considerably to the behavior of the particles in nucleation; for particles larger than 0.2 μ the activity remains practically independent of size, while for smaller particles it drops down quickly.

The correlation just reffered to was found to be expressed by the formula

$$1/(r+\Delta)=a-bT_c\,,$$

where r stands for the radius of particle (μ), T_c the temperature of nucleation ($^\circ K$), a, b and Δ the empirical constants. If the formula is obeyed, the plot of $1/(r+\Delta)$ against T_c should yield a straight line; that this is in fact the case is indicated in Fig. 5. The values assigned to Δ in carrying this out are listed in Table 4; they are of the order of magnitude as large as 35 to 60 times the diameter of water molecule. For the sake of completeness, the derivation of the formula will be given under.

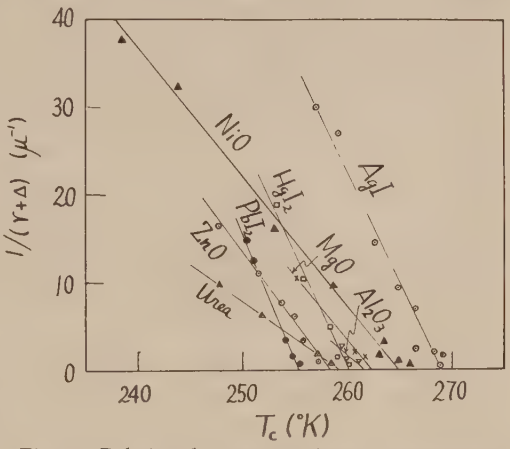

Fig. 5. Relation between nucleation temperature and $1/(r+\triangle)$ for various ice-nucleating substances.

Table 4. Assigned values of Δ in the formula $1/(r+\Delta)=a-bTc$

Nucleating particle	Δ (μ)
AgI	0.014
HgI_2	0.018
PbI_2	0.016
NiO	0.013
MgO	0.012
ZnO	0.010
Al_2O_3	0.010
$CO(NH_2)_2$	0.010

Suppose some one temperature T'_c, higher by x than the temperature of nucleation T_c and lower than the ice point T_0. If the notation $\mu_l(T'_c)$ denotes the chemical potential of supercooled water at the temperature T'_c and $\mu_s(T'_c)$ that

of ice, the difference of molar free energy between these states of water can be written by thermodynamics as

$$\mu_l(T'_c)-\mu_s(T'_c)=RT'_c\ln\frac{P_l(T'_c)}{P_s(T'_c)},$$

where R is the molar gas-constant, $P_l(T'_c)$ the vapor pressure, or more strictly the fugacity, of supercooled water at temperature T'_c and $P_s(T'_c)$ that of ice. Applying the Clapeyron-Clausius' relation to these two-phase equilibria at the temperatures between T_0 and T'_c, it follows that

$$\ln\frac{P_l(T'_c)}{P_s(T_0)}=-\frac{L_l}{R}\left(\frac{1}{T'_c}-\frac{1}{T_0}\right)$$

and

$$\ln\frac{P_s(T'_c)}{P_s(T_0)}=-\frac{L_s}{R}\left(\frac{1}{T'_c}-\frac{1}{T_0}\right),$$

L_l and L_s being the molar latent heat of vaporization, averaged over the interval of temperature, of liquid water and of solid ice, respectively. Combination of these leads to

$$\mu_l(T'_c)-\mu_s(T'_c)=RT'_c\left\{\frac{L_s-L_l}{R}\left(\frac{1}{T'_c}-\frac{1}{T_0}\right)\right\}, \qquad (1)$$

since

$$P_l(T_0)=P_s(T_0).$$

Consider now the water adsorbed on the surface of a nucleating particle of radius r and assume it to have grown up to a layer of ice or something like such of thickness Δ. Denoting its chemical potential by $\mu_s^{r+\Delta}(T'_c)$ and its vapor pressure by $P_s^{r+\Delta}(T'_c)$, there is obtained, again by thermodynaics,

$$\mu_s^{r+\Delta}(T'_c)-\mu_s(T'_c)=RT'_c\ln\frac{P_s^{r+\Delta}(T'_c)}{P_s(T'_c)},$$

the superscript $r+\Delta$ referring to the radius of the ice-covered particle, inclusive of the thickness of the ice layer. On the other hand, it holds for the vapor pressure over ice surfaces, according to the Thomson's equation defining the vapor pressure of a surface as determined by its radius of curvature, that

$$\frac{RT'_c}{M}\ln\frac{P_s^{r+\Delta}(T'_c)}{P_s(T'_c)}=\frac{2\gamma}{\rho}\frac{1}{r+\Delta},$$

where γ is the surface tension of ice against its vapor, M the molar weight of water in vaporous state and ρ the density of ice. From these,

$$\mu_s^{r+\Delta}(T'_c)-\mu_s(T'_c)=\frac{2\gamma}{\rho}\frac{M}{r+\Delta}. \qquad (2)$$

Upon equating the left sides of both (1) and (2) with each other and using T_c+x instead of T'_c, there results an expression

$$\frac{1}{r+\Delta}=\frac{\rho(L_s-L_l)}{2\gamma M}\left\{\left(1-\frac{x}{T_0}\right)-\frac{T_c}{T_0}\right\},$$

and this is transformed, by setting

$$\frac{\rho(L_s-L_l)}{2\gamma M}\left(1-\frac{x}{T_c}\right)\equiv a \quad \text{and} \quad \frac{\rho(L_s-L_l)}{2\gamma M}\frac{1}{T_0}\equiv b,$$

to the epuivalent form

$$1/(r+\Delta)=a-bT_c\,,$$

which is the formula hoped for, provided that

$$a=b(T_0-x).$$

It has been shown through the derivation above given that the slope, b, of the straight lines in Fig. 5 is a function of ρ/γ of the adsorption layer of water molecules on the particle; this could be a foothold in elucidating why the slope for the iodides are, as seen in the figure, larger than that for the oxides. It may well be that the magnitudes of both ρ and γ are regarded as depending upon the nature and extent of the interacrton of the nucleating substance with the water molecules adsorbed on it to build a layer in more or less ice-like state. An additional consideration wonld be hardly possible to be made, at the moment, from lack of the available information except that which has been obtained by Birstein (1954, 1955, 1956) from the adsorption studies carried out, using iodides of silver and lead, at several temperatues ranging $+25°$ to $-20°$C. According to his results, there is indication of the water molecules adsorbed being oriented to form an ice-like phase, and further, the differential heats of adsorption of water on the iodides appear to remain higher than its heat of liquefaction even after an adsorption layer of over 50 molecules thick has been formed; these will enable one to imagine that there should exist a field of force arising from the interaction between the adsorbed water and the iodide surface and extending outwards from one layer of adsorbed molecules to another through a distance, although for the present one is not confident of the manner in which the force is transmitted.

It has been known for some time that silver iodide acts most effectively as an ice nucleus, and also in the present investigation this is, as seen in Table 1, actually the case. This may be attributable, as generally accepted, (cf., e. g., Vonnegut, 1947; Birstein, 1954, 1955, 1956) to the close resemblance of silver iodide to ice in so far as the crystal symmetry and the atomic spacings are both concerned. However, the results tabluated in the table, taken together with those represented in Fig. 4, inform explicitly that the substances not belonging to the hexagonal system, say, oxides of nickel, magnesium and aluminium, carbonate and chloride of lead, mercuric iodide, etc., are more or less active than those of the hexagonal system such as zinc oxide, iodides of cadmium and lead; it may be suggested, in view of this fact, that the effectiveness of substances in ice nucleation would depend not only upon the crystallographic characterization like those afore said but also upon the geometrical conditions of the existing surface such as the arrangement of the lattice points as adsorption site and their affinity toward water, considered to be most probably of physical origin though of a sufficient magnitude to keep the molecules bound to the surface in successive layers and to develop them into an ice structure. Before the question of how ice crystals are initiated heterogeneously

on foreign solid particles can be answered, it will be necessary to go farther than is possible by discussion of average effects and to take into account the molecular picture of what happens on the surface of nucleus. The experimental data on hand should be thought as preliminary, and only enough to point the trend; further study now under way will shed light on the outstanding and unsolved aspects of the problem.

In conclusion, the authors express their gratitude to the Chūbu Electric Power Co., Ltd., Nagoya, under whose financial support the present investigation has been carried out.

References

(1) Birstein, S. J. (1954): Adsorption Studies of Heterogeneous Phase Transitions. *Geophys. Res. Pap.*, No. 32, Air Force Cambridge Res. Center, Cambridge, Mass., U. S. A.

(2) Birstein, S. J. (1955): The Role of Adsorption in Heterogeneous Nucleation, I: Adsorption of water Vapor on Silver Iodide and Lead Iodide. *J. Met.*, Vol. 12, pp. 324--331.

(3) Birstein, S. J. (1956): The Role of Adsorption in Heterogeneous Nucleation, II: Adsorption of Water Vapor on Photolyzed Silver Iodide. *Ibid.*, Vol. 13, pp. 395--398.

(4) Birstein, S. J. and Anderson, C. E. (1955): The Mechanism of Atmospheric Ice Formation, I: The Chemical Composition of Nucleating Agents. *Ibid.* 12, pp. 68--73.

(5) Fletcher, N. H. (1958): Size Effect in Heterogeneous Nucleation. *J. Chem. Phys.*, Vol. 29, pp. 572--576.

(6) Fukuta, N. (1958): Experimental Investigations on the Ice-Forming Ability of Various Chemical Substances. *J. Met.*, Vol. 15, pp. 17--26.

(7) Hosler, C. L. (1951): On the Crystallization of Supercooled Clouds. *Ibid.*, Vol. 8, pp. 326--331.

(8) Isono, K. and Komabayashi, M. (1954): The Influence of Volcanic Dust on Precipitation. *J. Met. Soc. Japan*, Vol. 32, pp. 345--353.

(9) Mason, B. J. (1959): Recent Developments in the Physics of Rain and Rain-Making. *Weather*, Vol. 14, pp. 81--97.

(10) Robertson, J. M. (1953): *Organic Crystals and Molecules.* Cornell Univ. Press, Ithaca, New York. (see Part II, p. 151).

(11) Sano, I. and Fukuta, N. (1956): Effects of water vapor, ammonia and hydrogen sulfide against the dacay of silver iodide smoke under irradiation of ultraviolet light. *J. Met. Soc. Japan*, Vol. 34, pp. 34--40.

(12) Sano, I. and Fukuta, N. (1956): Observations of the ice-nucleating temperature of some chemical substances. *J. Met. Soc. Japan*, Vol. 34, pp. 293--295.

(13) Sano, I., Fujitani, Y. and Kawase, K. (1958): An experiment on the supercooling of water-droplets containing foreign solid particles. *J. Met. Soc. Japan*, Vol. 36, pp. 112--117.

(14) Scheafer, V. J. (1953): Possible sources of natural ice nuclei found in the atmosphere. *Projet Cirrus, Final Rept., RL-785* (March 1953). G. E. Res. Lab., Schenectady, New York, Chapter 2, pp. 28--29.

(15) Vonnegut, B. (1947): The nucleation of ice formation by silver iodide. *J. Appl. Phys.*, Vol. 18, pp. 593--595.

(16) Vonnegut, B. (1949): Nucleation of supercooled water clouds by silver iodide smokes. *Chem. Rev.*, Vol. 44, pp. 276--289.

(17) Wyckoff, R. W. G. (1948, 1951, 1953): *Crystal Structures*, I, II, III. Interscience Publishers, New York.

On the Relation of the Generation and Passage of a Typhoon to Sea Surface Conditions

By

T. Ogata

Japan Meteorological Agency

1. Preface

It is well known about the interchange of heat between the sea surface and the lower atmosphere, for instance, W. C. Jacobs,[1] gave the following formula on this relation:

$$Q=145.4[(e_w-e_a)+0.01(T_w-T_a)]W_a \quad \text{gr cal/cm}^2\text{/day}, \qquad (1)$$

where the following units are used:

Q (heat content): gr cal/cm^2/day

e_w and e_a (water vapour tentions of sea surface and air):

inches of mercury,

W_a (Wind Velocity): knots, T_w (the sea surface temperature): degrees F

T_a (the air temperature): degrees F.

The first term of this formula indicates the heat transfer from the sea surface to the lower atmosphere by evaporation, that is by latent heat. The second term indicates sensible heat.

The author intends to consider the passage and generation of a typhoon, the condition of heat interchange between the sea surface and the lower atmosphere and the variation of marine conditions, and expresses the result of marine observation by bathythermograph during before and after the passage of typhoon.

2. On the marine condition of typhoon formation area

It is well known that the typhoon develops by the acquistion of a large quantity of heat and water vapour. And it is important that the area of high water temperature contributes to the formation and development of the typhoon. For example, in the Atlantic Ocean, it is said that the hurricane forms and develops often in the sea area where the water temperature is higher than 28°C.

According to the result of the author's research in the North Pacific Ocean, it is found also that the typhoon forms and develops mostly in the area where the sea surface temperature is higher than 28°C. Throughout the year, the typhoon forms rarely, except just one or two cases, in the sea area of the water temperature at around 27°C in the cold season, but most probably, the typhoon forms over the ocaen area

where the water temperature is above 28°C, and develops strongly when it is above 29°C.* Typhoon is considered not to form in the sea area where the water temperature is below 27°C.

It is often observed that temperature of the water gets as high as 30°C in the low latitude under the strong sunshine. When the disturbance is caused over such a high water temperature area, it often develops to a typhoon. This fact is easily understood if the heat energy is calculated by using formula (1), this heat

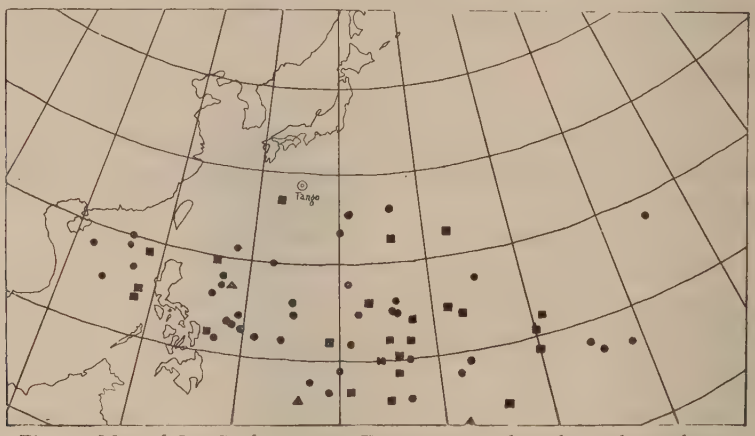

Fig. 1. Map of Sea Surface water Temperature when the typhoon forms.

Note Sea Surface water Temperature

▲ > 27.0

● > 28.0

■ > 29.0

value is very large. Fig. 1 shows the distribution of sea surface water temperature in a typhoon formation area which is obtained from the map of typhoon path and marine reports from 1956 to 1958. Comparing the map of marine report and the path of typhoon individualy, it is found that the typhoon moves toward the high water temperature area.

This fact is also pointed out by E. L. Fisher.[3]

3. On the variation of marine condition during before and after the typhoon passage**

The author examined the observation data of the Tango (Ocean weather station; 29°N, 135°E) to see how the sea condition between the sea surface to the middle

* B. I. Miller[2] states that hurricane can not form in the sea area where the sea surface temperature is below 26—27°C. Also H. P. Palmer and H. Riehl[6] state that the typhoon or hurricane forms seldom when it is below 28°C.

** The same marine condition observed when typhoon 5811 passed was also observed when typhoon 5821 passed.

layer when typhoon 5811 passed.

This typhoon with the central pressure 970 mb and maximum wind velocity 45m/s passed on the early morning of July 22 very near the Tango. We observed the maximum surface wind velocity 29.1m/s, the minimum pressure 990.5mb, and the maximum wave height 9m, and the distance between the center of the typhoon and our ship was 108 miles, and the wind above 20 m/s lasted for 22 hours. We observed the shallow and middle layer of the sea by B. T.

The result of the observation is shown in Fig. 2, 3, 4 and Table 1.

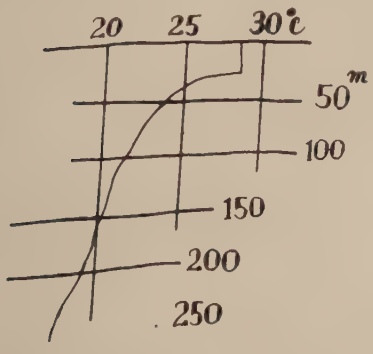

Fig. 2. Record of Bathythermograph
1958 July 20th
0840 Tango
SLD 25m
TCS −6m
DCS −0.5°C
SWT 28.1°C

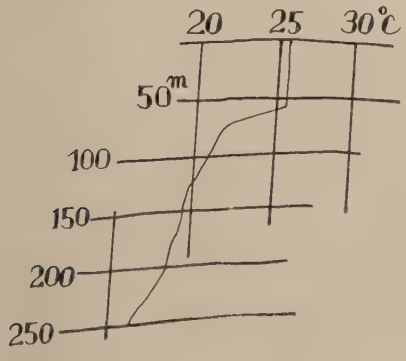

Fig. 3. 1958 July 23rd
0835 Tango
SLD 53m
TCS −6m
DCS −0.6°C
SWT 25.2°C

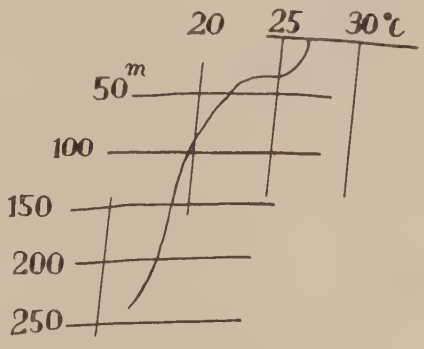

Fig. 4. 1958 July 26th
0845 Tango
SLD 10m
TCS −6m
DCS −0.2°C
SWT 26.3°C

Table 1. On the Variation of Sea Water Temperature from Sea Surface to 250m depth by Typhoon 5811 passage.

Depth \ Observation Date / Time	July 20 08 40	23 08 35	26 08 45	Aug. 6 08 40
Surface	28.1 °C	25.2 °C	26.3 °C	28.0 °C
10m	28.2	25.2	26.2	27.0
20m	28.2	25.2	25.8	26.7
30m	25.5	25.2	25.4	26.6
50m	23.4	25.2	21.7	23.3
75m	22.3	21.5	20.5	21.2
100m	21.1	20.3	19.7	20.4
150m	19.9	19.3	18.9	19.1
200m	19.0	18.5	18.4	17.9
250m	17.3	16.9	16.9	17.4
S.L.D	25m	53m	10m	0m

These data show that the marine condition indicates almost isothermal layer from the surface to 25m depth and high water temperature of 28.1°C before the passage of this typhoon, but the isothermal layer became deeper and water temperature dropped by 2.9°C and indicated 25.2°C after the passage of this typhoon. The layer deeper than 250m could not be observed by B. T., so although we can not say definitely the layer down to 300 m seems affected by the typhoon and the water temperature is lowered. Especially, the sea water temperature near the Tango dropped apparently at the last decade of July by the passage of this typhoon.

The marine report, Fig. 5 indicates this fact.

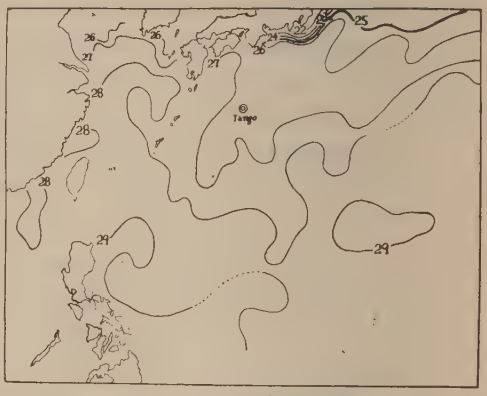

Fig. 5. Map of Sea Surface Temperature, Third tendays July 1958.

The feature of the sea area around the Tango like that of in the low latitude is the horizontal gradient of the sea water temperature is very gradual, and the difference of the sea water temperature is very small according to the variation of the position. Therefore the result of the sea observation indicated in Fig 2, 3 is understood to be not by the variation of position.

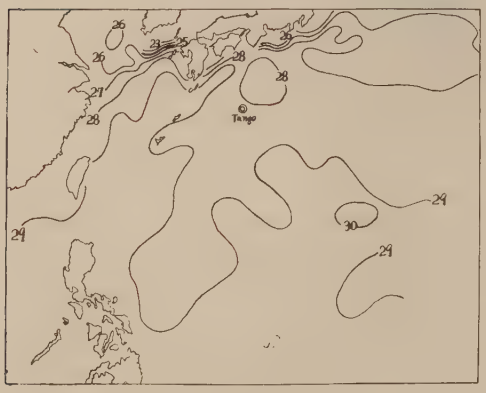

Fig. 6. Map of Sea Sutface Temporature, Third tendays August 1958.

The lowering of the sea water temperature continued for about 14 days. The sea surface water temperature recovered to 28°C on Aug. 6, and the marine condition almost recovered to that of the one before the typhoon 5811 passed. (see Fig. 6)

It is understood that distribution of the sea water temperature from the surface to the middle layer drops remarkably by the passage of a typhoon. An interesting fact is observed when the typhoon 5813* passed the neighboring sea area of the Tango, on July 28. (see Fig. 7)

* Typhoon 5813 was very weak, maximum wind velocity 16.7m/s, maximum wave height 7m at the Tango. And this typhoon was filled over this sea area to 1000mb, and soon after decayed.

For the reason of suddenly decaying of typhoon 5813 over this sea area, other reason can not be considered.

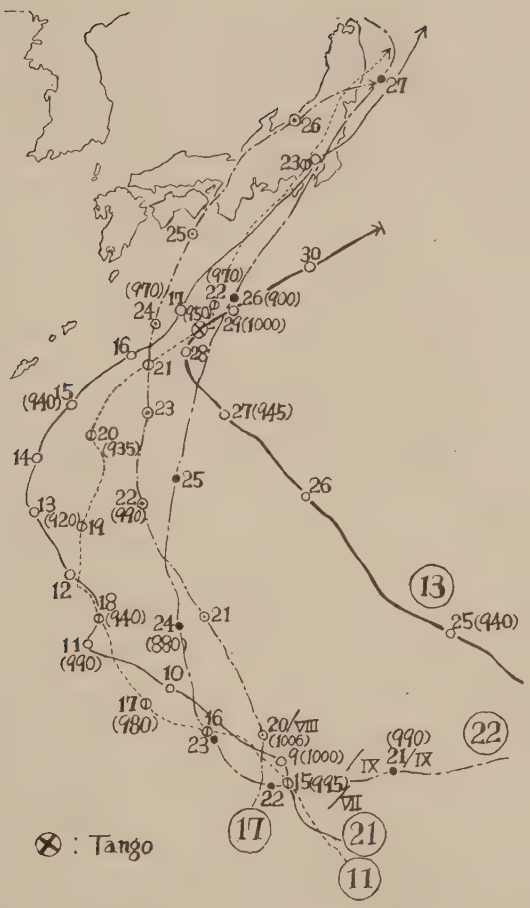

Fig. 7. Typhoon Track of passsage near the Tango, 1958.

This typhoon passed the east side of the track of the typhoon 5811, and approached to the Tango, suddenly the pressure of the center rose from 940mb to 990mb, and the stormy wind area reduced.

It is neccessary to consider why the strength of this typhoon weakened. This is very different from the case of typhoon 5811 which was not weakend until the time of landing on the mainland of Japan.

According to the marine condition, in this neighboring sea area, the drop of sea water temperature was nearly 3°C, and the sea water temperature indicated 25.2°C, so in this case it is understood that heat supply from the sea surface to the lower atmosphere was opposite direction compared with the case of typhoon 5811.

This fact agrees with the statement by E. L. Fisher[4] on the example of hurricane in the Atlantic ocean that the cold pool water caused by the passage

of a hurricane deters the approach of next hurricane and when the hurricane passes across the sea area of cold pool of water, it is definitely weakened.

Therefore once a strong typhoon passes the sea area, the marine condition changed and requires adequate intervals to recover the former marine condition.

The change of marine condition by the typhoon disturbance is considered from the point of external force. When the typhoon come to this sea area, in the center of the typhoon, the static water ascent from the surface is naturally caused by pressure fall.

In case of typhoon 5811, pressure difference between the center and the outside was about 30mb, so static water ascent is about 30cm. As the pressure center and maximum wind velocity of the typhoon was observed by the weather reconnaissance air plane while the observation of the wave haight near the center of the typhoon was not obtained. From the fact that the wave height of our observation was about 9m, it is presumed that the wave height near the centre will be around 12 or 13 metres.

In the sea where the typhoon passed, stirring of the water was caused by the wind wave, swell and static water ascent, and it is considered the temperature variation of such degree reached. The marine observation data of Muroto-typhoon (1939) before and after the typhoon passage by the Shumpu-maru, Kobe Marine Observatory indicated also the same fact.

On this fact, the generation of upwelling water by typhoon was demonstrated theoreticaly by K. Hidaka and Y. Akiba.[5] The variation of marine condition caused by the typhoon 5811 is supposed to be raised by the disturbanee near the water surface and the upwelling water. After the recovery of marine condition, when meteorological disturbance such as a typhoon forms in this sea area, it will be understood from another example that the disturbance will develop. The truth of this fact will be well understood when we see the typhoon 5817 passed this area deeping the pressure.

Finally, considering the heat exchange, the typhoon moves receiving sufficient supply of heat and water vapour from the water surface as explained, and thus maintaining and increasing its energy.

And on the other hand, the disturbance and upwelling water by the typhoon makes the sea water temperature lower from the surface to the middle layer, and for some time, the sea area is considered to become cold water pool area and meteorologically stable area. This fact well agrees with the fact that we are experienced to continue mild and calm sea for some intervals after typhoon passage.

Here, according to the marine report, middle decade of Aug. 1958 (see Fig. 8), it was realized considerably wide sea area of high water temperature field from the southern sea off Japan proper to the East china sea. The condition of this

Fig. 8. Map of Sea Surface Temperature, Second tendays August 1958.

sea area was thermally instable. Consequently, it can be seen when the typhoon approachs this area, it can move without being hindered thermaly or rather developing. As has already been stated, we can say from our obsevation data on the wider high water temperature area, as follows:—

I) In the sea area where a severe disturbance such as a typhoon has passed, so called the cold water pool formed by the upwelling of the cold water of middle layer appears and persists for some time.

II) This cold water pool is considered to be supplied heat easily, as this is in the low latitude area. But the heat capacity of sea water is very large compared with the atmosphere, and so this cold water area takes for a long time to recover to the previous state.

III) The space of typhoon generation is not at the same time concentrated in one area, but inclined to be scattered in wide areas. This phenomenum is observed through the pursuit of typhoon generating area.

IV) Therefore, the same sea area is considered to have a certain periodicity for the typhoon generation and passage. That is to say, the lower atmosphere receives energy from sea surface, thus thermal instability is formed small meteorological disturbance develops to a typhoon. Generally it requires some time to accumulate enough instable energy. Although the temperature distribution in the low latitude is considered to be almost uniform, it is not uniform.

The area of high water temperature is supposed to give the most favorable condition for a typhoon formation. This fact is considered to be able to affirm that the sea area in low latitude does not have large variation of water temperature,

as in the neighboring sea of Japan where warm and cold sea currents meet and make a complicated temperature distribution, and the horizontal gradient of water temperature in the low latitude is also very gradual with good conservativity of temperature distribution. As is seen in Fig. 7, in summer it existed the wide area of high water temperature above 30°C from the southern Ocean of Japan to the East China Sea. In February, also wide sea area with the temperature above 28°C existed in the low latitude from the equator to 10°N latitude. This fact indicates that even in the cold season there still is a chance for a typhoon formation (see Fig. 9).

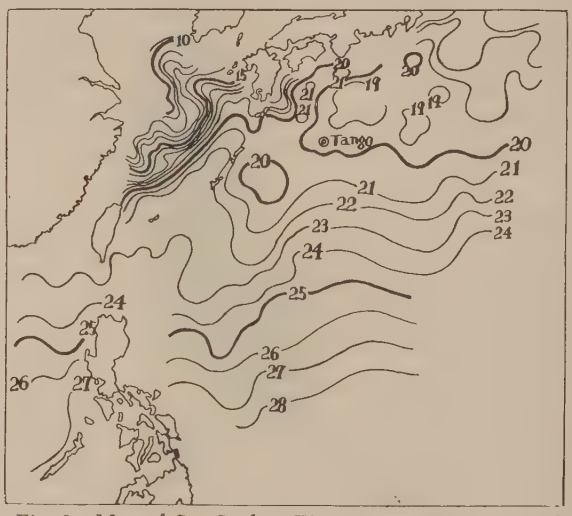

Fig. 9. Map of Sea Surface Water Temperature, Second tendays, February 1958.

4. The heat exchange between the sea surface and the lower atmosphere before and after typhoon passage

The amount of heat exchange computed by W. C. Jacobs formula (1) in case of typhoon 5811 is as follows:*—

Before the passage of typhoon 5811, that is July 19, the heat amount for 24 hours is +412.09 gr cal/cm²/day by latent heat and −10.26 gr cal /cm²/day by sensible heat, thus total heat is +401.83 gr cal/cm²/day, while after the passage, the sea surface cooled, and therefore heat removal is from the lower atmosphere to the sea surface on the contrary. The lower atmosphere indicated very stable weather condition. In this case the amount of the heat of the lower atmosphere acquired from the sea surface is by latent heat; — −56.52 gr cal/cm²/day, by

* The positive of heat value means the heat stream from sea surface to lower atmosphere and the negative is on the contrary.

sensible heat; — −12.93 gr cal/cm²/day, total amount is −69.44 gr cal/cm²/day. But before the passage of typhoon 5813, this value recovered till +295.23 gr cal/cm²/day, and after typhoon 5813 passed, this value dropped till +125.40 gr cal/cm²/day.

On this occasion, this typhoon could not acquire sufficient heat energy and weakend and so is considered to be unable to raise the upwelling water. Therefore, large variation of marine condition was not seen. Of course, on the occasion of calculation of the daily heat gain, for example, when the lower atmosphere looses labile heat for large scale of shower, and so it has a small labile heat account

But on this occasion, the lower atmosphere was not labile state to cause shower. Such an example, as typhoon 5811, was also seen distinctly on the case of typhoon 5817. Table 2 shows the variation of heat gain from the sea surface to the lower atmosphere when typhoons passed near the Tango, 1958.

Table 2. Calculation of Heat Supply from Sea Surface to Lower Atmosphere during before and after the Typhoon passage by Jacob's formula (1958) at Tango (29°N, 135°E)

Date	By Latent Heat	By Sensible Heat	Total	Remarks	unit
July. 19	+412.09	− 10.26	+401.83	Before Typhoon 5811 passage.	gr cal/cm²/day
23	− 56.52	− 12.93	− 69.44	After 5811 passage.	
26	+280.05	+ 15.18	+295.23	Before 5813 passage.	
30	+121.86	+ 3.54	+125.40	After 5813 passage. This value is small.	
Aug. 22	+345.15	+ 2.92	+348.07	Before 5817 passage.	
26	+148.61	− 2.92	+145.69	After 5817 passage. This value is small.	
Sept. 14	+544.48	+ 21.29	+565.67	Before 5821 passage. This value is large and Typhoon 5821 is strong.	
19	+297.54	+ 5.95	+303.49	After 5821 passage.	
24	+329.84	+ 41.76	+371.60	Before 5822 passage 5822 is strong.	
28	+232.30	+ 8.26	+240.56	After 5822 passage.	

Note: Pressure Center 5811(960mb), 5813(985mb), 5317(970mb), 5821(950mb), 5822(900mb).
Heat (+); Stream from Sea Water to Lower Atmosphere, Heat (−); on the Contrary.

This facts shows, when the heat gain after typhoon passage is small, it requires some interval till next typhoon approachs.

But when the heat gain is large, the period for approaching of the next typhoon is short, as seen in the example of typhoon 5821 and 5822, in which they came successively.

5. Conclusions

So far it has been difficult to make a map of marine condition covering wide area with the same accuracy throughout as the data available are not uniformly distributed over the area. While now it is getting possible to use data sufficiently accurate and dense for research. As is well known, the sea water is large and conservative heat source, compared with the atmosphere on the land and so the meteorological effect by sea water of our country is very large.

The heat and water vapour absorption of the lower atmosphere is more easily carried out on the ocean than on the land, and actually heat and water vapour exchange is easily and constantly going on between them throngh various processes. There are many theories on the formation and development of typhoon, at present time and it is supposed there are many factors contributing to them.

So it would be too bold to decide from only the marine condition, yet it is quite clear that it is an important factor for the typhoon formation and development. We also feel that the information on the marine condition is almost in dispensable for the improvement of accuracy of marine weather forecast. I wish to continue study on this field.

Aknowledgements: — I wish to express my gratitude to Dr. K. Terada, M. Higa and K. Tsuchiya, Japan Meteorological Agency, for their kind encouragements and advices for this study.

References

(1) Jacobs, W. C.: Large scale aspects of energy transformation over the oceans. *Compendium of Meteorology*, 1057—1070.

(2) Miller, Banner I. (1958): On the maximum intensity of hurricanes. *Jour. of Met.*, Vol. 15 184～195.

(3) Fisher, L. Edwin (1958): The exchange of energy between the sea and the atmosphere in relation to hurricane behaviour. *Jour. of Met.*, Vol. 15. 164～171.

(4) Fisher, L. Edwin (1958): Hurricane and the sea surface temperature field. *Jour. of Met.*, Vol. 15 328～333.

(5) Hidaka, Koji and Akiba, Yoshio (1955): Upwelling induced by a circular wind system. *Records of Oceanographic works in Japan*, Vol. 2 7—17.

(6) Riehl, H. (1954): *Tropical Meteorolology*, 281～300.

(7) Ogata, T (1955): On the relation between sea surface water temperature and air temperature. *Jour. of Met. Res.* Japan Met. Age., Vol. 7 No. 3, 159—168.

(8) Suda, K. (1943): *Kaiyo-no-Kagaku*, 720.

On the Wind Velocity Profile near the Surface and Accumulation of Sand Grains at a Coastal Sand Dune

By

Seiko Akai

Tottori Local Meteorological Observatory

1. Introduction

In this paper, the author investigated the relation between height and wind velocity near the surface that these observations were carried out by the author and his cocperators at coastal sand dune of Tottori (Fig. 1).

Wind velocities were counted every ten minutes by three Robinson's cup anemometers which were set up at three different heights near the surface both in the daytime and at night 22~23. Sept. and 16. Oct. 1955 when it was clear or cloudy. For reference, air temperature was measured and accumulation of drifting sand grains was observed at the same time during the observations of wind velocity.

Logarithmic law and power law in relation to height and wind velocity were applied to those observational data of wind velccity and also accumulation of sand grains was discussed by the observations on a hill and along its slope toward the coast and theoretical consideration.

2. Wind velocity by height near the surface

Results of observation are shown in Table 1.

Denoting $\overline{u}$ mean wind velocity, Z height on the surface respectively,

logarithmic law $\quad \overline{u} = A\log Z + B \quad (1)$

power law $\quad \overline{u} = \overline{u}_1 Z^p \quad (2)$

where A, B, $\overline{u}_1$, P are experimental constants.

Therefore, applying (1) and (2) to the observational data, we get Table 2 and Table 3 by graphical method and numerical calculation.

It was assumed that temperature gradient near the surface was very small, on the other hand though Richardson number was not examined almost in detail.

Anyhow it seems that both logarithmic and power laws fit considerably in Table 2 and Table 3.

3. Wind velocity on a hill and its slope

Model of vertical section of a slope along the coast is shown in Fig 2, and wind velocity was measured by three cup anemometers whose cups were set up with the height of one meter on the surface. Observational data are shown in Table 4.

Southerly wind blew down the slope and wind velocity was largest at point A, smallest at B, and became large again somewhat at C in night in Table 4. Sand

grains on the surface become more humid in night than at daytime, but drifting of sand grains was severe at A because of rather strong wind (6~8m/s), and sand grains were transported unceasingly toward B and C.

Especially the tendency that drifting sand grains accumulated at B as the wind velocity became smaller at B, was remarkable.

However the difference of wind velocity between B and C was very small at daytime in Table 4 when the northerly wind blowing up the slope was mild.

4. Wind velocity and accumulation of sand

As asserted in § 3., drifting sand grains accumulated strikingly at B in Fig. 2 in the case of rather strong southerly wind (6~8m/s), therefore the author tried a theoretical consideration of turning flow round a corner by the method of conformal representation.

In Fig. 3 and Fig. 4, taking Z-plane and W-plane, imaginary axis y and v axis, real axis x and u axis, ϕ, ψ, u, v and i denoting velocity potential, stream function, velocity component of x and y direction, unit of imaginary number respectively,

$$Z=x+iy, \quad W=f(Z)=f(x+iy)=\phi+i\psi$$

Now in the case of flow turning round a corner,

$$W=f(Z)=Z^n, \quad n \text{ constant} \tag{3}$$

as is well known

Putting $Z=re^{i\theta}$ in (3) and Fig. 3, $\phi+i\psi=r^n(\cos n\theta+i\sin\theta)$ consequently,

$$\phi=r^n\cos n\theta, \quad \psi=r^n\sin n\theta \tag{4}$$

These formulas represent a flow when turns round a corner of central angle $\frac{\pi}{n}$ where $\alpha=\frac{\pi}{n}$ or $n=\frac{\pi}{\alpha}$ in Fig. 5.

θ is measured counterclockwise from OA in (4).

For an example of numerical computation, considering that a slope is inclined by 45° to horizontal line, $n=\frac{\pi}{\alpha}=\frac{180}{180-45}=\frac{4}{3}$ in Fig. 6.

Therefore results of computation are shown in Table 5 and Fig. 7.

According to the above results, it is found that velocity of flow becomes smaller near O than near A and becomes larger again near B in Fig. 7.

Then it is concluded that drifting sand grains fall and accumulate near O in Fig. 7, corresponding to the swelling at B in Fig. 2; namely it coincides with observational result to some extent.

5. Summary

(i) Both logarithmic and power laws fit considerably to wind velocities in the layer within about 2m on the surface.

(ii) The fact that drifting sand grains accumulate at the part near the foot of a hill when wind blows down a hill with a slope toward the seashore, coincides with result by theoretical consideration of a flow round a corner to some extent.

Table 1. Wind velocities by height (observed).

Number of data	[1]			[2]			[3]		
Height from the surface Z(cm)	30	88	134	30	79	142	30	100	165
Mean wind Velocity $\bar{u}$ (m/s)	4.91	5.30	5.57	2.97	3.19	3.37	1.94	2.22	2.43
Mean air temperature (°C)	20.5	20.3	20.4	22.2	22.0	21.9	—	—	—
Position of observation in Fig. 1	①			②			③		
Period	19h 00~22.00 22. Sept. 1955			23h 00~02 00 22~23. Sept. 1955			14h 10~14 50 16. Oct. 1955		
Wind direction	S ~ SE			SW~SSW			NW~NE		

① on a hill, ② at the bottom of a barchan.

Table 2. Wind velocities by height (Calculated, by logarithmic law).

Number of bata	[1]			[2]			[3]		
A	1.00			0.601			0.662		
B	3.42			2.07			0.93		
Height from the Surface Z(cm)	30	88	134	30	79	142	30	100	165
calculated $\bar{u}$ (m/s)	4.90	5.36	5.55	2.96	3.21	3.36	1.91	2.25	2.40
$\bar{u}$cal. $-\bar{u}$obs. (m/s)	−0.01	+0.06	−0.02	−0.01	+0.02	−0.01	−0.03	+0.03	−0.03

Table 3. Wind velocities by height (Calculated, by power law).

Number of data	[1]			[2]			[3]		
$\bar{u}_1$	3.47			2.30			1.23		
p	0.096			0.076			0.132		
Height from the Surface Z(cm)	30	88	134	30	79	142	30	100	165
Calculated $\bar{u}$ (m/s)	4.81	5.33	5.55	2.97	3.19	3.34	1.93	2.26	2.41
$\bar{u}$ cal.$-\bar{u}$ obs. (m/s)	−0.10	+0.03	−0.02	±0.00	±0.00	−0.03	−0.01	+0.04	−0.02

Table 4. Wind velocities on a hill and its slope (Obsrved).

Position	A	B	C	Wind direction	Period of observation
$\bar{u}$ (m/s)	7.24	4.47	5.29	S ~ SSW	(night)
Air temperature (°C)	23.3	23.5	23.9		03^h 00~05 30 23. Sept. 1955
$\bar{u}$ (m/s)	3.67	1.96	1.85	NW ~ NNW	(daytime)
Air temperature (°C)	—	21.3	—		10^h 30~12 30 16. Oct. 1955

Table 5. Numerical values of γ in the case of n=4/3, for various values of velocity potential and stream function.

θ	$n\theta$	γ		γ		γ		γ		γ	
		$\phi=1$	$\psi=1$	$\phi=2$	$\psi=2$	$\phi=3$	$\psi=3$	$\phi=4$	$\psi=4$	$\phi=5$	$\psi=5$
0°	0°	1	∞	1.67	∞	2.28	∞	2.83	∞	3.34	∞
6	8	1.01	43.9	1.68	7.34	2.30	10.00	2.85	12.41	3.37	14.67
15	20	1.05	2.24	1.75	3.74	2.39	5.10	2.97	6.32	3.51	7.48
30	40	1.22	1.39	2.04	2.33	2.78	3.18	3.45	3.94	4.08	4.66
45	60	1.68	1.11	2.81	1.86	3.83	2.54	4.76	3.15	5.62	3.73
60	80	3.72	1.01	6.22	1.69	8.47	2.31	10.51	2.86	12.43	3.38
67.5	90	∞	1.00	∞	1.67	∞	2.28	∞	2.83	∞	3.34

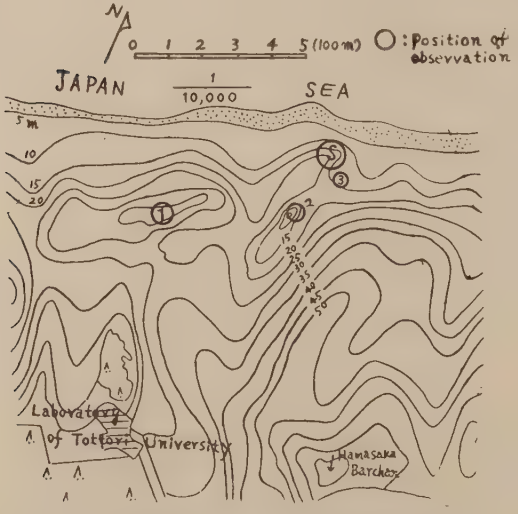

Fig. 1. Topographical map neighbouring the place of observation.

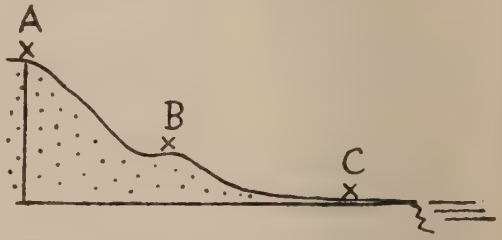

Fig. 2. Model of vertical section of a slope along the coast.

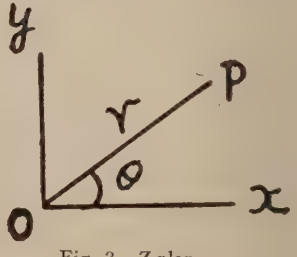

Fig. 3. Z-plane.

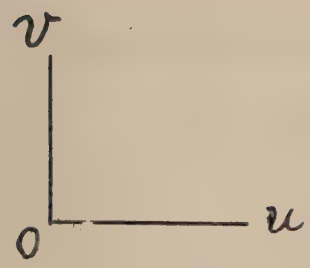

Fig. 4. W-plane.

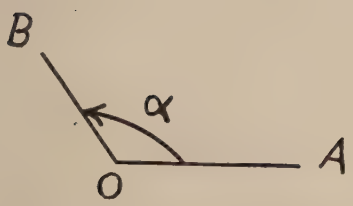

Fig. 5. Corner of central angle α.

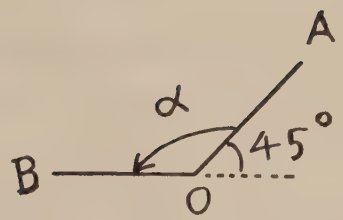

Fig. 6. Vertical section of a slope which has an angle of inclinaton to horizon 45°.

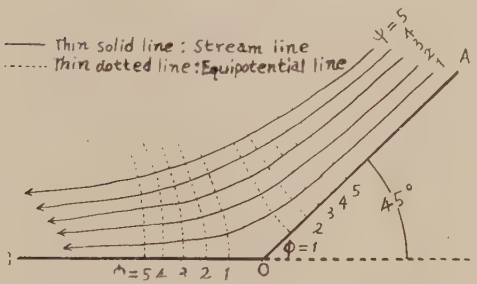

Fig. 7. Stream lines and equipotential lines of flow turning round a corner that its central angle is 135°.

References

(1) Sutton, O. G. (1953): *Micrometeorology.*

(2) Hara, M. (1932): *Untersuchungen über den Dünenwaldbau.* The College of Tottori.

(3) Sasaki, T. (1939): *Applied conformal representation.* Fusanbo, Tokyo.

On the Northwesterly Monsoon around Japan in Winter Season

By

Ken Akedo

Kobe Marine Observatory

1. Introduction

According to many attempts on the monsoon in winter season, the development of the continental high does not depend upon the accumulation of the polar air mass, but upon the dynamical development of long wave. From synoptic analysis it was concluded that the intensification of the ridge near 90°E, 150°—180°E and the deepening of the trough near 125°—130°E play the important role on the monsoon given in Table 1.

Table 1. Date of maximum wind velocity caused by winter monsoon at Kobe City during 1955–1959.

	Direction of maximum wind velaciiy	maximum wind velocity (m/s)
5～ 6th. Jan. 1955	W	14.0
10th. Jan. 1955	W	13.7
15～16th. Jan. 1955	W	14.9
17～18th. Jan. 1955	W	17.1
26th. Jan. 1955	WSW	1.0
11th. Feb. 1955	WNW	11.0
20～21th. Feb. 1955	WSW	19.3
7～ 8th. Jan. 1956	W	17.7
23～25th. Jan. 1956	WNW	15.8
28～29th. Jan. 1956	WSW	17.3
4～ 5th. Jan. 1956	W	16.5
21～22th. Dec. 1956	W	13.7
19～20th. Jan. 1957	WNW	11.5
30～31th. Jan. 1957	WNW	13.7
10～12th. Feb. 1957	WNW	12.2
29th. Dec. 1957	W	12.5
4～ 7th. Jan. 1959	W	13.7
2th. mar. 1959	WSW	11.8
11～12th. mar. 1959	W	14.9

2. Intensification of the ridge in the Atlantic Ocean

It is often observed that the state of intensification of long wave ridge propagates from west to east. As shown in Table 2, the intensification of the ridge near 90°E occurs in about five or six days after that of ridge in the Atlantic Ocean. In this case we estimate that a new ridge may be intensified in the west, even when the trough near that region is deepening, though the ridge is not well maked. These examples are given in the lower column of Table 2.

Table 2. The frequency of periods which the monsoon need to occur around Japan after the strong intensification of the ridge in the Atlantic Ocean (upper) and the deepening of the western trough in the Atlantic Ocean (lower).

Number of days	4	5	6	7	8	9	10
Frequency	—	6	7	—	2	—	—
Frequency	(1)	(1)	(2)	—	—	—	—

The outbreak of cold air mass occurs in one or two days after the appearance of the ridge near 90°E as shown in Table 3. The ridge near 90°E intensifies in five or six days after its development in the Atlantic Ocean. Its displacement may be considered to be so fast. But since the mean geostrophic wind speed is 10.9m/sec over 35°N - 65°N in January and February, 1956—1958, and the distance from 20°W to 130°E at 60°N is about 10000km, it will arrive at 90°E about six days later, provided that the long wave propagates with group velocity $C_G = 2_u$.

The strong development of ridge and trough is in general associated with that of the long wave. The group velocity C_G of the long wave (almost stationary wave length L_S =9000km) and that of normal cyclonic wave with its wave length $\frac{1}{3}\ L_S = 3000$km equal nearly to 2_u and u respectively as shown Fig. 1.

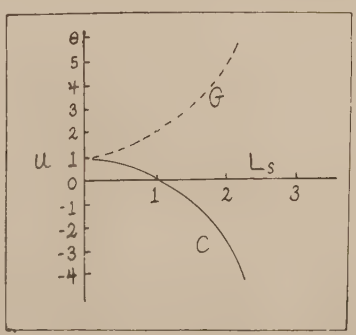

Fig. 1. Relations between wave velocity and zonal wind velocity.

As far as the outbreak of cold air is concerned with the intensification of the ridge near 90°E, it is necessary to consider both the long wave and the short wave, which propagate with the velocity of 2_u and u. The outbreak of the polar air occurs in about one or two days after the intensification of the ridg near 90°E, but the range of the periods fluctuates considerably. The fact is due mainly to the irregularity of the periods when the short wave ridge coincides with the long

wave ridge and the trigger action is to be operate after the intensification of long wave ridge near 90°E. There were a number of studies on the intensification of long wave due to energy propagation. Kadoya pointed out that it propagates with group velocity.

Table 3. The frequency of the periods which the monsoon need to occur around Japan after appearance of the ridge near 90E.

Number of days	0	1	2	3
Frequency	2	9	6	2

3. The effects of solenoid on the intensification of a ridge

Fig. 2 (a—f) represent 500mb charts of the northern hemisphere for the monsoon on the 15th and 16th of January in 1955. In this case, the maximum wind speed of 14.9m/s was observed at Kobe being rather stronger than in the normal monsoon. According to 500mb chart at 00 00 J.S.T. on the 10th of January (see Fig. 2a), a ridge intensiffed in eastern Atlantic Ocean. In this ridge the amplitude of isotherms was smaller than that of contour, while the interval between isotherms was not so small. On the 12th (Fig. 2b) a trough deepened in western Europe. Isotherms and contours intersected each other at right angle in the eastern region of trough. The solenoid in that region caused anticyclonic circulation.

Here, it should be noted that the amplitude of isotherms was larger than that of contour and the phase of isotherm retards in comparison with that of contour. Isotherms were almost paralled to contours in the vicinity of trough. On the 13th

Fig. 2. (a) 500 mb map 10 Jan. 1955 00 J.S.T.

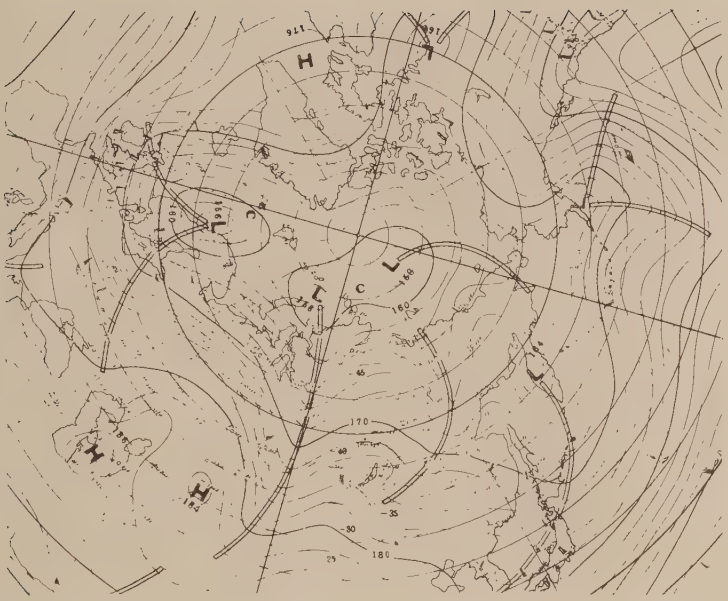

(b) 500 mb map 12 Jan. 1955 00 J.S.T.

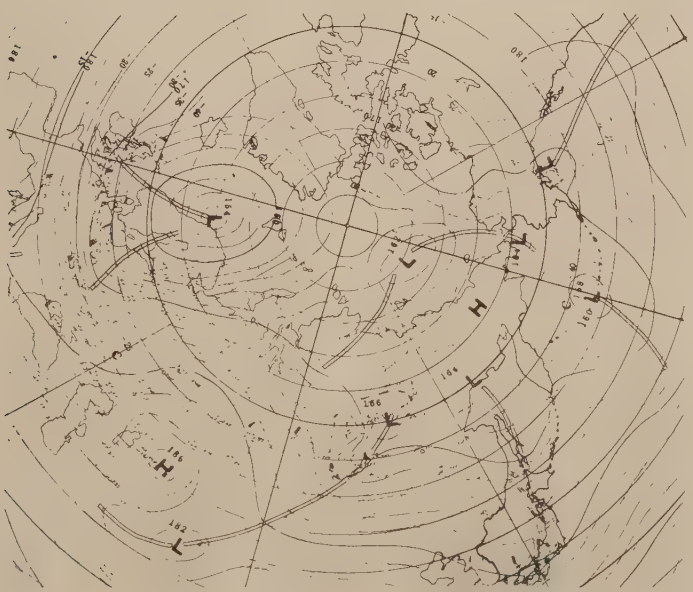

(c) 500 mb map 13 Jan. 1955 00 J.S.T.

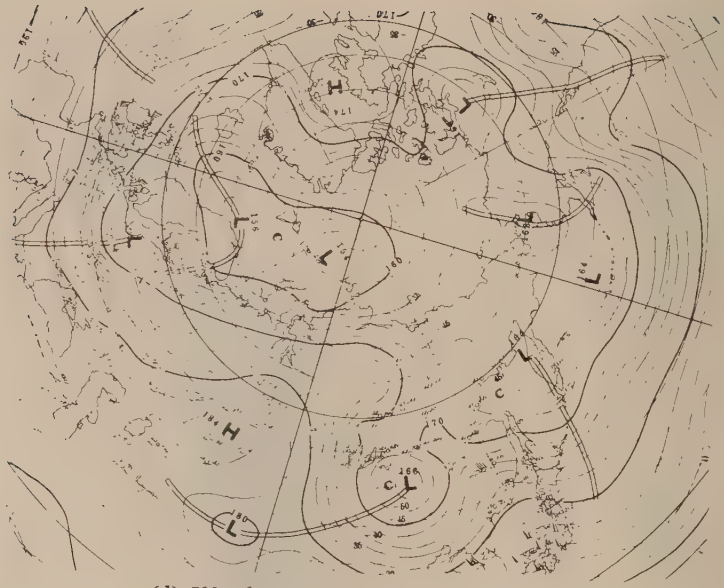

(d) 500 mb map 14 Jan. 1955 00 J.S.T.

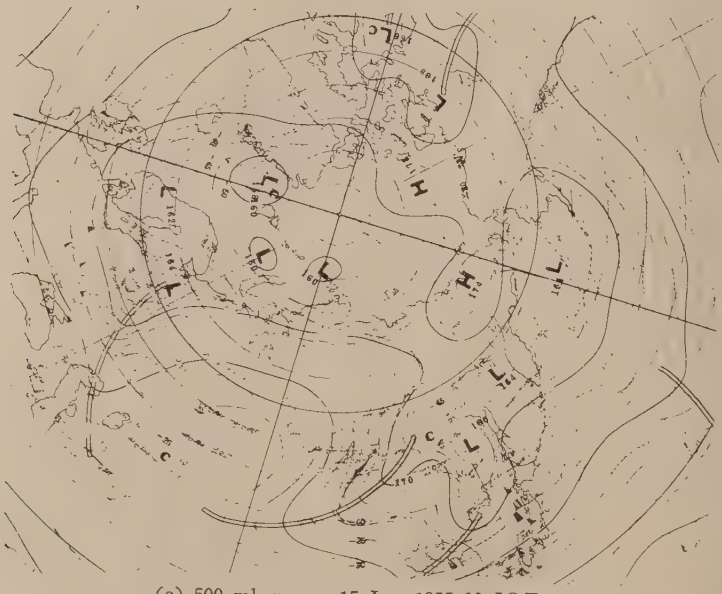

(e) 500 mb map 15 Jan. 1955 00 J.S.T.

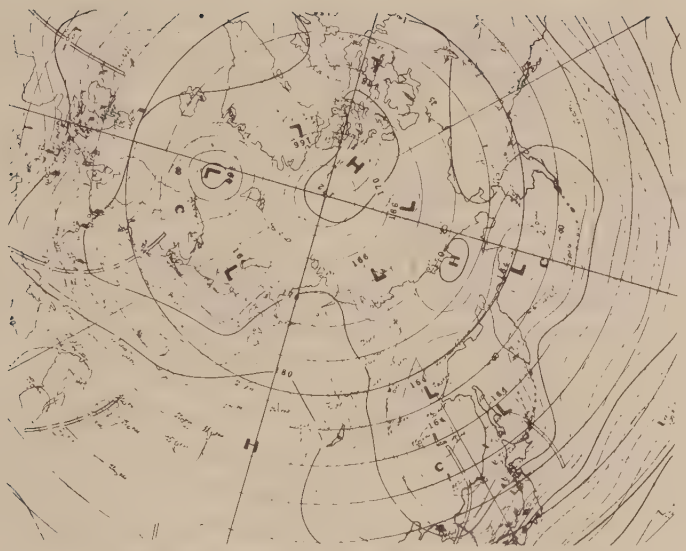

(f) 500 mb map 16 Jan. 1955 00 J.S.T.

(Fig. 2c) the trough nearly stagnated, and the ridge gradually intensified over the area where the anticyclonic circulation due to solenoid was formed and expanded east ward. In this case, the solenoidal effect was found over that region. On the 14th (Fig. 2d) ridge continued to intensify and finally arived at 90°E, while the rear trough did not deepened and the distance from ridge to trough expanded. On the 15th (Fig. 2e) and the 16th (Fig. 2f), the amplitude of the trough near 125°—130°E increased and thus the monsoon pattern was established.

Now, we shall discuss the solenoidal effects on the pattern. It has been usually considered that the effects of vertical solenoid on pressure patterns were large, whereas the effects of horizontal solenoid were not so large. As shown in Fig. 2, however, it has sometimes considerable large effects when the long wave developed. A wave is generally stable when the constant absolute vorticity is conserved. Then, considering the effects of solenoid and divergence in the following equation:

$$\frac{dz}{dt}+ZQ=N$$

where Z is absolute vorticity, Q divergence and N solenoid, the wave patterns may be unstable. The effect of divergence was studied by Goto. He has obtained the relation between the effect of convergence connected with jet stream and the intensification of the ridge near 90°E.

Here we shall discuss only the solenoid term. Fig. 3a—3d′ represent the relations between contour and isotherms. Figures on the left side express the initial state of wave and the change of wave pattern together with the effects of solenoid on the right side. Because of the effects of solenoid change at various circumstances,

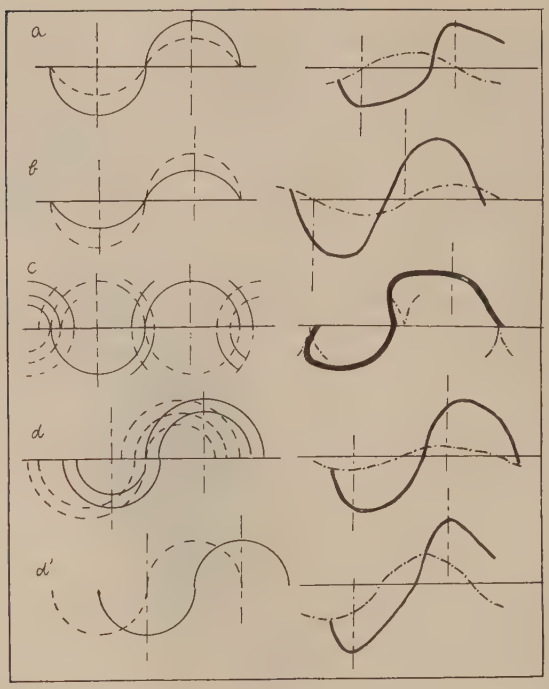

Fig. 3. Solenoidal effect.

(a) ——— Isotherm.
(b) — — — Initial locations of the trough and ridge.
(c) ——— Contour.
(d) — · — · — Solenoidal effect.
(e) ▬▬ Illustrating superposition of (c) and (d).
(f) ▬▬ The outline of wave pattern illustrated superposition of (c) and (d).

we consider that it has cyclonic or anticyclonic effects with the same order as the maximum amplitude of contour on the height change, when the isotherm and contour intersect each other at right angle, while it has no effect when both lines are parallel. Figures on the right illustrate the composite waves in which the phase difference is $\frac{1}{8}$ wave length with considering the effects of solenoid.

Now, provided that the amplitudes of isotherm and contour are A_I and A_C, respectively,

a) The case $A_I < A_C$

The wave retrogrades slightly and its amplitude decreases partly.

b) The case $A_I > A_C$

In this case the wave progresses slightly and its amplitude increases.

c) The case which isotherm and contour patterns are out of phase by $\frac{1}{2}$ wave length.

It is very difficult to draw the complete patterns with the effect of solenoid, since its effect is maximum at the distant area from the axes located between ridge and trough. The outline of wave pattern is shown in the figure on the right. Namely, the amplitude is almost constant. Its profile is steep on the both sides and also extends backward.

d) The case which the phase of isotherms retards in comparison with that of contour.

Fig. 3d represents the case where the phase difference is $\frac{1}{8}$ wave length. The amplitude of wave increases gradually and progresses slightly. The distance from ridge and trough tend to expand. Similarly, Fig. 3d' illustrates the case where

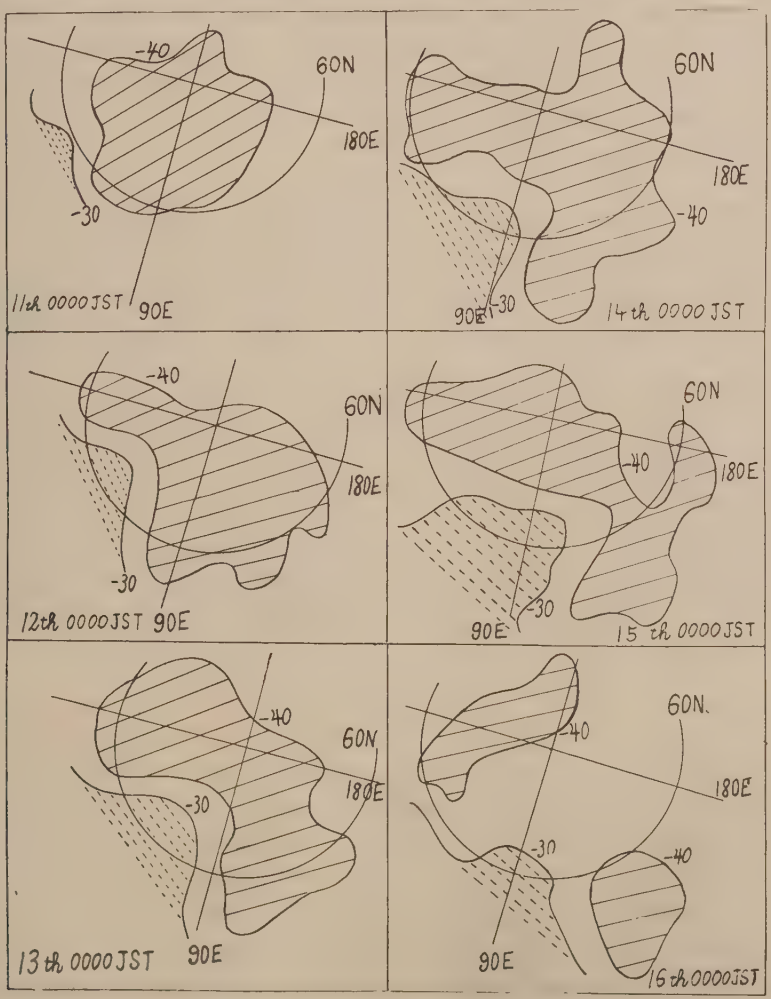

Fig. 4. Change of isotherm at 500 mb.

the phase difference is $\frac{1}{4}$ wave length. Its amplitude increases, but the wave does not progresses. When the phase of isotherm retard in comparison with that of contour by about 110°, the great increase in amplitude will be caused by the effect of solenoid. The larger the phase difference is, the greater the retrogression of wave is. Among the figures (a)-(d) the amplitude will be largest when figures (b) and (d) are combined. Pressure wave will be most unstable, when the amplitude of isotherms is larger than that of contours, and the phase of isotherms retards in comparison with that of contour. The above relations are evident from figures (2b) and (2c). In this case it should be noted that the distance from ridge to trough expands. Fig. 4 indicates the change of isotherms 30°C and 40°C at 500mb charts from 11th to 16th. As soon as the penetration of warm air with temperature of above 30°C occurs, the cold air near the polar region gradually spreads and moves southward. In this case the spreading of cold air is not affected by radiation cooling. Fig. 5 represents 500 mb and surface charts at 00 00 J.S.T. of 12 th with the thermal change at 500mb from 10th to 12th.

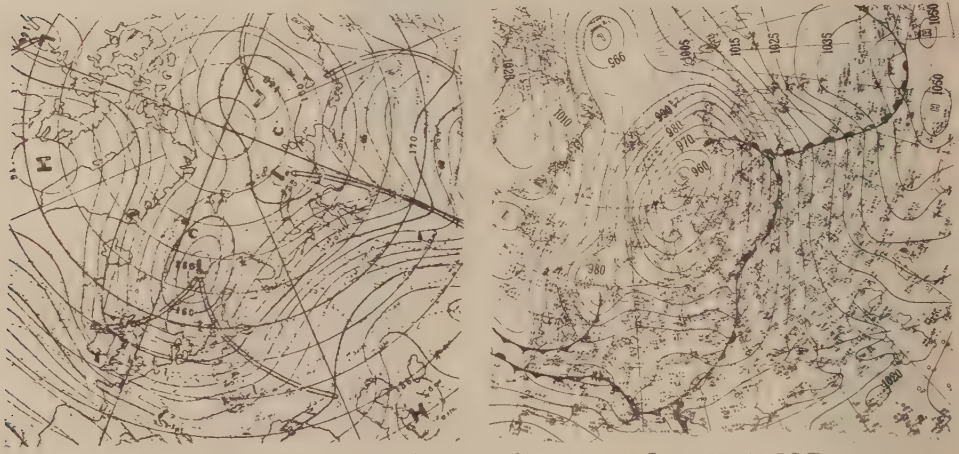

Fig. 5. 500 mb (a) and surfaee map (b). 12 Jan., 1955 00 J.S.T.
———— Contour.
- - - Isotherm.

From figure 5 we can see readily that the advection of warm air at 500 mb chart results from the exceptrional deepening of sea-level cyclone. A westerly wind exists over the downstream of trough situated near 30°E, owing to the effect of solenoid caused by warm air advection. The convergence formed by the westerly wind and southwesterly geostrophic wind makes the pressure rise in that region. The anticyclonic circulation caused by solenoid develops and reaches the trough situated near 90°E. The deepening of the adjoing trough to the east and southward movement of cold air occurs by the circulation. In this case we may consider

that the area of cold air will be spread by the downdraft of upper cold air. Therefore, it seems that the spreading of warm and cold areas as shown in Fig. 3 results from the effect of solenoid, which is formed by the abnormal deepening of cyclone over the northern part of Scandinavia Peninsula.

4. Deepening of the trough in vicinity of 125°E

It has been considered that the adjoiniing trough to the east deepens when the ridge near 90°E intensifies as shown in Fig. 6(a). Because the relative vorticity is negative if nearly zero absolute vorticityis conserved. In the case $A_I > A_C$ as shown in Fig. 6(b), the above characteristics and the deepening of trough should be promoted by anticyclonic circulation existing in the east side of ridge. The intensification of ridge near 90°E is almost included in type (b), but no example correspondiog to type (c) is found. Above all we may consider that the necessary condition for intensification of monsoon is the relative deepening of trough resulting from the intensification of the ridge to the east. Accordingly, the stronger the relative deepening of trough near 125°—130°E is, the larger the advection of cyclonic vorticity is. Thus, the strong deepening of extratropical cyclone occurs off Sanriku. The coupling of outbreak of cold air and isallobaric wind causes northwesterly monsoon to intensify. The relations between the monsoon and the existence of the ridge to the east are shown in Table 4.

Table 4. Relations between maximum wind velocity at Kobe City and the location of the eastern ridge.

Maximum wind velocity at Kobe City / Location of the eastern ridge	below 14.9 m/s	above 15.0 m/s
130°W～160°W	10	1
150°E～170°W	2	5

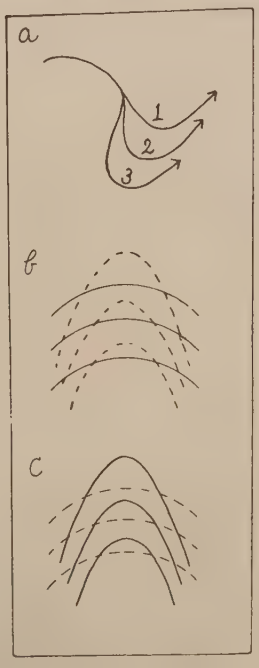

Fig. 6. ———— Contour.
- - - - - - Isotherm.

We find many examples to show that the wind velocity at Kobe is more than 15m/s when ridge exists over the region from 150°E to 170°E. Even in the monsoon caused by the strong ridge near 90°E in Fig. 2, the maximum wind velocity at Kobe is 14.9 m/s because of no existence of the ridge to the east. The ridge were studied by Kawanabe and Fujinori. The monsoon prevails when the curvature of isobars over Japan Sea is cyclonic, in contrast, it does not prevail when its curvature is anticyclonic or isobars stretches in a straight line from north to south. Besides this, the northwesterly gale falls gradually as soon as the pressure at Kobe stops to fall or tends to rise. (Perhaps the state at all stations in the western Japan may be similar to that at Kobe). The region over from Japan Sea to western Japan is the field of disvergence, when monsoon continues to prevail. However, monsoon falls as soon as its field turns to that of convergence. From these facts it may be found that the isallobaric wind caused by the deepening of extratropical cyclone has serious effects on the monsoon.

References

(1) Kadoya, K. (1954): On forecasting of the monsoon. *Umi to Sora*, Vol. 31. No. 1.

(2) Goto, T. (1959): On the abnormal development of the Siberian high. *Reported at the meeting for meteorological research of Kinki district.*

(3) Kawanabe, Y. (1956): Forecasting of the monsoon. *Reported at the meeting for meteorological research of Kinki district.*

(4) Fujinori, A. (1954): A form of the outbreak. *Reported at the meeting for meteorological research of Kinki district.*

(5) Bjerknes. J.: Extratropical cyclones. *Compendium of Meteorology.*

The Role of Vertical Structure of Atmospheric Circular Vortex in the Movement of its Center

By

Morizo Ōta

Kobe Marine Observatory

1. Introduction

At the center of a circular vortex, applying the formula of kinematic analysis to the tendency equation of atmospheric pressure at the earth's surface, it is readily seen that that the movement velocity of the disturbance center is separated into the components due to advection of air density and horizontal divergence of flow in the air column extended semi-infinitely upward. According to estimation of their orders, we can find that the former is the major portion of steering and, generally, in the case of mature tropical cyclones, the latter is almost negligible.

Furthermore, the present paper shows that the so-called steering level is determined by the vertical structure of the circular disturbance. Then, in practice, selecting five examples, Palmén's model of hurricane, the typhoons Kezia, Kitty, Jane and Marge, their steering levels are computed respectively. Thus, it is concluded that the role of vertical structure of the circular vortex is very important in the steering of the vortex center.

2. Considerations on the movement of circular disturbance

In the well-known tendency equation of surface pressure with neglect of topographic influence,

$$-\frac{\partial P_0}{\partial t} = g\int_0^\infty \nabla \cdot (\rho \mathbf{V})dz = g\int_0^\infty \mathbf{V}\cdot\nabla\rho dz + g\int_0^\infty \rho\nabla\cdot\mathbf{V}dz \tag{1}$$

putting $$\mathbf{V}^* = \frac{1}{P_0}\int_0^{P_0}\mathbf{V}\,dP \tag{2}$$

we obtain $$-\frac{\partial P_0}{\partial t} = \mathbf{V}^*\cdot\nabla P_0 + P_0\nabla\cdot\mathbf{V}^* \tag{3}$$

where, except asterisk, the above notations are as usual respectively.

Here, at the center of surface pressure assuming $\frac{\partial^2 P_0}{\partial x^2} = \frac{\partial^2 P_0}{\partial y^2} = \frac{1}{2}\nabla^2 P_0$,

thhe movement velocity of pressure center is expressed by

$$\mathbf{C} = \frac{-\nabla\left(\frac{\partial P_0}{\partial t}\right)}{\frac{1}{2}\nabla^2 P_0} \tag{4}$$

Applying this formula of kinematic analysis to Eq. (3), Petterssen's formula is obtained as follows;

$$C = V^* + \frac{2P_0}{\nabla^2 P_0}\nabla(\nabla \cdot V^*) \tag{5}$$

This formula is very simple and convenient, but its physical meaning is too obscure for us to discuss theoretically. Therefore, substituting from the tendency equation immediately into Eq. (4), the authors has derived another formula which is more complicated but more distinct in physical meaning than Petterssen's formula.

Now, in the vicinity of a pressure center, separating various elements into fundamental fields and circular disturbances by means of the common method, we can put

$$\left.\begin{aligned} &V = \overline{V} + V', \ \rho = \overline{\rho} + \rho', P_0 = \overline{P_0} + P_0' \\ &V \cdot \nabla \rho = (V \cdot \nabla \overline{\rho}) + (V \cdot \nabla \rho)' \end{aligned}\right\} \tag{6}$$

and, $V \cdot \nabla \rho$ may be expanded as follows;

$$V \cdot \nabla \rho = \overline{V} \cdot \nabla \overline{\rho} + \overline{V} \cdot \nabla \rho' + V' \cdot \nabla \overline{\rho} + V' \cdot \nabla \rho'$$

Accordingly, we obtain

$$\overline{(V \cdot \nabla \rho)} = \overline{V} \cdot \nabla \overline{\rho} \tag{7}$$

$$(V \cdot \nabla \rho)' = \overline{V} \cdot \nabla \rho' + V' \cdot \nabla \overline{\rho} \tag{8}$$

where, $V' \cdot \nabla \rho' = 0$, under the assumption of the circular disturbance. Furthermore, for the sake of simplicty, we shall assume that the axis of the disturbance center is almost vertical.

Now, putting

$$C_a = 2g\nabla \int_0^\infty V \cdot \nabla \rho \, dz / \nabla^2 P_0 \tag{9}$$

$$C_d = 2g\nabla \int_0^\infty \rho \nabla \cdot V \, dz / \nabla^2 P_0 \tag{10}$$

the movement of pressure center is expressed by

$$C = C_a + C_d \tag{11}$$

Here, C_a is the component derived from substituting the advection term of the right-hand side of Eq. (1), and C_d is the component which depend upon the divergence term of Eq. (1).

First of all, considering the advection component C_a, as $(V \cdot \nabla \rho)' >> \overline{(V \cdot \nabla \rho)}$ and $\nabla^2 P_0' >> \nabla^2 \overline{P_0}$, the following equation is approximately derived from Eq. (9).

$$C_a = 2g\nabla \int_0^\infty (V \cdot \nabla \rho)' \, dz / \nabla^2 P_0' \tag{12}$$

Now, let C_1 and C_2 be first and second terms of the right-hand side of the equation derived from combining Eq. (8), and Eq. (12). Then,

$$C_a = C_1 + C_2 \tag{13}$$

where

$$C_1 = 2g\nabla \int_0^\infty \overline{V} \cdot \nabla \rho' \, dz \,/\, \nabla^2 P_0 \tag{14}$$

$$C_2 = 2g\nabla \int_0^\infty \overline{V'} \cdot \nabla \overline{\rho} \, dz \,/\, \nabla^2 P_0' \tag{15}$$

However, in Eq. (14), $\nabla(\overline{V} \cdot \nabla \rho') = \frac{1}{2} \nabla^2 \rho' V$ under the assumption that $\nabla \rho' = 0$, $\frac{\partial^2 \rho'}{\partial x \partial y} = 0$, and $\frac{\partial^2 \rho'}{\partial x^2} = \frac{\partial^2 \rho'}{\partial y^2} = \frac{1}{2} \nabla^2 \rho'$ near the disturbance center. Combining these relations and Eq. (14), we get

$$C_1 = g \int_0^\infty \nabla^2 \rho' \overline{V} \, dZ \,/\, \nabla^2 P_0' \tag{16}$$

Next, let us consider the other component C_2. At the disturbance center, assuming

$$\left.\begin{aligned} &\frac{\partial u'}{\partial x} = \frac{\partial v'}{\partial y} = \frac{1}{2} Q', \quad \frac{\partial v'}{\partial x} = -\frac{\partial u'}{\partial y} = \frac{1}{2} \zeta' \\ &\frac{\partial^2 \overline{\rho}}{\partial x^2} = 0, \quad \frac{\partial^2 \overline{\rho}}{\partial^2 y^2} = 0, \quad \frac{\partial^2 \overline{\rho}}{\partial x \partial y} = 0 \end{aligned}\right\} \tag{17}$$

it is found that

$$\nabla \int_0^\infty (\overline{V'} \cdot \nabla \overline{\rho}) \, dZ = \frac{1}{2} \int_0^\infty (Q' \nabla \overline{\rho} + \zeta' \nabla \overline{\rho} \times \boldsymbol{k}) \, dZ = \frac{1}{2g} \nabla \int_0^{\overline{P}_0} Q' \, d\overline{P} + \frac{1}{2g} \nabla \int_0^{\overline{P}_0} \zeta' \, d\overline{P} \times \boldsymbol{k}$$

where $\boldsymbol{k}$ is the vertical unit vector. Furthermore, using the relations,

$\frac{1}{\overline{P}_0} \int_0^{\overline{P}_0} d\overline{P} \approx \frac{1}{P_0} \int_0^{P_0} dP = *$, $\nabla Q' = 0$, $\nabla \zeta' = 0$ at the center, we obtain

$$\nabla \int_0^\infty (\overline{V'} \cdot \nabla \overline{\rho}) \, dZ \approx \frac{1}{2g} (Q'^* \nabla \overline{P}_0 + \zeta'^* \nabla \overline{P}_0 \times \boldsymbol{k})$$

Substituting the above equations to Eq. (15), an approximate expression of C_2 is derived as follows;

$$C_2 \approx (Q'^* \nabla \overline{P}_0 + \zeta'^* \nabla \overline{P}_0 \times \boldsymbol{k}) / \nabla P_0'$$

Then, putting $\frac{\nabla^2 P_0'}{f\rho} = \zeta'_{g_0}$, $\frac{-\nabla \overline{P}_0}{f\rho} \times \boldsymbol{k} = \overline{V}_{g_0}$, we obtain

$$C_2 \approx \frac{Q'^*}{\nabla^2 P_0'} \nabla \overline{P}_0 - \frac{\zeta'^*}{\zeta'_{g_0}} \overline{V}_{g_0} \tag{18}$$

Of course, ζ'_{g_0} is the disturbance of geostrophic vorticity and $\overline{V}_{g_0}$ is the fundamental geostrophic wind respectively at sea level.

Next, we shall consider the divergence component C_d. Here, putting $\nabla \cdot V = Q$, as $\nabla^2 P_0 \approx \nabla^2 P_0'$ in Eq. (10), it is found that

$$C_d \approx 2g \nabla \int_0^\infty \rho \, Q \, dZ \,/\, \nabla^2 P_0' = \frac{2\nabla(Q^* P_0)}{\nabla^2 P_0'}$$

Therefore, substituting $Q^* - \bar{Q}^* + Q'^*$ and $P_0 = \bar{P}_0 + P_0'$ to the above relation the divergence component C_d is expressed by

$$C_d \approx \frac{2}{\nabla^2 P_0'} \left(\bar{Q}^* \nabla \bar{P}_0 + \bar{P}_0 \nabla \bar{Q}^* + Q'^* \nabla \bar{P}_0 + P_0' \nabla \bar{Q}^* \right) \quad (19)$$

Owing to the effect of changing fundamental field caused by hoizontal divergence, the first and second terms of the right-hand side of Eq. (19) are the components associated with the infuence on the movement of the apparent pressure center which is derived from the sum of the fundamental field and the disturbance. And they have nothing to do with the movement of the pure disturbance P_0' center at all. On the other hand, the third and fourth terms have relations to the disturbance center movement influenced by horizontal divergence.

In the case of the component C_a, it has the component concerned with the movement of the apparent center also, but this is almost negligible, and so it may be seen that the component C_a is concerned with only the pure disturbance center.

3. Estimated orders of various components

In the component C_a, C_1 acts the most important part which is the major portion of the so-called steering current. The details of this components shall be explained later, and, in this chapter, we shall estimate the orders of various components in C_2 and C_d.

Then, in order to consider the first term of the right-hand side of Eq. (18), the estimated orders of essential elements shall be arranged as follows;

$$Q'^* \sim 10^{-6} \text{ to } 10^{-7}(C.G.S.), \qquad \nabla^2 P_0' \sim 10^{-9}(C.G.S.),$$
$$| \nabla \bar{P}_0 | \sim 10^{-4}(C.G.S.) \quad ,$$

Thus, we obtain $\left| \frac{Q'^*}{\nabla^2 P_0'} \nabla \bar{P}_0 \right| \sim 10^{-3}$ to 10^{-4}m, $\sec^{-1}$ and it is found that this is quite negligible.

Next, let us examine the second term of Eq. (18), $-\frac{\zeta'}{\zeta'_{g0}} \bar{V}_{g0}$. First of all, it is necessary for us to discuss the method of computation of vorticity near the disturbance center. Near the center of such a remarkable vortex as a tropical cyclone, the centrifugal force is excessively larger than the deviating force due to the earth's rotation, in the equation of motion, and so it is readily seen that the cyclostrophic wind is more suitabe than the geostrophic wind for computation of vorticity. Therefore, surface geostrophic vorticity ζ'_{g0} becomes about one hundred times as large as ζ'^* applying cyclostrophic vorticity to computation of ζ'^*. Hence, $\left| \frac{\zeta'^*}{\zeta'_{g0}} \bar{V}_{g0} \right| \sim 10^{-1}$m $\sec^{-1}$ and this is generally negligible also. Accordingly, it follows from the above-mentioned explanations that the component C_2 offers no problem in general.

In the case of component C_d, if we assume $| \bar{Q}^* | \sim 10^{-6}$ to $10^{-7}(C.G.S.)$,

$\left| \nabla \overline{Q^*} \right| \sim 10^{-14}$ to 10^{-15}(*C.G.S.*), $\overline{P_0} \sim 10^{6}$(*C.G.S.*), $\left| \nabla \overline{P_0} \right| \sim 10^{4}$(*C.G.S.*), we obtain in Eq, (19), $\left| \frac{2}{f^2 P_0'} \overline{Q^*} \nabla \overline{P_0} \right| \sim 2\times10^{-1}$ to 2×10^{-2}m sec^{-1}, $\left| \frac{2}{f^2 P_0'} \overline{P_0} \nabla \overline{Q^*} \right| \sim 2\times10^{-1}$ to 2×10^{-2}m sec^{-1}. Here, according to the relation that the third term of Eq. (19), is just twice as large as the first term of Eq. (18), $\left| \frac{2}{f^2 P_0'} Q^* \nabla \overline{P_0} \right| \sim 2\times10^{-3}$ to 2×10^{-4}m sec^{-1} is obtained, and under the assumption that $\left| P_0' \nabla \overline{Q^*} \right| \sim 3\times10^{-2}$ $\overline{P_0} \nabla \overline{Q^*}$ in Eq. (19), it is found that $\left| \frac{2}{f^2 P_0'} P_0' \nabla \overline{Q^*} \right| \sim 6\times10^{-3}$ to 6×10^{-4}m sec^{-1}

Accordingly, the magnitudes of various terms in Eq. (19), are very small and quite negligible except the second term of Eq. (19). The second term is small also and this is out of the queetion in general, but, in the case when $f^2 P_0' << 10^{-9}$ (*C.G.S.*) at the center of a weak depression, this component has influence on the movement of surface pressure center in some degree. However, as stated at the end of chapter 2, this effect is connected with only the movement of the apparent pressure center, and independent of the pure disturbance center. Consequently, C_d offers no problem also, as for the movement of the circular disturbance.

4. Considerations on the steering level

As the orders of various components except C_1 have been estimated in the above chapter, we must, now, consider the most important component C_1 which is regarded as the steering current of the circular vortex approximately.

First of all, in order to simplify the computation, the following relation shall be assumed;

$$\overline{V} = \overline{V}_0 + Az \qquad (20)$$

where A is a vectorial constant which shows the lapse rate of wind in the fundamental field. Here, as soon as we see Eq. (20), we can find the contradiction that $\lim_{Z\to\infty} \left| \overline{V} \right| = \infty$ is derived. But we have $\lim_{Z\to\infty} \left| \rho \overline{V} \right| = 0$ taking accout of the fact that the air density decreases exponentially with height. Thus, in order to compute the component C_1 approximately, we need not consider the extremely high level of atmosphere. Strictly speaking, in the stratosphere, we must assume another model which is different from Eq. (20), but the air density in the stratosphere is so small that the surface pressure is nearly given by the weight of the air column, only in the troposphere.

According to circumstances, Eq. (20), is too simple to express the fundamental condition in the troposphere, and it is more accurate to use the equations including the higher orders with respect to height. However, in the above case, we can

determine $\boldsymbol{A}$ and $\overline{\boldsymbol{V}}_0$ in Eq. (20), as constants by the well-known method of least squares where we may use the quantities proportional to $r^2\rho'$ as the weights of data. Consequently, we can obtain the sufficient approximation for computation of the component $\boldsymbol{C}_1$ applying such a simple relation as Eq. (20), to the semi-infinite column of the air.

But it should be beared in mind that the steering level derived from the above method of least squares is due to the supposed model expressed by Eq. (20), and so this is not the actual steering level in the case when the higher orders are considerable.

Now, combining Eq. (16), Eq. (20), and $r^2 P_0' = g\int_0^\infty r^2 \rho' dz$, it is found that

$$\boldsymbol{C}_1 = g\int_0^\infty r^2\rho'(\overline{\boldsymbol{V}}_0 + \boldsymbol{A}z)dz / r^2 P_0' = \overline{\boldsymbol{V}}_0 + \boldsymbol{A}g\int_0^\infty r^2\rho' Z dz / r^2 P_0'$$

puttnig $\boldsymbol{C}_1 = \overline{\boldsymbol{V}}_0 + \boldsymbol{A}h$ (21)

the steering level h is shown by

$$h = \frac{g}{r^2 P_0'}\int_0^\infty r^2\rho' Z dz \tag{22}$$

In the other expression of h, owing to $r^2\rho' = -\frac{1}{g}\frac{\partial}{\partial z}r^2 P'$, $\lim_{Z\to\infty} z r^2 P' = 0$ and Eq. (22), we have

$$h = \frac{1}{r^2 P_0'}\int_0^{r^2 P_0'} Z d(r^2 P') = \frac{1}{r^2 P_0'}\int_0^\infty r^2 P' dZ \tag{23}$$

Next, in view of the static balance, the vertical distribution of the air pressure is given by

$$P = P_0 e^{-\int_0^Z \frac{g}{RT} dZ} \tag{24}$$

Furthermore, putting

$$\frac{g}{RT^*} = K \tag{25}$$

where T^* is the mean temperature of the air column averaged vertically with respect to air pressure, we obtain, near the disturbance center,

$$r^2 P' \approx r^2 P_0' e^{-KZ} + P_0 e^{-KZ}\frac{K}{T^*}\int_0^Z r^2 T' dZ \tag{26}$$

Here, we may approximately substitute the air temperature at 500-mb surface for T^*.

Now, as for the vertical distribution of $r^2 T'$, it is already known that they are undulating near the center, and so the following assumption shall be taken,

$$r^2 T' = \tau_0 + \sum_{n=1}^\infty \tau_n e^{i(\sigma_n Z + \theta_n)} \tag{27}$$

where τ_0, τ_n, σ_n, θ_n are harmonic constants, and n is denoted by integer. Then, combining Eqs. (23), (26), (27), and taking the real part, we obtain

$$h \approx \frac{1}{K} + \frac{P_0 \tau_0}{\rho^2 P_0' T^* K} + \sum_{n=1}^{\infty} (A_n \sin \theta_n + B_n \cos \theta_n) \tag{28}$$

where

$$A_n = \frac{-P_0 \tau_n \sigma_n}{\rho^2 P_0' T^* (K^2 + \sigma_n^2)}, \quad B_n = \frac{P_0 \tau_n K}{\rho^2 P_0' T^* (K^2 + \sigma_n)^2} \tag{29}$$

Moreover, putting

$$h_0 = \frac{P_0 \tau_0}{\rho^2 P_0' T^* K}, \quad h_n = A_n \sin \theta_n + B_n \cos \theta_n \tag{30}$$

a simple formula is obtained as follows;

$$h \approx \frac{1}{K} + \sum_{n=0}^{\infty} h_n \tag{31}$$

5. Practical computations

From the foregoing, it follows that the major portion of the steering current is given by the component C_1 and we can compute the approximate height of the steering level from Eqs. (29), (30), and (31). In this chapter, we shall have several examples of computation under the assumption that tropical cyclones are nearly regarded as symetric circular disturbances.

Now, concerning the vertical structure of the mature hurricane, Palmén has proposed a model mainly due to the Miami-New Orleans hurricane which hit the Florida Peninsular in Sept., 1947. In the case of the typhoon connected with Japan, Arakawa has published his study on the vertical structure of the typhoon Kitty which struck the Kanto district during Aug. 31 to Sept. 1, 1949, and another study by Masuda and Takeuchi shows the case of the typhoon Kezia which passed across the Kyushu district during 13 to 14 in Sept. 1950, immediately after the typhoon Jane hit the Kyushu disttrict.

As stated above, now, we have three typical examples invesigated by four meteorologists concerning the vertical structures of tropical cyclones. Then, we shall apply the foregoing considerations to them practically.

Here, for the sake of convenience, with respect to the property ψ, let $\Delta\psi = \psi_c - \psi_s$ where ψ_c is the property at the center, and ψ_s is the averaged property at the distance d from the center. Using the temperaturatre T instead of the property ψ, Fig. 1 shows the variations of ΔT with height where $d = 100$km in the present three cases.

According to this figure, it is readily seen that, in all cases, the air in the central region is much warmer than the surrounding air in the most part of the troposphere. Moreover, in the cases of the typhoon Kezia and Palmén's model, we can find two warm cores at the levels of 3 to 4km and 9 to 10km. However,

in the case of Kitty, we have only one warm core at the level of about 14km owing to filtration of negligibly small irregularity of the ΔT profile curve, and it should be noted that the level of this core is by far the highest of all examples.

Returning to the ΔT profiles of Kezia and Palmén's model, it is of interest that both of them are so analogous to each other that Fig. 1 indicates the correlation between them deriving a simple experimental formula $\Delta T_K \approx 0.47\ \Delta T_P$ where the subscripts K and P are concerning Kezia and Palmén's model respectively.

Now, as shown in Fig. 2, the vertical distributions of $\nabla^2 \rho$ in the central region of disturbance are derived from Fig. 1, Eq. (26), and $P=\rho RT$, putting $d=100$km. As readily seen, all profiles in this figure illustrate roughly exponential decrease with height, but, for details, they have a maximum within the extent of 1 to 4km level, that is, at about 1.5km in the cases of Palmén's model and the typhoon Kezia and at about 3.5km in the case of the typhoon Kitty.

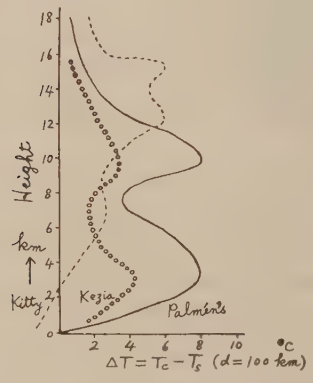

Fig. 1. Examples of vertical distribution of ΔT, where T_c is temprature at center and T_s is average temperature at distance 100km from center.

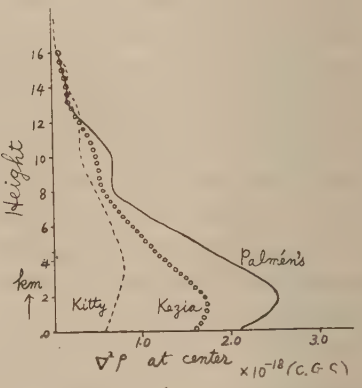

Fig. 2. Examples of vertical distribution of $\nabla^2 \rho$ at center of tropical cyclone.

Here, for the approximate computation of Laplacian, it is convenient to use the finite-difference formula $\nabla^2 \psi \approx \dfrac{-4\Delta\psi}{d^2}$. Then, $\nabla^2 \rho$, $\nabla^2 T$, $\nabla^2 P$, etc. are able to be estimated from $\Delta\rho$, ΔT, ΔP, etc. (Let us use $d=100$km hereafter.) Therefore, instead of Eq. (27), we can use the following equation disregarding negligible heigher terms,

$$\Delta T \approx \Delta T_0 + \Delta T_1 \cos\left(\frac{2\pi}{H_1} + \theta_1\right) + \Delta T_2 \cos\left(\frac{2\pi}{H_2} + \theta_2\right) \tag{32}$$

where ΔT_0 is the residual constants, and, for the others, subscripts 1, 2 are concerning the long and short waves respectively.

Table 1. Showing vertical structure of each case.

	ΔT_0	ΔT_1	ΔT_2	H_1	H_2	θ_1	θ_2
Palmén's	3.1	3.8	2.8	28	8	$2\pi-1.34$	π
Kezia	1.5	1.8	1.3	28	8	$2\pi-1.34$	π
Kitty	×	4.7	×	42	×	$\pi+1.17$	×
Unit	°C	°C	°C	km	km	radian	radian

Thus we obtain, in Table 1, computed constants of Eq. (32) from the abovementioned three examples. Moreover, Table 2 indicates surface pressure distributions corresponding to Table 1 where P_{0c} shows the surface pressure at the center.

Table 2. Showing surface pressure distribution of each case, where P_{0c} = surface pressure at center.

	P_{0c}	ΔP_0	$\nabla^2 P_0$
Palmén's	956	−40	1.6
Kezia	960	−30	1.2
Kitty	975	−17	0.7
Unit	mb	mb	10^{-9}(C·G.S.)

After all, we can obtain Table 3 which denotes various elements concerned with the steering level, from substitutioins of Table 1 and 2 into Eqs. (30), and (31), assuming $\frac{1}{K} \approx 8.0$km.

Table 3. Showing various elements concerned with height of steering level (unit: km).

	h_0	h_1	h_2	h
Palmén's	−2.2	−2.3	+0.1	3.6
Kezia	−1.4	−1.5	0.0	5.1
Kitty	×	−2.4	×	5.6

Here, judging from this table, we may disregard the value of h_2 as well as h_3. Hence, for the approximate computation of h, we shall be practically satisfied with the following simple formula,

$$h \approx \frac{1}{K} + h_0 + h_1 \tag{33}$$

In other words, the effect of the short wave whose wave-length is less than about 10km is able to be ignored, and, conversely, that of the long wave whose wave-length is larger than about 20km is rather effective to the steering level. The residual

warming effect h_0 is comparable to the long wave effect h_1 in general.

In the foregoing we have discussed the results of practical computations of three examples. Then, let us shift our consideration to the other cases.

For instance, Simpson says in his paper owing to aircraft reconnaissance "In 1951 an exploration of the lower and middle vortex of Typhoon Marge provided some insight into the magnitude of temperature gradients which can exist in very large storms. At 18,000 feet a temperature fall of of more than 18°C in 60 miles was observed in flying out of the eye".

Besides, in another case, there is a study on the thermal structure of the typhoon Jane in 1950 by Masuda and Takeuchi. But, unfortunately, their data are not so detailed as those of the typhoons Kezia and Kitty, because the center of Jane was always out of the 100km radius from the ocean station named Tare situated at 29°N, 135°E whose aerological data are utilized to a time isopleth by the above investigators.

Then, in order to estimate the ΔT profile near the center for the case of Jane also, we must be satisfied with a roughly approximate method as given below. Now, let S_1 denote the shortest distance of Tare from the center of Jane and S_2 another distance between them, and we shall have two opportunities of putting $S_2 - S_1 = 100$km. Next, let T_1 and T_2 denote the temperature at Tare corresponding to S_1 and S_2 respectivey. Thus, the mean of $T_2 - T_1$ taken twice may be regared as the roughly approximate value of ΔT.

In this way, we can estimate the vertical distribution of ΔT at the center of Jane as shown in Fig. 3. Judging from this figure, it is supposed that a remarkable warm core exists at the level of about 13km where $\Delta T \approx 11$°C in the case of Jane.

Now, let us try to compute the steering level h approximately for the cases of Marge and Jane also, although their data are not so detailed as those of Kitty and Kezia, where the following is assumed roughly in their thermal structures,

$$\Delta T \approx \Delta T_1 \cos\left(\frac{2\pi}{H_1} Z + \theta_1\right) \tag{34}$$

And, finally, we shall obtain the estimated vertical structures of Marge and Jane as given in Table 4 where $h \approx 4.9$km for Marge and $h \approx 4.1$km for Jane.

Table 4. Showing estimated vertical structures of the typhoons Marge and Jane.

	ΔT_1	H_1	θ_1	h
Marge	18°C	22km	$\frac{3}{2}\pi$	4.9km
Jane	11°C	48km	$\frac{5}{2}\pi$	4.1km

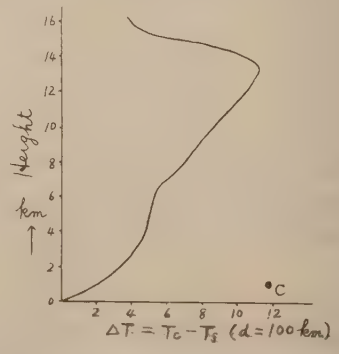

Fig. 3. Estimated vertical distribution of ΔT at center of the typhoon Jane.

6. Conclusions and remarks

At the end of this paper, summarizing the foregiong discussions and supplying some remarks on the present problem, the following articles shall be arranged:

(Ⅰ) Although the movement velocity of the atmospheric circular disturbance is expressed by the vectorial sum of the components associated with advection of air density and horizontal divergence of flow in the air column extended semi-infinitely upward, the former component is much more predominant than the lattter in mature tropical cyclones.

(Ⅱ) The steering current of the developed circular disturbance is, on account of the above article, mainly due to the mean fundamental current averaged along the vertical air column in the central region of the disturbance where the weight at each level is proprtional to the intensity of the air density disturbance (Refer to Eq. (16)).

(Ⅲ) The steering level of the tropical cyclone is considerably influenced by its vertical structure near the center. According to actual computations, it is supposed that the steering levels are within the extent of 3 to 6km.

(Ⅳ) The more remarkable the warm core is, the lower the steering level becomes in the central region of the tropical cyclone, while the stronger the circulation is, the weeker the warm core effect becomes. Generally, both effects seem to be cancelled each other. For instance, the case of the typhoon Marge in 1951 may be regarded as one of the typical cases.

(Ⅴ) In the foregoing, the assumptions are forced to be taken roughly at places so as to simplify the problems which are too difficult to be solved immediately.

For example, we have assumed that any tropical cyclone is a symetric circular vortex, actual temperature is able to be substituted into virtual temperature approximately, the axis of the disturbance center is nearly vertical, etc.

Nevertheless, the results in this paper may be satisfactory enough for us from the semi-quantitative point of view.

(Ⅵ) In general, concerning the steering current, we make it a rule to use the geostrophic current instead of the actual current in the fundamental field. However, it should be necessarry for us to consider ageostrophic components for computation of the steering current.

Although it is of interest to investigate the above problem indeed, the author intends to reserve them for another occasion.

References

(1) Palmén, E. (1948): *Geophysica, Helsingfors*, Vol. 3, p. 26.

(2) Arakawa, H. (1950): *Papers in Meteorology and Geophysics*, Vol. 1, No. 2—4, p. 217.

(3) Masuda, Y. and Takeuchi, M. (1951): *Papers in Meteorology and Geophysics*, Vol. 2. No. 3—4, p. 234.

(4) Simpson, R. H. (1955): *Proceedings of the Unesco Symposium on Typhoons*, p. 129.

Some Statistical Studies on Typhoons attacking Japan Islands

By

K. Koenuma

Japan Meteorological Agency

1. Japan Islands are frequently attacked by typhoons every year. Of these, some are of considerable intensity, causing huge damages in our country. Concerning these typhoons, such as the Muroto Typhoon and the Makurazaki Typhoon etc., detailed studies have been done respectively. Here, we intend to try some statistical studies of typhoons, approaching and landing Japan Islands.

2. Let us first consider typhoons, approaching or landing Japan Islands in recent ten years of 1949—1958. In this period, we have experienced 27 typhoons which gave rise to more or less damages in our country. The annual and monthly distributions of these typhoons are shown in Table 1 and Table 2.

Table 1.

Year	freq.
1649	3
50	3
51	3
52	1
53	1
54	5
55	1
56	3
57	3
58	4
Total	27

Table 2.

Month	freq.	%
6	3	11.1
7	3	11.1
8	7	25.9
9	13	48.2
10	1	3.7
Total	27	100.0

As seen from the tables, the annual number of typhoons which attack Japan Islands varies from year to year, while the typhoon season is limited in summer and autumn. Further, their numbers in both season are nearly the same, though, in autumn, they concentrate in September, amounting to so much as 48.2%. Also,

as we know already by experience, typhoons in September, are generally intense, bringing much damages in our country. For example, in recent ten years, there were ten typhoons which caused damages including 100 or more victims. Of these, the Toyamaru Typhoon and the Kanogawa Typhoon are most famous. The former sunk the ferry steamer Toyamaru in 1954, giving rise to 1761 victims, while the latter sacrificed 1269 persons owing to the huge flood of the Kano River.

3. Next, we shall proceed to consider the intense typhoons which attacked Japan Islands in sixty years since 1900. Among numerous typhoons which we have experienced in these years, we shall here take 59 typhoons which gave rise to the lowest pressure of 975mb. or less at some land stations in Japan. Such observed lowest pressure may be more preferable for our purpose than that of typhoon center.

To know the frequency of typhoon of different intensity, we have classified these 59 typhoons into five types, according to their lowest pressure above mentioned with interval of 15mb., as shown in Table 3.

Table 3.

type	pressure interval	freq.
A	901 — 915 mb.	1
B	916 — 930 〃	2
C	931 — 945 〃	3
D	946 — 960 〃	13
E	960 — 975 〃	40
Total		59

As seen in the table, the most intense type A was experienced once for sixty years, while the type B occured twice for the same period. The former is the famous Muroto Typhoon in Sept. 1934 which caused huge storm damages in Kansai District.

To see the general features of attacking of these typhoons, their frequencies for every five years are given in Table 4. It shows us that their attackings seem to become more frequent in the latter half of sixty years. As regards their monthly distribution, Table 5 explains that their general aspects are nearly the same already stated in the previous article. However, in this case, we have experienced more typhoons in autumn than in summer, especially in case of ones whose observed lowest pressure are below 960mb.

Table 4.

Year	below 975mb	below 960mb	below 945mb	below 930mb
1900 — 1904	6	2	1	0
05 — 9	2	1	0	0
10 — 14	4	0	0	0
15 — 19	5	1	1	0
20 — 24	3	0	0	0
25 — 29	1	0	0	0
30 — 34	5	4	1	1
35 — 39	5	1	0	0
40 — 44	8	2	0	0
45 — 49	5	1	1	1
50 — 54	8	4	1	0
55 — 59	7	3	1	1
Total	59	19	6	3

Table 5.

month	below 975		below 960	
	freq.	%	freq.	%
6	1	1.7	0	0
7	8	5.1	1	5.3
8	18	30.5	4	21.0
9	28	47.5	11	57.9
10	8	13.5	2	10.5
11	1	1.7	1	5.3

In this connection, we shall notice ten typhoons which caused huge damages in our country, including 1000 or more victims since 1900. As seen in Table 6, all these tyhpoons but two, occured in autumn. Consequently, it may be said that typhoons in autumn are far more intense than those in summer on the neighbouring seas of Japan.

Table 6.

No.	Month	Year	Name	Remark
1	Aug.	1910		Flood of the Tone River.
2	Oct.	1917		Storm damages and high water of the Tokyo Bay.
3	Sept.	1934	Muroto	Storm damages and high water of the Osaka Bay.
4	Aug.	1942		Storm damages and high water of the Suō nada.
5	Sept.	1945	Makurazaki	Storm damages in western Japan.
6	Sept.	1947	Cathrine	Flood of the Tone River.
7	Oct.	1951	Ruth	Storm damages in western Japan.
8	Sept.	1954	Toyamaru	Maritime calamity of the Toyamaru.
9	Sept.	1958	Kanogawa	Flood of the Kano River.
10	Sept.	1959	Isewan	Storm damages and high water of the Ise Bay.

4. Typhoons are formed in the tropical regions of the western Pacific, especially on the neighbouring seas of the Marshall, Mariana and Caroline Islands. They develop gradually, owing to the released heat energy of condensation in the unstable tropical air of high temperature and humidity. As for the typhoons approaching Japan Islands, they become gradually less intense, owing not only to the decrease of heat energy of condensation but to the topographic friction.

According to K. Takahashi, the mean monthly frequencies of their formations and attackings to our country are given in Table 7.

Table 7.

Month	formation		attackings to Japan.	
	freq.	%	freq.	%
1	0.2	0.9	—	—
2	0.2	0.9	—	—
3	0.2	0.9	—	—
4	0.4	1.7	—	—
5	0.9	3.8	—	—
6	1.4	5.9	0.1	2.7
7	4.1	17.4	0.8	21.6
8	5.7	24.3	1.2	32.4
9	4.8	20.4	1.2	32.4
10	3.1	13.2	0.3	8.1
11	1.5	6.4	0.1	2.7
12	1.0	4.2	—	—
sum	23.5	100.0	3.7	99.9

As seen from the table the formation of typhoons extends all over the year, but it is more frequent in summer than in autumn, showing its maximum in August. Attackings of typhoons to our country are also more frequent in summer than in autumn, though they are the same in August and September. From these facts, it may be naturally supposed that the developement of typhoons is more favourable in summer than in autumn. However, this seems to be inconsistent with Table 5 and 6 in the previous article. Then, what is the season in which typhoons might develop most ?

To answer this problem, we shall refer to Table 8 in which the monthly mean pressures and positions of centers of 27 typhoons, treated in art. 2, are shown when they are in most developed state on the southern sea of Japan. It tells us that the typhoon in September develop more than those in August, though those in other months are so scanty as to discuss their developement. At any rate, it may be said that typhoons in autumn seems to be more intense than those in summer.

Table 8.

Month	mean press.	mean lat.	freq.
6	948	22	3
7	965	26	3
8	943	26	7
9	937	25	13
10	924	22	1

5. It may be generally said that all typhoons tend to decay gradually, approaching Japan Islands. This is true for all typhoons in summer, but it is not true for some typhoons in autumn.

When autumn comes, the cold continental air begins to predominate over Mongolia and Siberia. Therefore, when a typhoon approaches Japan Islands in this season, this cold air is withdrawned to its center, forming a front with the tropical air and changing the feature of typhoon. In such case, two types of typhoons are noticed, one being a rainy type and the other a windy type.

When the cold air is withdrawned to the typhoon from north, a front is formed nearly parallel to the latitude. In this case, the typhoon can not move fastly and decays gradually, bringing heavy rainfall along the front or on the slope of mountaineous regions, Such is the rainy type typhoon. The Cathrine Typhoon in 1947 and the Kanogawa Typhoon in 1958 belong to this type. The Kanogawa Typhoon developed to the extent that its central pressure was so deep as 880mb. on the

southern sea of Japan. When it approached to the Izu Peninsula, a front is formed through the peninsula by the cold air, coming from north. As a result, it began to decay gradually, but gave rise to enormous rainfall in the vicinity of the peninsula.

On the other hand, when the cold air comes from northwest, a front tends to form along Japan Proper. In this case, as the air masses on both sides of the front are in the unstable state, the typhoon travels very fast along the front, maintaining its energy and causing very strong southerly wind in the eastern quadrant. This is the windy type typhoon. The Muroto Tyhpoon in 1934 is a typical example of this type. The most intense typhoons attacking Japan Islands, seem to belong to this type, though details are left for future.

昭和35年3月20日印刷
昭和35年3月25日発行

編集兼発行人　神戸海洋気象台
神戸市生田区中山手通7丁目

印刷人　高輪忠二

印刷所　高輪印刷株式会社
神戸市兵庫区中道通2丁目6